ADVANCED FORMATION FLIGHT CONTROL

THESIS

Michael J. Veth
Second Lieutenant, USAF

AFIT/GE/ENG/94D-30

DEPARTMENT OF THE AIR FORCE
AIR UNIVERSITY
AIR FORCE INSTITUTE OF TECHNOLOGY

Wright-Patterson Air Force Base, Ohio

AFIT/GE/ENG/94D-30

ADVANCED FORMATION FLIGHT CONTROL

THESIS

Michael J. Veth
Second Lieutenant, USAF

AFIT/GE/ENG/94D-30

The views expressed in this thesis are those of the author and do not reflect the official policy or position of the Department of Defense or the U. S. Government.

AFIT/GE/ENG/94D-30

ADVANCED FORMATION FLIGHT CONTROL

THESIS

Presented to the Faculty of the Graduate School of Engineering

of the Air Force Institute of Technology

Air University

In Partial Fulfillment of the

Requirements for the Degree of

Master of Science in Electrical Engineering

Michael J. Veth, B.S. Electrical Engineering

Second Lieutenant, USAF

December, 1994

Acknowledgements

I would like to thank my thesis advisor, Dr. Meir Pachter, for his guidance throughout this thesis research. His unique combination of scientific excellence and practicality serve as a model for which I can only hope to follow. I would also like to thank my parents, John and Jacquelyn Veth, for their support and encouragement. I owe what I am today to their tireless guidance throughout my life.

Michael J. Veth

Table of Contents

		Page
Acknowledgements		ii
List of Figures		vii
List of Tables		xii
List of Symbols		xiii
Abstract		xv
I.	Introduction to Advanced Formation Flight Control	1-1
	1.1 Overview of Thesis	1-1
	1.2 Motivation for Formation Flight Control	1-2
	1.3 Background Information for Thesis Effort	1-3
	1.4 Research Objectives and Questions	1-5
	1.5 Assumptions	1-7
	1.6 Criterion for Success	1-8
	1.7 Materials and Equipment	1-9
	1.8 Conclusion	1-9
II.	Literature and Concept Review	2-1
	2.1 Development of Formation Flight Control Systems	2-1
	2.2 Previous AFIT Research	2-2
	2.3 Equation of Coriolis	2-3
	2.4 Conclusion	2-3

Page

III. Model and Simulation Development 3-1

3.1 Aircraft/Autopilot Models 3-1

3.2 Formation Coordinate System 3-5

3.3 Kinematic Equations 3-5

3.4 Simulation Description 3-9

3.5 Simulation Rendering Using Aviator 3-11

IV. Formation Hold Autopilot 4-1

4.1 Procedure 4-1

4.2 Linearization of Kinematic Equations 4-1

4.3 Development (First-order models) 4-2

4.3.1 Control Laws 4-3

4.3.2 Determination of Controller Gains 4-4

4.4 Evaluation of First-Order Controllers 4-7

4.5 Development (Second-Order Models) 4-12

4.6 Determination of Controller Gains 4-13

4.7 Evaluation of Controller with Second-Order Models 4-13

4.8 Formation Geometry Change Maneuvers 4-18

4.9 Controller Summary 4-22

4.10 Conclusion 4-22

V. Energy Tracking 5-1

5.1 Introduction 5-1

5.2 Energy Conservation Problem 5-1

5.2.1 Controller Derivation 5-2

5.2.2 Performance Metric 5-4

5.3 Energy Tracking Controller Analysis 5-4

5.4 Formation Geometry Change Maneuvers 5-9

Page

5.5 Controller Summary 5-12

5.6 Conclusion 5-12

VI. Autopilots for Flying Circular Paths 6-1

6.1 Problem Description 6-1

6.1.1 Linearization 6-1

6.2 First-order Models 6-4

6.2.1 Proportional Control Law 6-5

6.2.2 Stability Envelope Determination Using Routhian Analysis 6-5

6.2.3 Choosing K_{xp} and K_{yp} 6-8

6.2.4 Proportional Controller Analysis 6-9

6.2.5 Adding Integral Action 6-11

6.2.6 Proportional Plus Integral Controller Analysis . . . 6-12

6.2.7 Simulation Using Nonlinear Dynamics 6-17

6.2.8 Simulation Using Nonlinear Dynamics and Rate Limits 6-19

6.3 Second-order Models 6-21

6.3.1 Proportional Controller Design Using Successive Loop Closures 6-22

6.3.2 Proportional Controller Analysis 6-22

6.3.3 Adding Integral Action 6-27

6.3.4 Proportional Integral Controller Analysis and Comparison 6-27

6.3.5 Simulation Using Nonlinear Kinematics 6-28

6.3.6 Simulation Using Both Nonlinear Kinematics and Rate Limits 6-29

6.4 Trajectory Variations 6-34

6.5 Controller Summary 6-37

6.6 Conclusion 6-37

Page

VII. Proportional and Integral Control of Nonlinear Systems 7-1

7.1 Introduction 7-1

7.2 Linearization 7-2

7.3 PI Control 7-4

7.4 Example 7-7

7.5 Linearization - Induced Mismatches 7-8

7.6 Integral Action in Robust Control 7-17

7.7 Conclusions 7-18

VIII. Analysis and Conclusions 8-1

8.1 Objectives of Research Met 8-1

8.1.1 Incorporation of Second-Order Models - Analysis . . 8-1

8.1.2 Energy Tracking 8-1

8.1.3 Circular Path Autopilot 8-2

8.1.4 Analysis of Subtleties Encountered in the Linearization Design Process 8-2

8.2 Conclusions and Specific Lessons Learned 8-2

8.3 Recommendations for Further Study 8-3

8.4 Formation Assembly Problem 8-4

8.5 Summary 8-7

Bibliography BIB-1

Vita VITA-1

List of Figures

Figure		Page
1.1.	Trail Formation	1-4
1.2.	Diamond Formation	1-5
1.3.	Diamond Formation Heading Change Maneuver	1-6
1.4.	Trail Formation Altitude Change Maneuver	1-7
1.5.	Trail to Diamond Formation Change Maneuver	1-8
2.1.	Three Dimensional Aircraft Response	2-2
2.2.	Inertial and Rotating Frames of Reference [3:Figure 1.7]	2-4
3.1.	First-Order Aircraft Models	3-3
3.2.	Comparison of First and Second-Order Responses	3-4
3.3.	Second-Order Aircraft/Autopilot Models	3-4
3.4.	Inertial Reference Frame and Separation Distances	3-6
3.5.	Wing's Rotating Reference Frame and Separation Distances	3-7
3.6.	Relative Motion Diagram	3-8
3.7.	Simulation Model	3-10
4.1.	Proportional Formation Flight Controller Block Diagram	4-5
4.2.	Proportional Inner Loop (Y) Feedback Root-Locus	4-5
4.3.	Proportional Outer Loop (X) Feedback Root-Locus	4-6
4.4.	C-130A: Diamond Formation, Linear Response, 30^o Heading Change	4-7
4.5.	C-130A: Diamond Formation, Linear Response, $25\frac{ft}{sec}$ Velocity Change	4-8
4.6.	C-130A: Diamond Formation, Nonlinear Response, 30 Degree Heading Change	4-9
4.7.	C-130A: Diamond Formation, Nonlinear Response, $25\frac{ft}{sec}$ Velocity Increase	4-9

Figure Page

4.8. C-130A: Diamond Formation, Nonlinear Response, 30 Degree Heading Change *Revised X-Channel Gain* 4-10

4.9. C-130A: Diamond Formation, Nonlinear Response, 30 Degree Heading Change *Reyna: solid; New: dashed* 4-10

4.10. C-130A: Diamond Formation, Nonlinear Response, 25 $\frac{ft}{sec}$ Velocity Change *Reyna: solid; New: dashed* 4-11

4.11. Proportional Inner Loop (Y) Feedback Root-Locus *Second-Order models* 4-14

4.12. Proportional Outer Loop (X) Feedback Root-Locus *Second-Order Models* 4-15

4.13. C-130A: Diamond Formation, Linear Response, 30 Degree Heading Change *Second-Order Models* 4-15

4.14. C-130A: Diamond Formation, Linear Response, 25 $\frac{ft}{sec}$ Velocity Change *Second-Order Models* 4-16

4.15. Heading Change Comparison. Linear: Solid, Nonlinear: Dashed . . . 4-16

4.16. Velocity Change Comparison. Linear: Solid, Nonlinear: Dashed 4-17

4.17. Left Turn with Formation Translation 4-19

4.18. Left Diamond to Trail Formation Change 4-19

4.19. Left Diamond to Trail Formation Change Lissajous Figure 4-20

4.20. Left Diamond to Right Diamond with a 30 degree Left Turn 4-20

4.21. Left Diamond to Right Diamond with a 30 degree Left Turn Lissajous Figure 4-21

5.1. Comparison of Planar (Solid) and Energy Tracking Controller (dashed) *(30 Degree Heading Change)* 5-5

5.2. Performance Indices *(30 Degree Heading Change)* 5-6

5.3. Comparison of Planar (Solid) and Energy Tracking Controller (dashed) *(10 fps Velocity Increase)* 5-6

5.4. Performance Indices *(10 fps Velocity Increase)* 5-7

5.5. Comparison of Planar (Solid) and Energy Tracking Controller (dashed) *(Combination Maneuver) — 30° Heading Change, 100 ft Altitude Change, and 15 fps Velocity Increase)* 5-7

Figure Page

5.6. Performance Indices *(Combination Maneuver — 30° Heading Change, 100 ft Altitude Change, and 15 fps Velocity Increase)* 5-8

5.7. Left Diamond to Trail Formation Change — *Planar (Solid), Energy Tracking Controller (Dashed)* 5-9

5.8. Left Diamond to Trail Formation Change Performance Index 5-10

5.9. Left Diamond to Right Diamond with a 30 degree Left Turn — *Planar (Solid), Energy Tracking Controller (Dashed)* 5-10

5.10. Left Diamond to Right Diamond with a 30° Left Turn Performance Index 5-11

6.1. Circular Path Autopilot Visualization 6-2

6.2. Range of Stability for Values of K_{xp} and K_{yp} *(Shaded Region)* 6-7

6.3. Linearized Formation Flight Control System with Proportional Feedback 6-8

6.4. First-order, Proportional Linear Autopilot Response ($\overline{X} = \overline{Y} = 0$) . . 6-9

6.5. First-order, Proportional Linear Autopilot Response ($\overline{X} = \overline{Y} = 500$) . 6-10

6.6. First-order, Proportional Linear Autopilot. 10 $\frac{ft}{sec}$ Velocity Increase Response ($\overline{X} = \overline{Y} = 0$) 6-11

6.7. First-order, Proportional Linear Autopilot. 10 degree Heading Change Response ($\overline{X} = \overline{Y} = 0$) 6-13

6.8. First-order, Proportional Linear and Nonlinear Autopilot Response ($\overline{X} = \overline{Y} = 0$) 6-13

6.9. First-order, Proportional Linear and Nonlinear Autopilot Response ($\overline{X} = \overline{Y} = 500$) 6-14

6.10. First-order, Proportional Plus Integral, Linear Autopilot Response ($\overline{X} = \overline{Y} = 0$) 6-14

6.11. First-order, Proportional Plus Integral, Linear Autopilot Response ($\overline{X} = \overline{Y} = 500$) 6-15

6.12. First-order, Proportional Plus Integral, Linear Autopilot. 10 $\frac{ft}{sec}$ Velocity Increase Response ($\overline{X} = \overline{Y} = 0$) 6-15

6.13. First-order, Proportional Plus Integral, Linear Autopilot. 10 degree Heading Change Response ($\overline{X} = \overline{Y} = 0$) 6-16

Figure Page

6.14. First-order, Proportional Plus Integral, Nonlinear Autopilot Response ($\overline{X} = \overline{Y} = 0$) 6-17

6.15. First-order, Proportional Plus Integral, Nonlinear Autopilot Response ($\overline{X} = \overline{Y} = 500$) 6-18

6.16. First-order, Proportional Plus Integral, Nonlinear Autopilot Response w/ Rate Limits ($X_0 = Y_0 = 10ft$) 6-19

6.17. First-order, Proportional Plus Integral, Nonlinear Autopilot Response w/ Rate Limits ($X_0 = Y_0 = 510ft$) 6-20

6.18. First-order, Proportional Plus Integral, Nonlinear Velocity Response w/ and w/o Rate Limits ($X_0 = Y_0 = 510ft$) 6-20

6.19. Proportional Inner Loop (Y) Feedback Root-Locus *(Second-Order Models)* 6-22

6.20. Proportional Outer Loop (X) Feedback Root-Locus *(Second-Order Models)* 6-23

6.21. Second-Order, Proportional, Linear Autopilot Response ($\overline{X} = \overline{Y} = 0$) 6-24

6.22. Second-Order, Proportional, Linear Autopilot Response ($\overline{X} = \overline{Y} = 500$) 6-24

6.23. Second-Order, Proportional, Linear Autopilot 10 $\frac{ft}{sec}$ Velocity Increase Response ($\overline{X} = \overline{Y} = 0$) 6-25

6.24. Second-Order, Proportional, Linear Autopilot 10 degree Heading Change Response ($\overline{X} = \overline{Y} = 0$) 6-25

6.25. First-Order, Proportional, Linear and Nonlinear Autopilot Response ($\overline{X} = \overline{Y} = 0$) 6-26

6.26. Proportional Plus Integral Inner Loop (Y) Feedback Root-Locus *(Second-Order Models)* 6-27

6.27. Proportional Plus Integral Outer Loop (X) Feedback Root-Locus *(Second-Order Models)* 6-28

6.28. Second-order, Proportional Plus Integral, Linear Autopilot Response ($\overline{X} = \overline{Y} = 0$) 6-29

6.29. Second-order, Proportional Plus Integral, Linear Autopilot Response ($\overline{X} = \overline{Y} = 500$) 6-30

Figure Page

6.30. Second-order, Proportional Plus Integral, Linear Autopilot. 10 $\frac{ft}{sec}$ Velocity Increase Response ($\overline{X} = \overline{Y} = 0$) 6-30

6.31. Second-order, Proportional Plus Integral, Linear Autopilot. 10 degree Heading Change Response ($\overline{X} = \overline{Y} = 0$) 6-31

6.32. Second-order, Proportional Plus Integral, Nonlinear Autopilot Response ($\overline{X} = \overline{Y} = 0$) 6-31

6.33. Second-order, Proportional Plus Integral, Nonlinear Autopilot Response ($\overline{X} = \overline{Y} = 500$) 6-32

6.34. Second-order, Proportional Plus Integral, Nonlinear Autopilot Response w/ Rate Limits ($X_0 = Y_0 = 10ft$) 6-32

6.35. Second-order, Proportional Plus Integral, Nonlinear Autopilot Response w/ Rate Limits ($X_0 = Y_0 = 2500ft$) 6-33

6.36. Second-order, Proportional Plus Integral, Nonlinear Velocity Response w/ and w/o Rate Limits ($X_0 = Y_0 = 2500ft$) 6-33

6.37. Trajectory Radius Change from 20054 ft to 10000 ft (at T = 300s) . . 6-34

6.38. Trajectory Velocity Change from 350 fps to 375 fps, ($atT = 300s$) . . 6-35

6.39. Combination Trajectory Radius and Velocity Change, ($atT = 300s$) . 6-35

6.40. Circular Path Initialization, ($0 \leq T \leq 300s$) 6-36

6.41. Combination Trajectory Radius and Velocity Change Lissajous Figure, ($300 \leq T \leq 600s$) 6-36

7.1. Phase Plane Response of Proportional/Integral Controller 7-8

7.2. Linear Point Circle Autopilot Model 7-13

7.3. Linear and Nonlinear Comparison (Proportional) 7-14

7.4. Linear and Nonlinear Comparison (With Integral Controller) 7-16

8.1. Optimal Formation Assembly (Two Aircraft) 8-5

8.2. Formation Assembly (Suboptimal Reformulation) 8-6

List of Tables

Table		Page
3.1.	First Order Aircraft/Autopilot Time Constants	3-2
3.2.	Aircraft/Autopilot Saturation Values	3-2
3.3.	Second-Order Aircraft/Autopilot Parameters	3-3
4.1.	Formation Flight Controller Gains	4-22
5.1.	Energy Tracking Formation Flight Controller Gains	5-12
6.1.	Circular Path Formation Flight Controller Gains	6-37

List of Symbols

Symbol		Page
$\dot{R}_i$	vector velocity in the i reference frame	2-3
$\dot{R}_p$	vector position as seen from the p reference frame	2-3
ω_{ip}	vector angular velocity of p with respect to i	2-3
R_p	vector position in the p reference frame	2-3
τ_ψ	heading time constant	3-1
τ_v	velocity time constant	3-1
τ_h	altitude time constant	3-1
V_{WL}^W	lead velocity with respect to the wing aircraft	3-6
ω_W^W	angular velocity of wing	3-6
R_{WL}^W	position of leader with respect to the wing aircraft	3-6
V_W^W	inertial velocity of the wing aircraft	3-6
V_L^W	inertial velocity of the lead aircraft	3-6
Ψ_E	heading error	3-7
V_L^L	velocity of lead aircraft	3-7
k_v	velocity mixer constant	4-4
k_ψ	heading mixer constant	4-4
ψ_L	lead heading	4-4
v_L	lead velocity	4-4
K_{xp}	X channel proportional gain	4-4
K_{yp}	Y channel proportional gain	4-4
$\overline{X}$	nominal X separation	4-4
$\overline{Y}$	nominal Y separation	4-4
$\overline{V}$	nominal velocity	4-4
ψ_{cmd}	heading command	4-4
g	gravitational acceleration	5-1

Symbol		Page
H_W	wing aircraft altitude	5-1
T	aircraft thrust	5-2
D	aircraft drag	5-2
m	aircraft mass	5-2
H_{wc}	wing altitude command	5-3
H_L	lead altitude	5-4
R	nominal radius of circular path	6-3
ω	angular rate	6-3
γ	toe-in angle	6-3
Ψ_{wc}	wing heading command	6-3
$\frac{Y(s)}{\Psi_{cmd}(s)}$	inner loop transfer function	6-8
$\frac{X(s)}{V_{cmd}(s)}$	outer loop transfer function	6-8
V_{max}	maximum aircraft velocity	6-29
$\overline{X}(t)$	nominal trajectory state	7-3
$\overline{U}(t)$	nominal trajectory controls	7-3
K_P	proportional feedback gain	7-7

Abstract

In this thesis, the formation flight control problem is continued from four previous theses. Automatic formation flight involves controlling multiple aircraft equipped with standard Mach-hold, altitude-hold, and heading-hold autopilots to maintain a desired distance from a lead aircraft or "rabbit". Changes in the rabbit's states are treated as disturbances to the system and rejected. Previous research is advanced in the following areas. Higher-order aircraft/autopilot models are included into the design and a new feedback control law is employed, resulting in more accurate simulations. An energy tracking scheme is developed and is shown to reduce wing aircraft energy excursions. Finally, the formation hold autopilot is modified to allow the wing aircraft to orbit a stationary reference point on the earth at a desired range, airspeed, and altitude. The importance of the disturbance rejection capability of the controller is demonstrated through comparisons of linearized model predictions with nonlinear simulations. The design tradeoffs between performance and robustness are emphasized.

ADVANCED FORMATION FLIGHT CONTROL

I. Introduction to Advanced Formation Flight Control

1.1 Overview of Thesis

Traditional flight control entails the design of controllers which achieve desired handling qualities over a range of plant variations by using the aircraft's control surfaces in response to pilot command inputs. *Formation* flight control, however, differs from traditional flight control design in a number of ways. Formation flight control, as presented here, seeks to use the aircraft's existing flight control systems to maintain formation with other similarly equipped aircraft. Whereas traditional flight control focuses on the dynamics associated with aircraft, the formation flight system consists of a number of individual aircraft and their associated dynamics. The resulting control problem is rich and provides insights into linear control systems design which are not obvious in the traditional flight control arena.

The first chapter introduces the Formation Flight Control problem. The background, assumptions, research questions, and scope are addressed.

The second chapter reviews current literature on formation flight control. Related work is discussed and the relative importance to this thesis is noted.

The third chapter defines the aircraft models used in the thesis. The standard kinematics are derived and nonlinear simulations are introduced. This chapter should enable the reader to easily reproduce the results from this research.

The fourth chapter extends Reyna's formation flight control work from March of 1994. The control law is modified to improve performance by changing the feedback gains to provide lead heading and velocity tracking. Second-order models developed by Buzogany [3] are incorporated into the design procedure and simulation. As in previous theses, lead heading and velocity commands introduce disturbances into the system.

The fifth chapter extends the energy minimizing concept pioneered by Buzogany and enhanced by Reyna. The energy conserving technique developed by Buzogany enabled the wing aircraft to vary altitude to eliminate energy excursions. Unfortunately, wing aircraft capability was limited because the wing aircraft was unable to track energy changes by the leader. Reyna extended the capability of the controller by developing an energy minimizing controller which enabled the wing aircraft to track energy changes and thereby reduce wing energy swings. The energy tracking controller developed in this thesis extends this concept by decomposing the energy problem into two parts: aircraft/autopilot commands which are energy tracking and commands which are energy conserving. This decomposition allows the design of the two controllers independently, improving performance and providing further insights into the energy tracking concept.

The sixth chapter introduces an advanced application of formation flight control research. The circular path autopilot concept allows an aircraft to automatically fly about a fixed point on the earth, at a prespecified range and velocity. The leader is a computer generated target (or "rabbit") following the ideal orbit path. The formation flight controller is thus responsible for maintaining the aircraft's desired position relative to the fictitious leader. The development and performance of this advanced formation flight control autopilot is studied. Apart from obvious military applications entailing surveillance, or laser designating an earth-bound target, civilian applications are also envisaged, e.g., automatically flying aircraft in a "stack" in an airport traffic pattern.

The seventh chapter investigates the subtle factors involved when designing linear controllers for nonlinear systems. The chapter reveals insights into possible pitfalls and motivations for the use of proportional plus integral (PI) control in this research effort.

The final chapter summarizes the findings of this research, provides conclusions, and makes recommendations for future research.

1.2 Motivation for Formation Flight Control

The mission of today's Air Force requires aircraft that are able to perform a wide variety of roles. Current flying missions vary from air-to-air combat to cargo and personnel

transport to surveillance. Technological advances have increased the capability of aircraft; however, these advances have come at a cost of increased complexity [16].

The complexity of aircraft has contributed to a definite increase in pilot workload. More importantly, some systems have even caused the pilot to become saturated with inputs [3]. In other words, the pilot is unable to keep track of all of the systems and begins to ignore data. A good example of this phenomena was discovered during the Vietnam era, where at times an aircraft missile warning system would provide so much data to the pilots that they would begin to ignore the system entirely, completely negating the effect of the system [16]. Another example of this occurs on a daily basis in the A-10 Thunderbolt II. The Head Up Display (HUD) is a visual display which projects information directly into the line of sight of the pilot, attempting to increase effectiveness. This system can be used to display an enormous amount of data. It turns out, however, that pilots become saturated with too much data and frequently opt to use a setting which displays the minimum information possible [8].

A specific mission which has a great potential for causing pilot saturation is the Air Force Special Operations Forces (SOF). An unclassified description of the SOF mission describes the following conditions under which pilots must operate. The missions emphasize concealment and secrecy and may require long range penetration behind enemy lines. To reduce the probability of detection, the missions are primarily flown at night, in tight formation, and at very low altitudes [20]. Finally, these formations may consist of like or dissimilar aircraft, depending on mission requirements.

These missions require pilots to perform a very heavy workload. When flying in close formation, at low altitude, and under darkness or in poor weather conditions, there is little room for pilot error. Current technology needs to be utilized to take over the demanding task of maintaining formation. This advancement will reduce the pilot workload, increasing endurance, and overall mission effectiveness [16],[5],[3], and [14].

1.3 Background Information for Thesis Effort

C-130 aircraft/autopilot models are employed in this thesis for the following reasons:

- C-130s are currently used by the Special Operations Forces
- Previous AFIT theses used the C-130 models. This enables comparison with previous results.

In previous research, two basic formations were investigated. They included the trail and diamond formations. The formations are illustrated in figures 1.1 and 1.2, respectively.

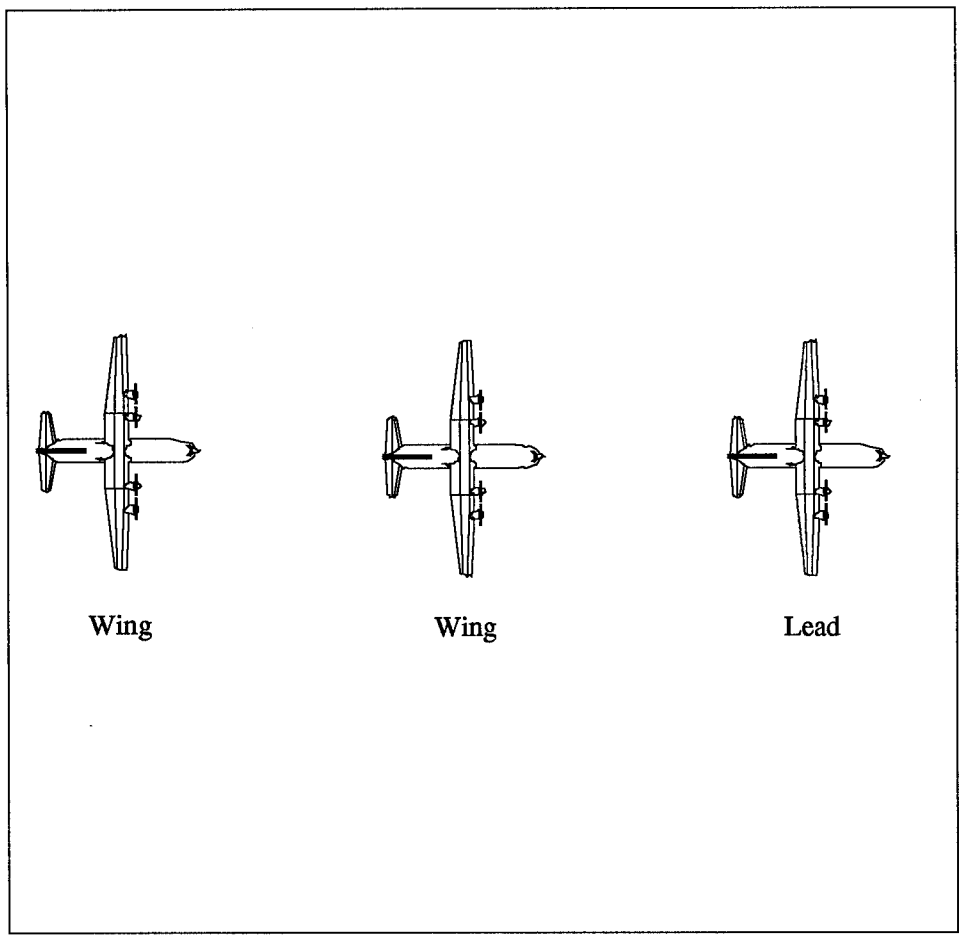

Figure 1.1 Trail Formation

The different formations are noted because they each have different uses in the SOF mission. The trail formation enables aircraft to cover a minimum amount of land during the flight. Conversely, the diamond formation covers more area, but allows easier visibility between aircraft.

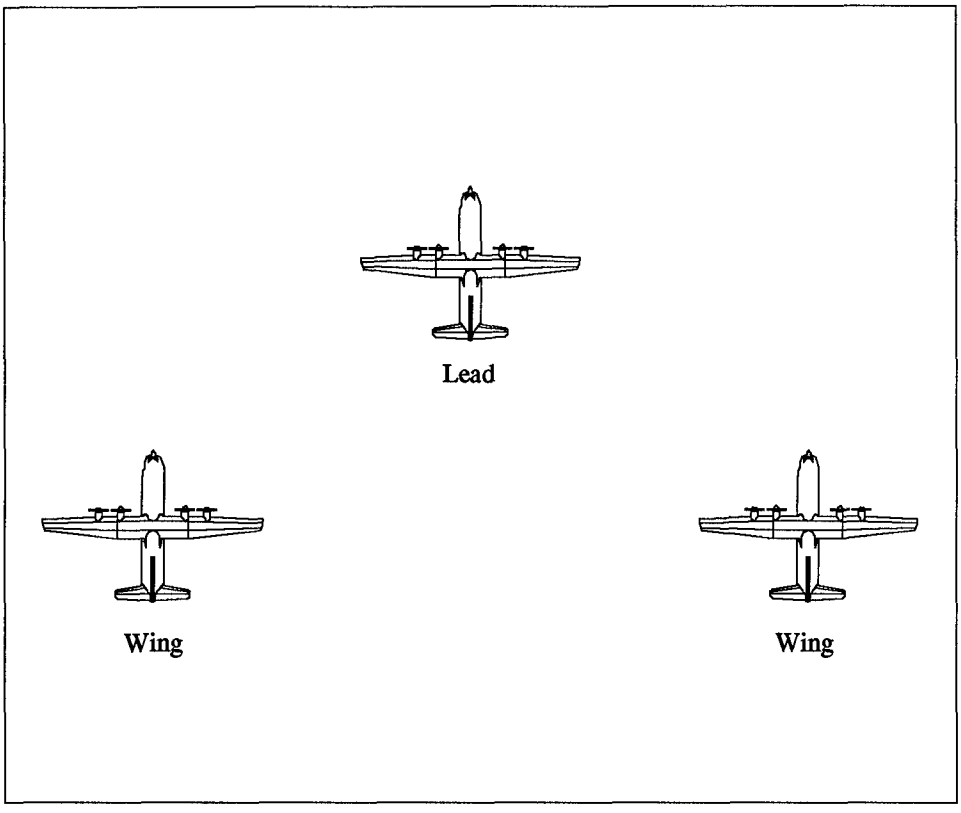

Figure 1.2 Diamond Formation

The formation flight control paradigm, as presented in this research, allows for changes in formation geometry during flight as well as changes in the formation velocity, heading, and altitude. Illustrations of select maneuvers are shown in Figures 1.3-1.5.

This thesis focuses primarily on the diamond formation. This enables convenient comparison with Reyna's results as well as addressing the problem with more interesting dynamics.

1.4 Research Objectives and Questions

The first step of this research is to verify the previous AFIT results from the equations of motions to the nonlinear SIMULINK simulations. By gaining full confidence in previous work, the foundation for further research is established.

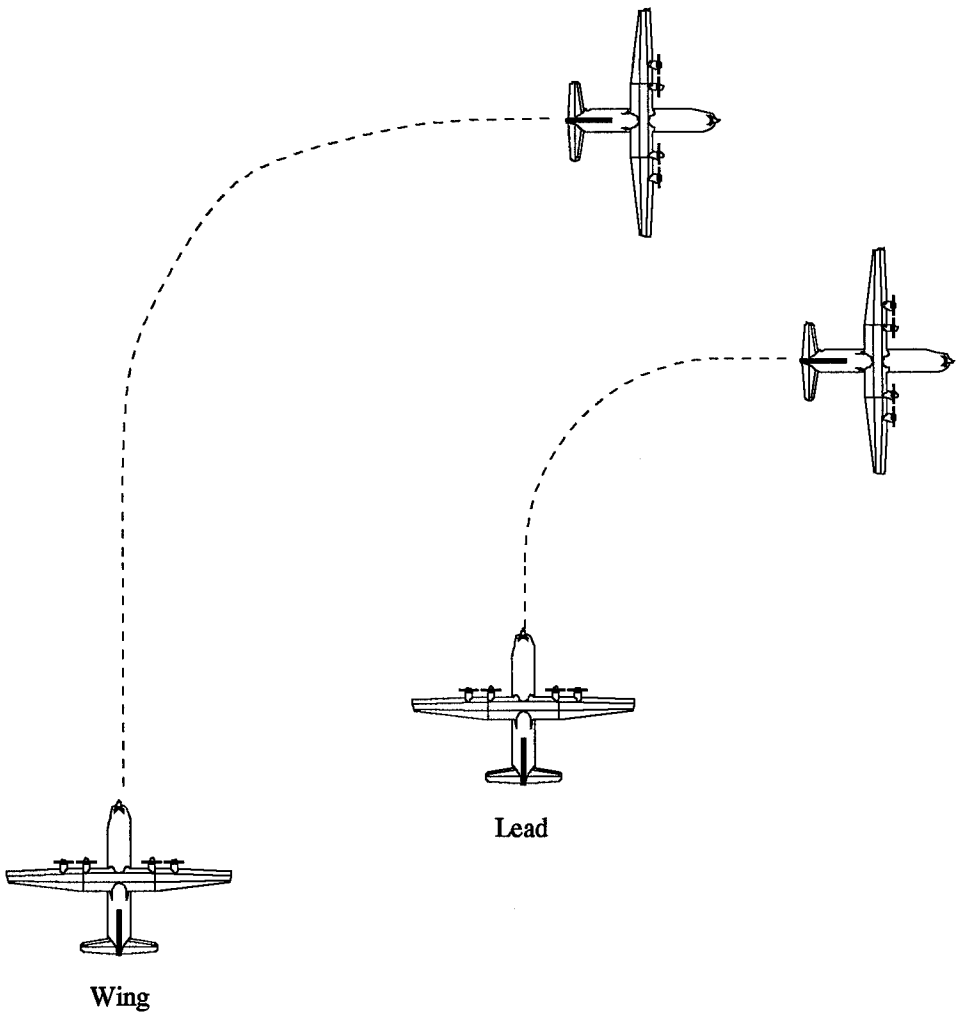

Figure 1.3 Diamond Formation Heading Change Maneuver

Once verification is complete, the second-order models are incorporated into the simulation. The models are evaluated in both two and three dimensional analysis using SIMULINK. The results are used to adjust controller gains to improve formation response.

The energy minimization problem is investigated and, if possible, improvements are made to provide a more desirable response. A metric used to objectively rate controller performance is derived.

The circular path autopilot generator is incorporated into the simulation and evaluated using a wide range of test conditions. The ability of the controller to fly a given

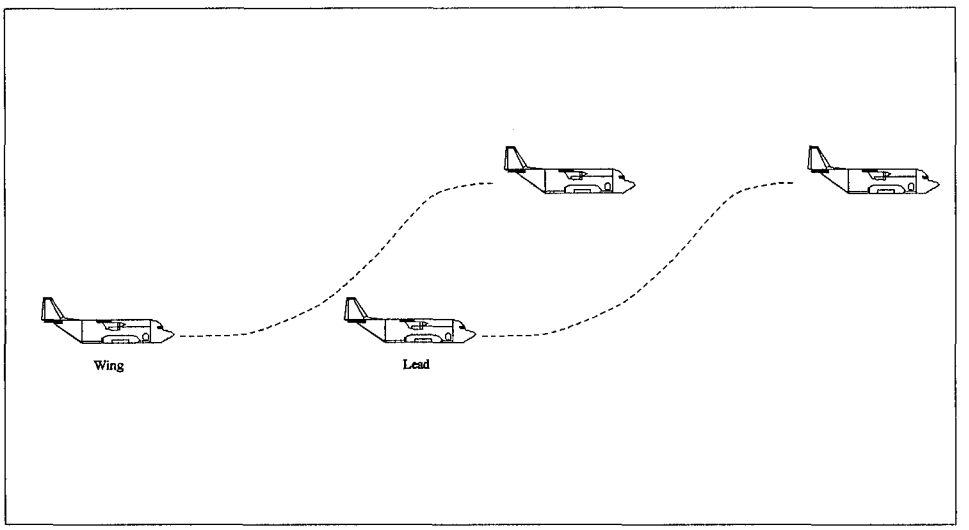

Figure 1.4 Trail Formation Altitude Change Maneuver

path without errors is measured. The controller gains are adjusted to achieve acceptable response.

The final task is to undertake a rigorous analysis of the subtleties associated with controller design for nonlinear systems. The benefits of integral action are explored. Finally, nonlinear formation simulations data is incorporated into Aviator to create a visual representation of aircraft response.

1.5 Assumptions

The primary goal of this thesis is the study of a unique control system application. Assumptions are made to restrict the focus of this research to the design of a formation flight control system. Assumptions are also made which limit the amount of work to a level appropriate for a Master's thesis. This thesis is a continuation of previous work and is intended to serve as a basis for extension to a "real world" application. The assumptions are:

- Each aircraft in the formation has the following autopilots in place:
  a) Mach-Hold Autopilot
  b) Heading-Hold Autopilot
  c) Altitude-Hold Autopilot

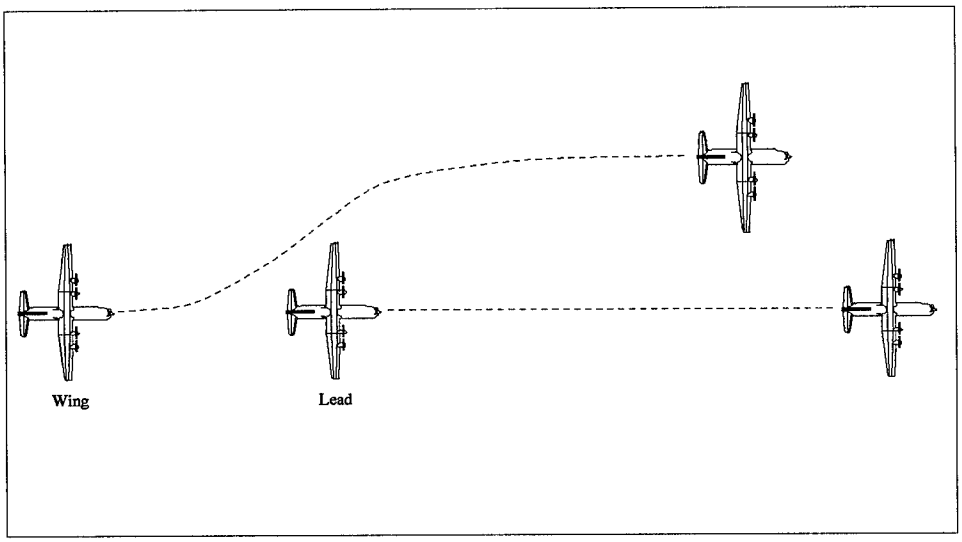

Figure 1.5 Trail to Diamond Formation Change Maneuver

All autopilots are decoupled. In other words, altitude changes can be made independently of altitude and heading changes, etc.

- The controller has access to the following ideal measurements: lead velocity, lead heading, and X and Y separation distances.
- Initial conditions for all simulations are straight and level flight.
- Aircraft/autopilot models are considered to be time invariant over the simulation time period (< 250 seconds).
- The formation flight control system uses continuous time measurements. No digital implementations are considered.

1.6 Criterion for Success

When designing a control system, it is important to establish a thumbprint to specify desirable output responses. The formation flight control system must meet the following criteria:

- The control system must maintain commanded formation with zero steady-state error.
- Other aircraft and terrain obstacles must be avoided.

- A critically damped response is desired ($\zeta = 1$). This eliminates unnecessary and undesirable excursions by the wing aircraft.
- The system must be robust over a wide range of command inputs, even commands which are large.

1.7 Materials and Equipment

All simulations are performed using the Matlab 4.0 analysis package. Matlab 4.0 is sold by Mathworks and uses double precision arithmetic and standard command files to execute computations and is available for a wide variety of platforms. A Runge-Kutta 4th order differential equation solver is used in all nonlinear simulations. The equipment and software is provided by the Department of Electrical and Computer Engineering in the Navigation and Flight Control Lab, Room 133, Air Force Institute of Technology. In addition, the thesis document is written using LaTeXdocument preparation software.

1.8 Conclusion

This thesis continues the development of a formation flight control system. These automatic formation flight control systems decrease pilot workload and increase safety and efficiency.

II. Literature and Concept Review

2.1 Development of Formation Flight Control Systems

The formation flight control problem is certainly not new. The military has been actively studying this topic since the early 1960s [16]. A variety of techniques have been used, each with its own merits. The most noteworthy of these techniques is discussed in the following section.

The earliest formation flight control systems were used to control drone aircraft to test the effectiveness of air-to-air weapons against enemy formations. The Navy used two separate controllers to fly formations of QF-9 drone aircraft as early as 1963. The wing drone maneuvered itself to keep the lead aircraft in the center of a TV screen [16]. Although this system performed adequately for simple commands, it was limited to only two aircraft because of difficulties with coordination and fine adjustment of the flight control system (FCS).

Another noteworthy system used to control drone aircraft was developed in the mid seventies by the Army and IBM. This system was able to control multiple QF-102 aircraft in take-off, missile attack evasions, and landing modes [16]. The system met specifications in all modes. This implementation, however, required direct access to the aircraft flight control system, making modification to other aircraft extremely difficult.

The current approach to flying difficult formations is to augment the pilot's ability to locate the lead aircraft [3]. Special Operations Forces may use a system known as IFPS (Intra-Formation Positioning System) which is developed by Loral. IFPS combines Forward Looking Infrared (FLIR), Terrain Following (TF), and a HAVE QUICK II data-link system to improve formation flight capability during darkness and adverse weather by providing formation data to the pilot. These visual enhancement systems help to increase mission capability, but still require the pilot to manually fly the formation. This can lead to pilot saturation, which increases the chance of midair collision or impact with low level obstructions [20].

2.2 *Previous AFIT Research*

The development of an automatic outer loop formation control system has been the focus of previous AFIT research. A simple planar control system for first-order aircraft models was initially studied [16]. A multivariable controller was designed which gave favorable results and proved the initial viability of the approach. The design was extended by using proportional-integral control in conjunction with a linear mixer [5]. The PI system successfully controlled aircraft in planar movements using first-order aircraft/autopilot models. Further research focused on evaluating true three-dimensional maneuvers [3] (Figure 2.1) and a controller which conserved wing aircraft energy level was implemented. Throttle fluctuations were eliminated, minimizing fuel consumption, but preventing the aircraft from tracking changes in lead altitude or velocity. A solution to the limitations of the energy conserving controller was to allow wing energy fluctuations, but to make them as small as possible [14]. This energy minimizing technique demonstrated the ability to track lead altitude and velocity changes, while reducing fuel consumption and achieving adequate formation performance.

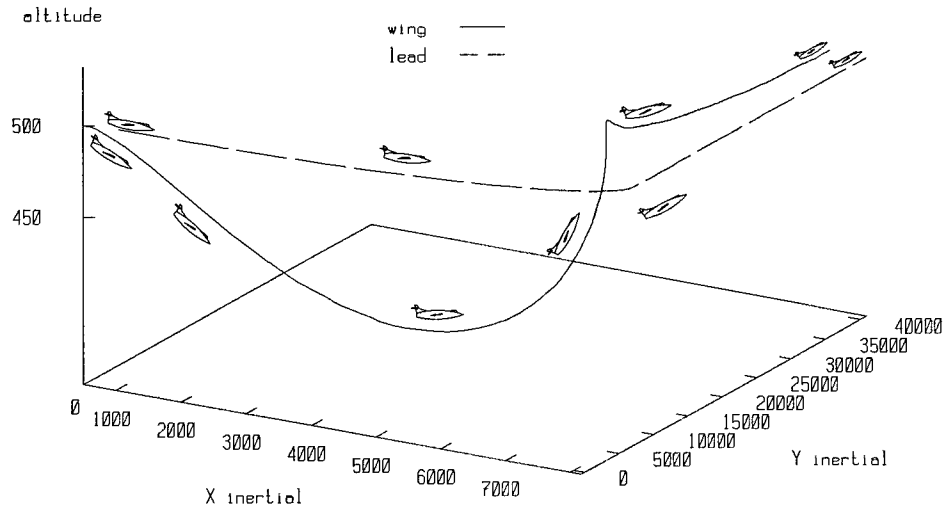

Figure 2.1 Three Dimensional Aircraft Response

2.3 *Equation of Coriolis*

In order to express the formation flight control problem kinematics, reference frames must be established in the inertial and wing aircraft frames. The subsequent rotations caused by maneuvering aircraft within the formation require a mathematical function relating vectors in different, rotating frames. The Equation of Coriolis performs this function.

According to Blakelock [2], "The motion of an object as viewed from a reference frame is equal to the motion as seen from the moving frame, plus the motion resulting from the relative angular velocity of the moving frame with respect to the reference frame" [2][page 489]. Using this equation provides the basis for converting individual aircraft heading and velocity into separation distances. This is an essential part of the design process. In equation form, the Equation of Coriolis is

$$\dot{R}_i = \dot{R}_p + \omega_{ip} \times R_p \tag{2.1}$$

where (Figure 2.2)

- $\dot{R}_i$ = the vector velocity of the point in the i reference frame
- $\dot{R}_p$ = the vector position of the point in question as seen from the p reference frame
- ω_{ip} = the vector angular velocity of the p reference frame with respect to the i reference frame
- R_p = the vector position of a point in the p frame

2.4 *Conclusion*

Although significant progress has been made, there are still issues which the previous research does not address [14]. For instance, the proposed research begins by incorporating second-order aircraft models into the nonlinear simulation. As shown in Figure 3.2, second-order models exhibit a more realistic aircraft response, namely by adding subtle delays to the system [13]. Finally, the formation-assembly phase must be addressed to complete the requirements of an implementable formation flight control system.

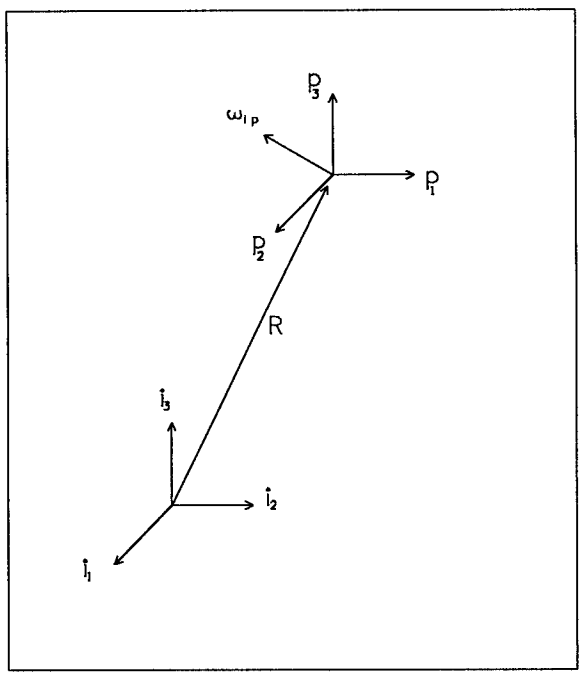

Figure 2.2 Inertial and Rotating Frames of Reference [3:Figure 1.7]

III. Model and Simulation Development

This chapter outlines the models and kinematic equations used in the nonlinear simulation. Sufficient information is provided to enable the reader to reproduce the results of the research.

3.1 Aircraft/Autopilot Models

The development of the aircraft/autopilot models was accomplished by Rohs [16], Dargan [5] and Buzogany [3]. Since no autopilot models were explicitly available, models were obtained by designing a custom autopilot system around C-130H aircraft models provided by Lockheed. The autopilot system included heading-hold, Mach-hold, and altitude-hold autopilots. Due to the inherent properties of aircraft autopilots, the models exhibited overdamped, decoupled responses. Using system identification techniques, first-order models were developed using rate limited, decoupled, first-order differential equations. The first-order aircraft/autopilot models are specified in equations (3.1) - (3.3).

$$\dot{\Psi} = -\frac{1}{\tau_\psi}\Psi + \frac{1}{\tau_\psi}\Psi_c \tag{3.1}$$

$$\dot{V} = -\frac{1}{\tau_v}V + \frac{1}{\tau_v}V_c \tag{3.2}$$

$$\dot{H} = -\frac{1}{\tau_h}H + \frac{1}{\tau_h}H_c \tag{3.3}$$

where,

τ_ψ = heading time constant

τ_v = velocity time constant

τ_h = altitude time constant

The time constants and saturation values used in this thesis are specified in Tables 3.1 and 3.2. The first-order aircraft/autopilot models are illustrated in Figure 3.1.

Second-order aircraft/autopilot models were developed by Buzogany [3] in order to more accurately represent the "true" aircraft/autopilot system. The most disturbing prob-

Parameter	Value
τ_ψ	$\frac{1}{1.5}$ sec
τ_v	$\frac{1}{3}$ sec
τ_h	2 sec

Table 3.1 First Order Aircraft/Autopilot Time Constants

Parameter	Lower Limit	Upper Limit
Velocity	$304\frac{ft}{sec}$	$422\frac{ft}{sec}$
Acceleration	$-5\frac{ft}{sec^2}$	$2.5\frac{ft}{sec^2}$
Turn Rate	-3 $\frac{deg}{sec}$	$3\frac{deg}{sec}$
Vertical Velocity	$-42\frac{ft}{sec}$	$8\frac{ft}{sec}$

Table 3.2 Aircraft/Autopilot Saturation Values

lem with first-order models is the presence of instantaneous heading rate and vertical velocity changes. Figure 3.2 compares an overdamped second-order response with a first-order response. While heading and altitude response was significantly improved using second-order models, it was found that velocity response was modelled more precisely using a first-order model with a larger time constant. Thus, the "second-order" models and time constants are specified in equations (3.4) - (3.6). The respective nonlinear saturation values remain identical to those specified in Table 3.1. The second-order models are illustrated in Figure 3.3.

$$\ddot{\Psi} = -\left(\frac{1}{\tau_{\psi_a}} + \frac{1}{\tau_{\psi_b}}\right)\dot{\Psi} - \frac{1}{\tau_{\psi_a}\tau_{\psi_b}}\Psi + \frac{1}{\tau_{\psi_a}\tau_{\psi_b}}\Psi_c \tag{3.4}$$

$$\dot{V} = -\frac{1}{\tau_v}V + \frac{1}{\tau_v}V_c \tag{3.5}$$

$$\ddot{H} = -\left(\frac{1}{\tau_{h_a}} + \frac{1}{\tau_{h_b}}\right)\dot{H} - \frac{1}{\tau_{h_a}\tau_{h_b}}H + \frac{1}{\tau_{h_a}\tau_{h_b}}H_c \tag{3.6}$$

The time constants used in the second-order models are specified in Table 3.3.

Parameter	Value
τ_{ψ_a}	1.838 sec
τ_{ψ_b}	1.838 sec
τ_v	10 sec
τ_{h_a}	0.615 sec
τ_{h_b}	7.692 sec

Table 3.3 Second-Order Aircraft/Autopilot Parameters

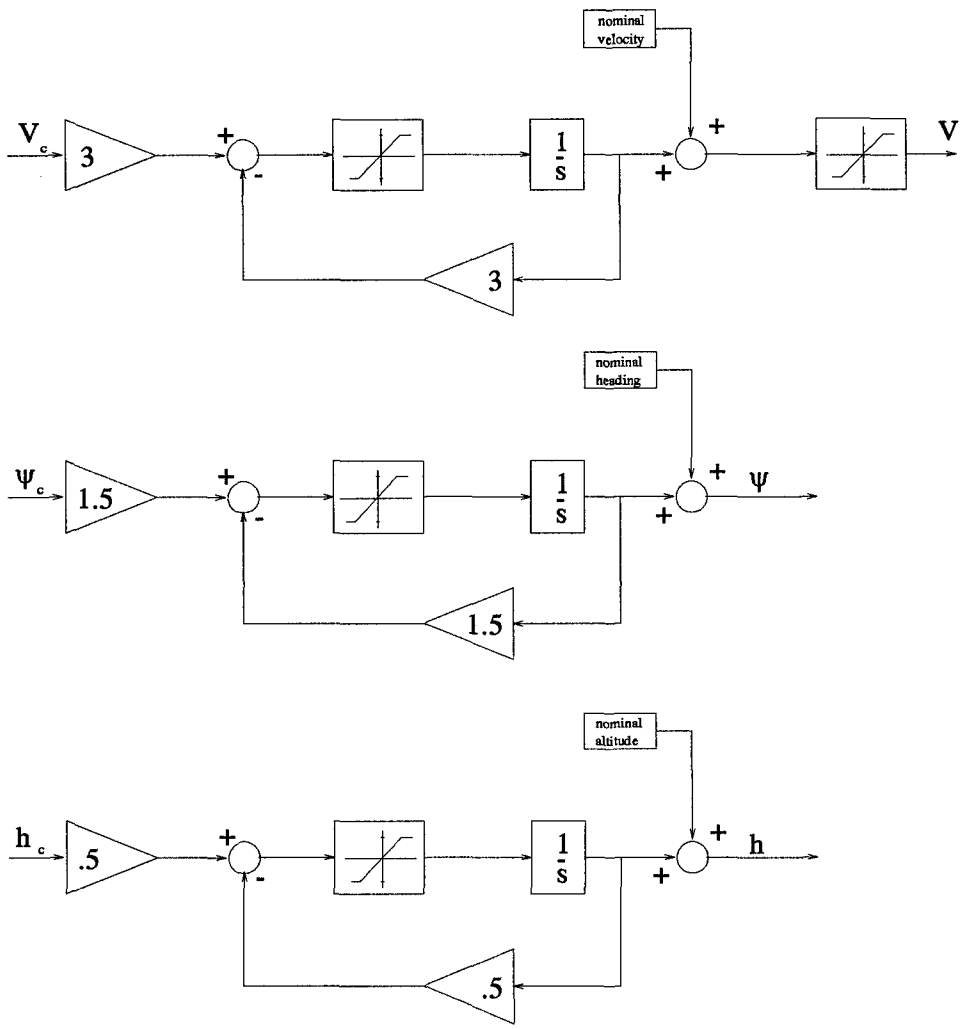

Figure 3.1 First-Order Aircraft Models

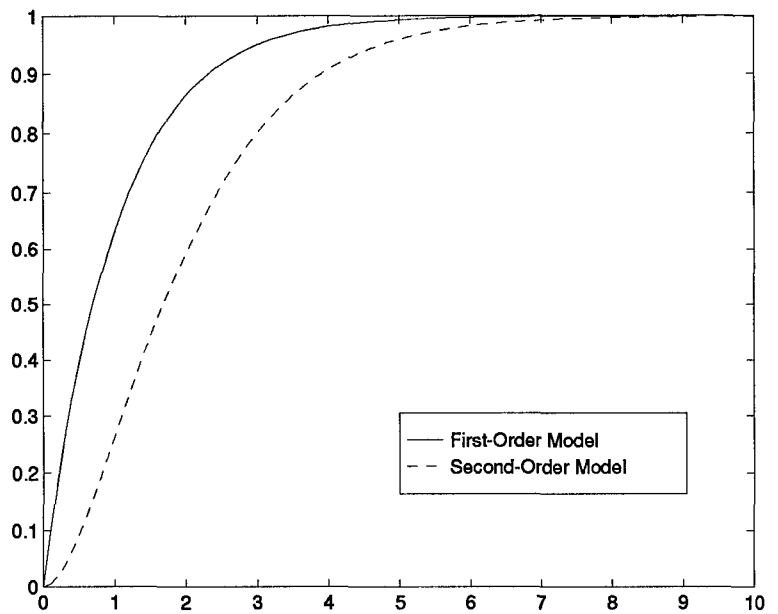

Figure 3.2 Comparison of First and Second-Order Responses

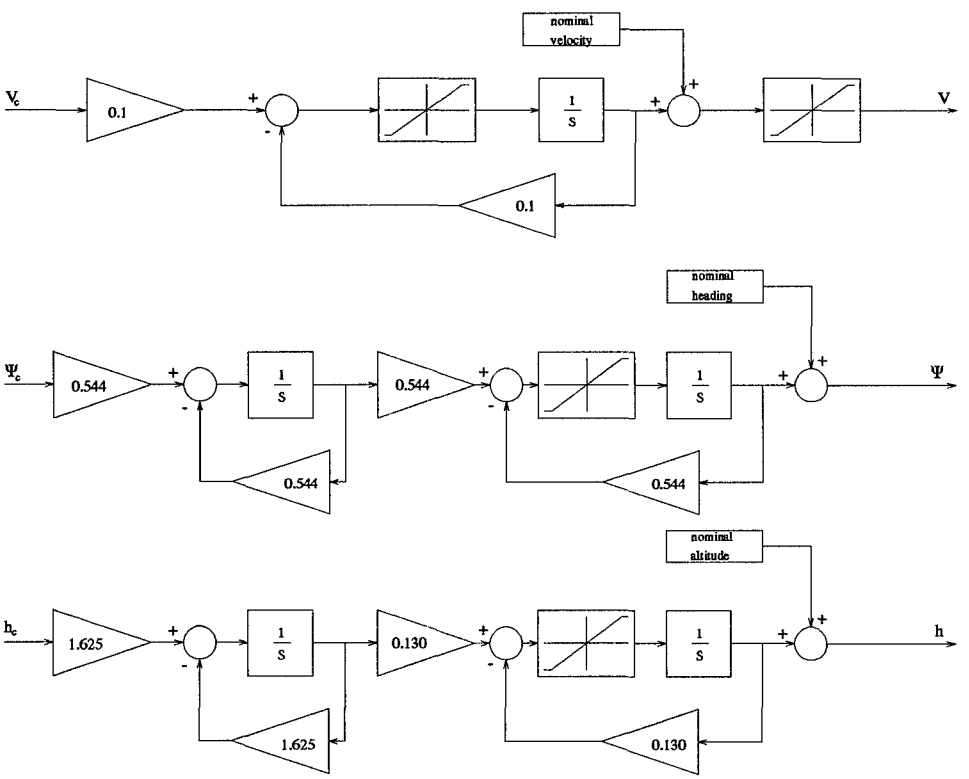

Figure 3.3 Second-Order Aircraft/Autopilot Models

3.2 Formation Coordinate System

The coordinate system used in this thesis is identical to that of Dargan [5], Buzogany [3], and Reyna [14]. The analysis of the system kinematics uses two coordinate frames:

- Inertial base frame
- Rotating reference frame centered on wing aircraft

The base frame is an inertial North-East-Down system. For the purposes of this research, the earth is considered to be flat and inertially fixed. The inertial reference frame and separation distances are shown in Figure 3.4.

The wing aircraft frame is centered on the wing aircraft. The x axis is in the flight direction (i.e., aligned with the velocity vector), the y axis points out the starboard wing, and the z axis points toward the earth. The x and y separation distances are measured in the wing frame (Figure 3.5).

3.3 Kinematic Equations

In order to simulate the kinematics associated with the formation flight control model, kinematic equations must be derived. This has already been done by Dargan [5], Buzogany [3], and Reyna [14]. Reyna's derivation is repeated here to ensure clarity (from [14], pages 3:6-10).

Using the Equation of Coriolis (Chapter II), the velocity of the lead with respect to the wing has been found by Dargan as

$$V_{WL}^{W} = V_{L}^{W} - \omega_{W}^{W} \times R_{WL}^{W} - V_{W}^{W} + \omega_{W}^{W} \times R_{W}^{W} \tag{3.7}$$

where the following convention is followed:

- The superscript indicates the reference frame.
- The subscript indicates the parameter described by the vector or a relation between two parameters.

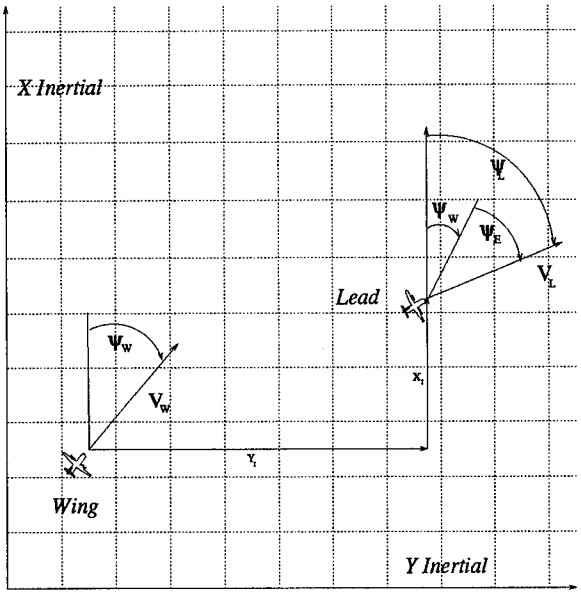

Figure 3.4 Inertial Reference Frame and Separation Distances

For example,

- V_{WL}^{W} = velocity of the lead aircraft with respect to the wing, in the wing's reference frame
- ω_{W}^{W} = angular velocity of the wing aircraft in the wing's reference frame
- R_{WL}^{W} = position of the lead aircraft with respect to the wing in the wing's reference frame
- V_{W}^{W} = inertial velocity of the wing aircraft in its own reference frame
- V_{L}^{W} = inertial velocity of the lead aircraft in the wing's reference frame

The development of the kinematic equations is based on the geometry defined in Figure 3.6. The following relationships are defined:

$$\Psi_E = \Psi_L - \Psi_W \tag{3.8}$$

$$\omega_W^W = \begin{bmatrix} 0 \\ 0 \\ \dot{\Psi}_W \end{bmatrix} \tag{3.9}$$

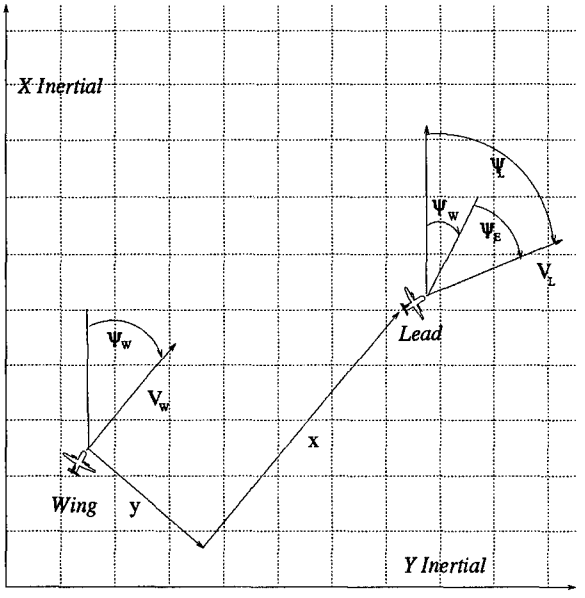

Figure 3.5 Wing's Rotating Reference Frame and Separation Distances

$$R_{WL}^{W} = \begin{bmatrix} x^W \\ y^W \\ z^W \end{bmatrix} \tag{3.10}$$

$$V_{W}^{W} = \begin{bmatrix} V_W \\ 0 \\ 0 \end{bmatrix} \tag{3.11}$$

$$V_{L}^{L} = \begin{bmatrix} V_L \\ 0 \\ 0 \end{bmatrix} \tag{3.12}$$

$$R_{W}^{W} = \begin{bmatrix} 0 \\ 0 \\ 0 \end{bmatrix} \tag{3.13}$$

where,

Ψ_E = heading error

V_L^L = velocity of the lead aircraft in its own reference frame

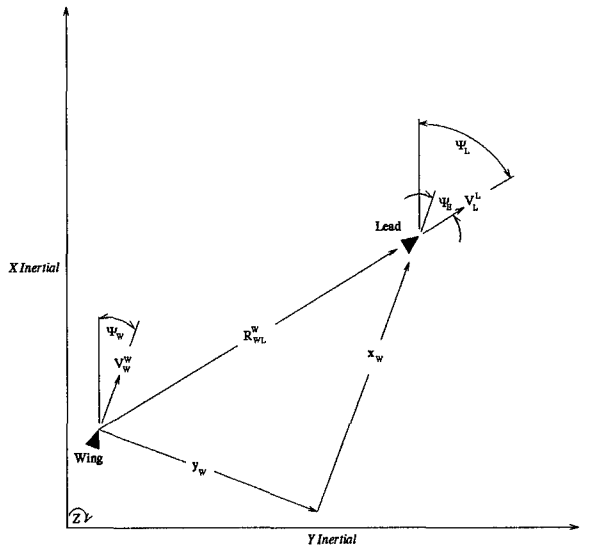

Figure 3.6 Relative Motion Diagram

In order to solve (3.7), V_L^L must be transformed into the wing reference frame. A Direction Cosine Matrix (DCM), developed by Dargan [5], is used to perform the rotation. Dargan found the DCM to be

$$C_L^W = \begin{bmatrix} cos\Psi_E & -sin\Psi_E & 0 \\ sin\Psi_E & cos\Psi_E & 0 \\ 0 & 0 & 1 \end{bmatrix} \tag{3.14}$$

V_L^W is found using by substituting (3.12) and (3.14) into the following equation

$$V_L^W = C_L^W V_L^L = \begin{bmatrix} V_L cos\Psi_E \\ V_L sin\Psi_E \\ 0 \end{bmatrix} \tag{3.15}$$

Substituting (3.9)-(3.11), (3.13), and (3.15) into equation (3.7) yields

$$V_{WL}^W = \begin{bmatrix} V_L cos\Psi_E \\ V_L sin\Psi_E \\ 0 \end{bmatrix} - \begin{bmatrix} 0 \\ 0 \\ \dot{\Psi}_W \end{bmatrix} \times \begin{bmatrix} x^W \\ y^W \\ z^W \end{bmatrix} - \begin{bmatrix} V_W \\ 0 \\ 0 \end{bmatrix} + \begin{bmatrix} 0 \\ 0 \\ \dot{\Psi}_W \end{bmatrix} \times \begin{bmatrix} 0 \\ 0 \\ 0 \end{bmatrix} \tag{3.16}$$

$$V_{WL}^{W} = \begin{bmatrix} V_L cos\Psi_E \\ V_L sin\Psi_E \\ 0 \end{bmatrix} - \begin{bmatrix} -\dot{\Psi}_W y^W \\ \dot{\Psi}_W x^W \\ 0 \end{bmatrix} - \begin{bmatrix} V_W \\ 0 \\ 0 \end{bmatrix} \quad (3.17)$$

Separating (3.17) into scalar components yields

$$\dot{x}^W = V_L cos\Psi_E + \dot{\Psi}_W y^W - V_W \quad (3.18)$$

$$\dot{y}^W = V_L sin\Psi_E - \dot{\Psi}_W x^W \quad (3.19)$$

$$\dot{z}^W = 0 \quad (3.20)$$

Equations (3.18) - (3.20) describe the kinematics of the formation (X and Y separations) in terms of the individual aircraft's heading and velocity. The altitude (Z) separations are non-dynamic and are simply the difference between the aircraft altitudes.

3.4 Simulation Description

The nonlinear simulation is performed using SIMULINK dynamic simulation software included in the Matlab package. SIMULINK provides an intuitive interface as well as a high quality nonlinear differential equation solver. In order to provide an easy to use tool for future research, a modular description of the formation flight control problem is created. The simulation model is illustrated in Figure 3.7. This allows future formation flight control researchers to easily modify the aircraft models or controller.

The formation flight control simulation is composed of two tiers of system inputs. The lower tier consists of commands available to the pilot of the wing aircraft(s). This allows control of separation distances which in turn dictate the formation geometry. The upper tier controls the entire formation's heading, speed and altitude. The upper tier commands are considered to reside onboard the lead aircraft.

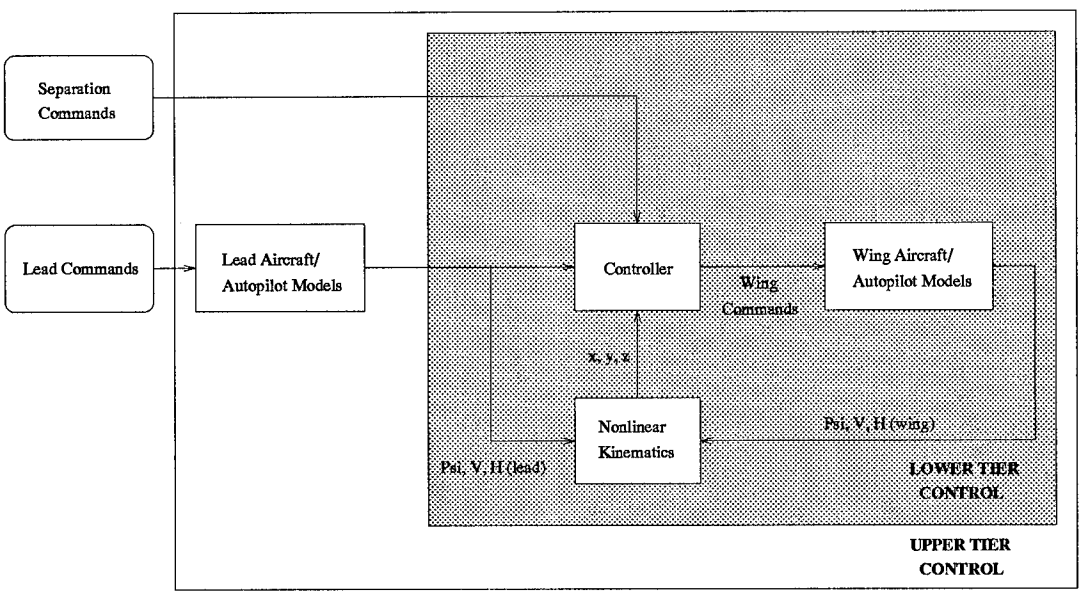

Figure 3.7 Simulation Model

3.5 Simulation Rendering Using Aviator

One of the problems with past AFIT formation flight control research is the difficulty in visualizing three dimensional formation maneuvers. In this thesis, research is devoted to developing an interface which simulates the formation flight control system in Aviator. Aviator is a network based flight simulator developed by Artificial Horizons which runs on the Sun SPARC family of workstations. Aviator provides a visual interface to a virtual world based on the computer network.

To accomplish this objective, a program (ctool) is written in C for the Openlook X-Windows standard which simulates the real time dynamical system. The operator is given control of simulated control panels which would reside on the individual formation aircraft. The lead aircraft autopilot command interface serves to guide the formation using altitude, heading and airspeed commands. The wing aircraft are controlled by commanding X, Y and Z separation distances. The aircraft positions and orientations are computed using difference equations at a sampling rate of 10 hertz. The respective data for all aircraft is transferred into the virtual world of Aviator running on another SPARC station connected via an ethernet connection.

The circular path autopilot designed in Chapter V is also implemented as a real time option in the lead aircraft control panel. During the simulation, the circular path autopilot can be engaged and the radius and velocity parameters controlled. This addition yields insights into real-world implementation of control systems as well as the complexities present in the three-dimensional dynamics of the formation flight control problem.

The program is available via ftp from *flight.wpafb.af.mil.* Contact the system administrator for details.

IV. Formation Hold Autopilot

4.1 Procedure

The design and testing of a new control law for the formation hold autopilot is considered in this chapter. The initial evaluation uses first-order aircraft models. This makes the initial design less complex and allows comparison of the new control law with the previous design developed by Reyna [14]. Next, the controller is designed and tested using second-order models.

The design method is based upon a conventional approach. The nonlinear kinematics and aircraft models are linearized about an equilibrium trim condition. Feedback gains are determined using successive loop closures and root-locus analysis. Gains are chosen to obtain desirable response.

The goal of the design is to achieve robust formation maintenance in the presence of full system nonlinearities. A minimum overshoot is desired.

4.2 Linearization of Kinematic Equations

The equations of motions, developed in Chapter III are repeated below for clarity.

$$\dot{X} = V_L cos(\Psi_L - \Psi_W) + \dot{\Psi}_W Y - V_W \tag{4.1}$$

$$\dot{Y} = V_L sin(\Psi_L - \Psi_W) - \dot{\Psi}_W X \tag{4.2}$$

The equilibrium trim conditions for this linearization are

$$X = \overline{X} + x$$

$$Y = \overline{Y} + y$$

$$V_L = \overline{V} + v_L$$

$$V_W = \overline{V} + v_W$$

$$\Psi_L = \overline{\Psi} + \psi_L$$
$$\Psi_W = \overline{\Psi} + \psi_W$$

Substituting the above trim conditions into equations (4.1) and (4.2), using the method of small perturbations, and eliminating the higher order terms yields the following linearized kinematics, which are used in the linear analysis.

$$\dot{x} = v_L - v_W + \dot{\psi}_W \overline{Y} \tag{4.3}$$
$$\dot{y} = \overline{V}(\psi_L - \psi_W) - \dot{\psi}_W \overline{X} \tag{4.4}$$

4.3 Development (First-order models)

The initial analysis uses first-order aircraft/autopilot models. The linearized kinematics (4.1), (4.2) and first-order linear aircraft/autopilot models are combined into the following state space form

$$\frac{d}{dt}\begin{bmatrix} x \\ v_W \\ y \\ \psi_W \\ v_L \\ \psi_L \end{bmatrix} = A\begin{bmatrix} x \\ v_W \\ y \\ \psi_W \\ v_L \\ \psi_L \end{bmatrix} + B\begin{bmatrix} v_{wc} \\ \psi_{wc} \end{bmatrix} + \Gamma\begin{bmatrix} v_{lc} \\ \psi_{lc} \end{bmatrix} \tag{4.5}$$

where the A, B, and Γ matrices are, respectively,

$$A = \begin{bmatrix} 0 & -1 & 0 & -\frac{\overline{Y}}{\tau_\psi} & 1 & 0 \\ 0 & -\frac{1}{\tau_V} & 0 & 0 & 0 & 0 \\ 0 & 0 & 0 & \frac{\overline{X}}{\tau_\psi} - \overline{V} & 0 & \overline{V} \\ 0 & 0 & 0 & -\frac{1}{\tau_\psi} & 0 & 0 \\ 0 & 0 & 0 & 0 & -\frac{1}{\tau_V} & 0 \\ 0 & 0 & 0 & 0 & 0 & -\frac{1}{\tau_\psi} \end{bmatrix}$$

$$B = \begin{bmatrix} 0 & \frac{\overline{X}}{\tau_\psi} \\ \frac{1}{\tau_V} & 0 \\ 0 & -\frac{\overline{X}}{\tau_\psi} \\ 0 & \frac{1}{\tau_\psi} \\ 0 & 0 \\ 0 & 0 \end{bmatrix}$$

$$\Gamma = \begin{bmatrix} 0 & 0 \\ 0 & 0 \\ 0 & 0 \\ 0 & 0 \\ \frac{1}{\tau_V} & 0 \\ 0 & \frac{1}{\tau_\psi} \end{bmatrix}$$

4.3.1 Control Laws. Two control laws are evaluated in this section. The proportional plus integral control law developed by Reyna [14] is:

$$v_{wc} = k_{xp} e_x + k_{xi} \int_0^t e_x \, dt \tag{4.6}$$

$$\psi_{wc} = k_{yp} e_y + k_{yi} \int_0^t e_y \, dt \tag{4.7}$$

where,

$$
\begin{aligned}
e_x &= k_x x + k_v(v_L - v_W) \\
e_y &= k_y y + k_\psi(\psi_L - \psi_W)
\end{aligned}
$$

The new control law proposed in this thesis eliminates the "mixer" constants k_v and k_ψ and adds direct state feedback of ψ_L and v_L. As revealed by the following analysis, the need for integral action is eliminated. The control law used is shown in equations (4.8) and (4.9).

$$v_{wc} = v_L + K_{xp}x \tag{4.8}$$

$$\psi_{wc} = \psi_L + K_{yp}y \tag{4.9}$$

4.3.2 Determination of Controller Gains. The controller gains K_{xp} and K_{yp} are determined using successive loop closures. Root-locus analysis is used to determine gains which give the desired response with the least amount of overshoot ($\zeta \cong 1$). This ensures that maneuvers are accomplished in "minimum" time without excessive excitation of the aircraft. Due to the rate limit nonlinearities in the system, it is inherently beneficial to choose relatively low controller gains. This helps to avoid forcing the system against its rate limits and resulting in uncontrollability. The controller block diagram is shown in Figure 4.1.

The controller is designed about the nominal left diamond formation ($\overline{X} = \overline{Y} = 500$ ft) at a nominal velocity ($\overline{V}$) of $350\frac{ft}{sec}$. The procedure begins by closing the unity feedback ψ_L and v_L loops. Next, the root-locus is examined for the $\frac{Y(s)}{\Psi_{cmd}(s)}$ transfer function obtained from the above A matrix. The root-locus is shown in Figure 4.2.

The resulting gain, determined to produce a critically damped response, is $K_{yp} = 6.14 \times 10^{-2}$. The ψ_{cmd} loop is now closed and the $\frac{X(s)}{V_{cmd}(s)}$ is determined. The resulting root-locus is shown in Figure 4.3. Again, a gain of $K_{xp} = 0.75$ is chosen, yielding a critically damped response.

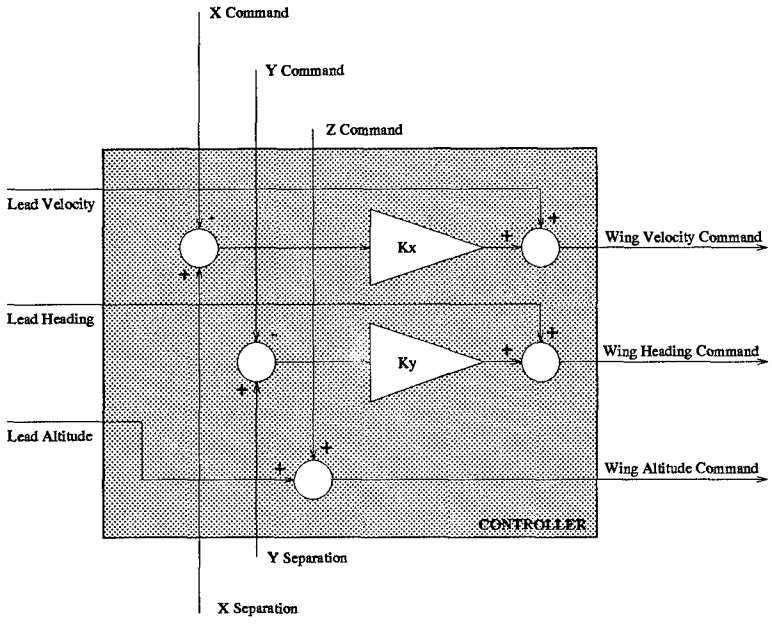

Figure 4.1 Proportional Formation Flight Controller Block Diagram

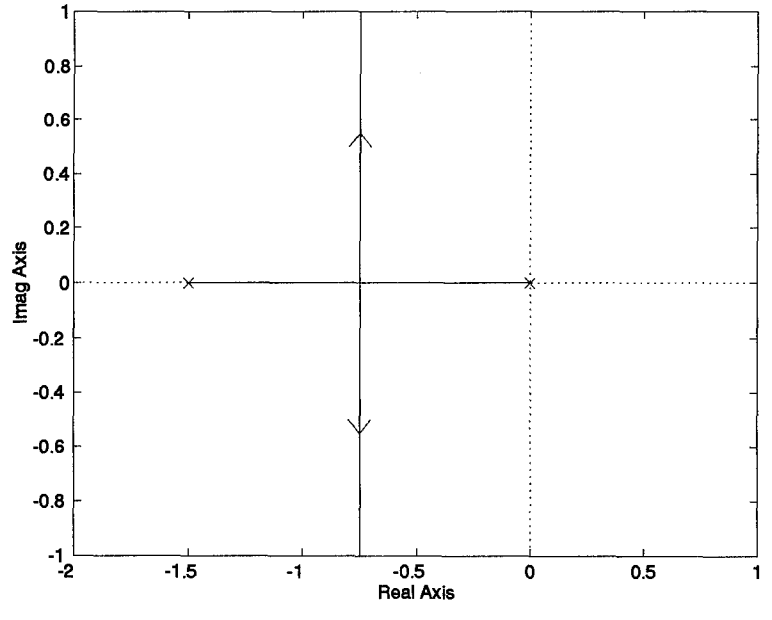

Figure 4.2 Proportional Inner Loop (Y) Feedback Root-Locus

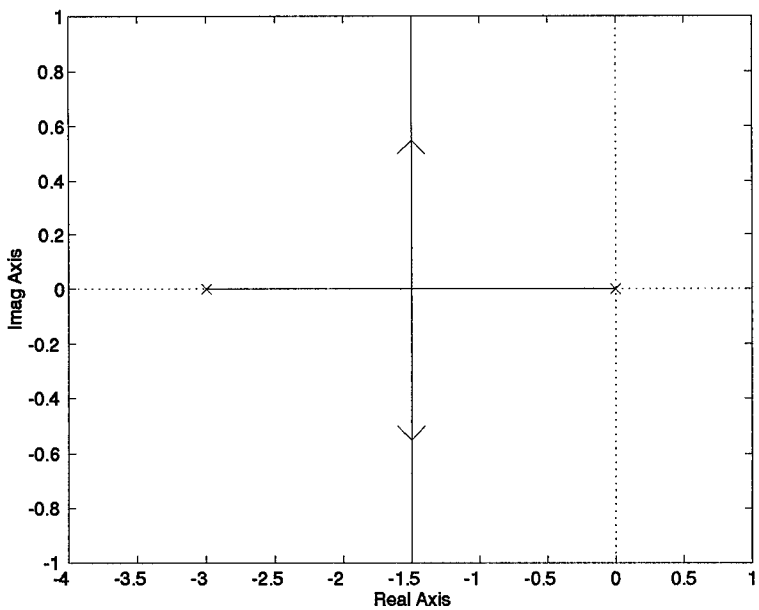

Figure 4.3 Proportional Outer Loop (X) Feedback Root-Locus

4.4 Evaluation of First-Order Controllers

Evaluation of the control system proceeds in the following manner. The initial evaluation focuses on the response of the linear system. Next, the controller is tested using the fully nonlinear simulation. The results for the new control law are compared to the previous design by Reyna [14].

The controller tests consist of two maneuvers:

1. $+30^o$ heading change maneuver
2. $+25\frac{ft}{sec}$ velocity increase

A 500 ft diamond formation is used in each test case. This ensures that a level of X-Y coupling is included. Note that the maneuvers are technically two dimensional, with no altitude excursions. Three dimensional maneuvers are addressed in Chapter V.

The responses of the linearized system to a 30 degree right turn and a $25\frac{ft}{sec}$ leader velocity increase are shown in Figures 4.4 and 4.5. The responses are both overdamped and successfully compensate for the disturbance in the lead channel. This confirms the validity of the loop closure technique in rejecting disturbances.

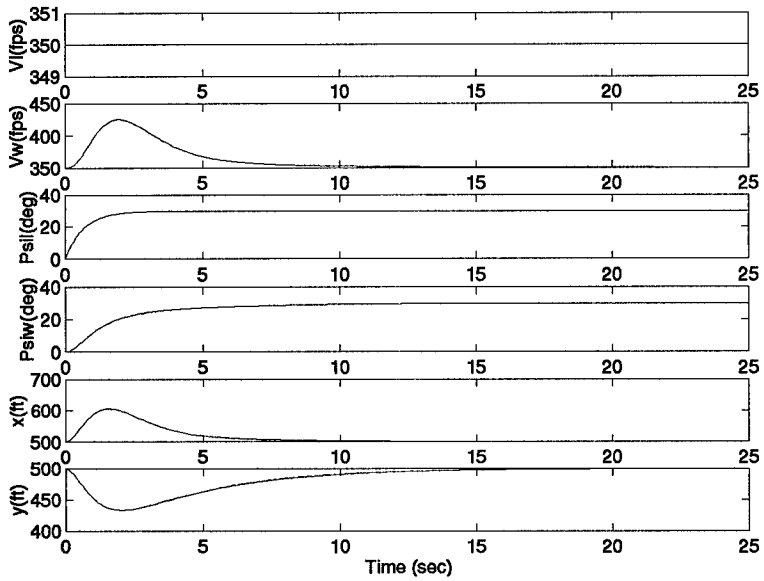

Figure 4.4 C-130A: Diamond Formation, Linear Response, 30^o Heading Change

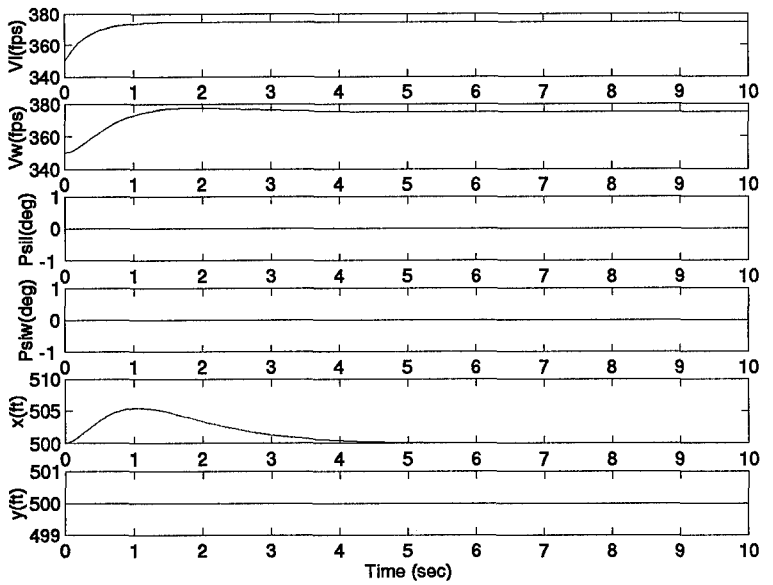

Figure 4.5 C-130A: Diamond Formation, Linear Response, $25\frac{ft}{sec}$ Velocity Change

The addition of system nonlinearities adds a slight complication. Figures 4.6 and 4.7 show the nonlinear simulation results for the heading and velocity change maneuvers, respectively. Note that the heading change causes an overshoot in the X channel. Figure 4.6 clearly shows that this is a direct result of the wing velocity rate limit. In order to obtain a better response, the X channel proportional gain, K_{xp}, is reduced to $K_{xp} = 0.4$. Repeating the heading change simulation with the new gain produces a much more desirable response and is shown in Figure 4.8.

Comparison of the new control scheme with that of Reyna [14] yields interesting results (see Figures 4.9 and 4.10). The heading change response shows a fundamental difference between the two controller designs. While the new controller was designed to achieve an overdamped response, Reyna's was not. Both the X and Y separations exhibit overshoot in Reyna's controller which causes their settling time to be longer than that of the new controller. The velocity increase response shows the differences in the X channel even more clearly. Note that the new controller settles much more quickly than Reyna's.

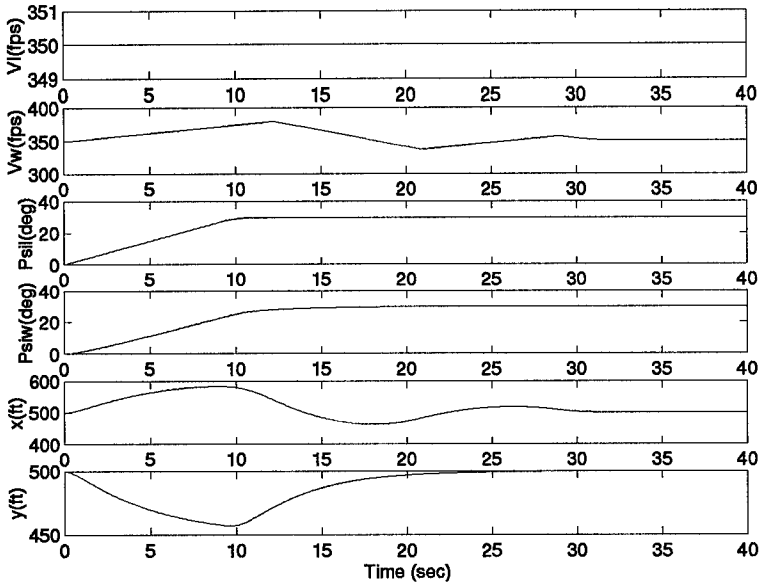

Figure 4.6 C-130A: Diamond Formation, Nonlinear Response, 30 Degree Heading Change

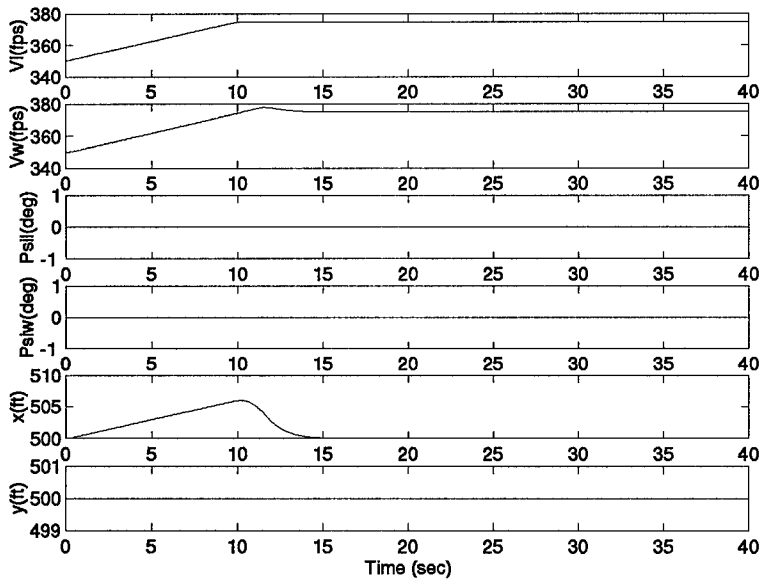

Figure 4.7 C-130A: Diamond Formation, Nonlinear Response, $25\frac{ft}{sec}$ Velocity Increase

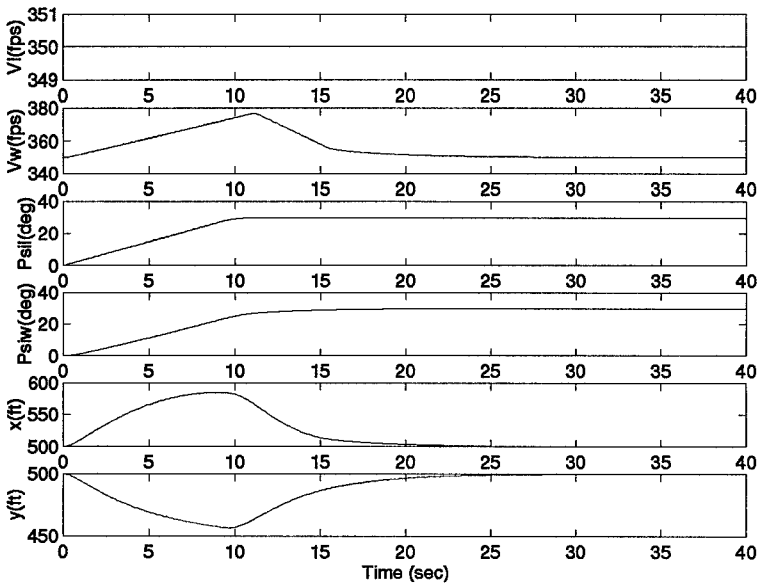

Figure 4.8 C-130A: Diamond Formation, Nonlinear Response, 30 Degree Heading Change
Revised X-Channel Gain

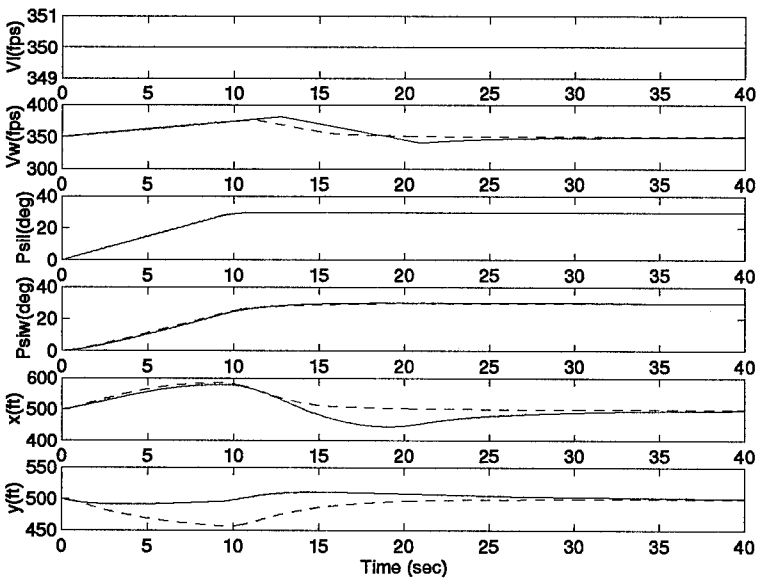

Figure 4.9 C-130A: Diamond Formation, Nonlinear Response, 30 Degree Heading Change
Reyna: solid; New: dashed

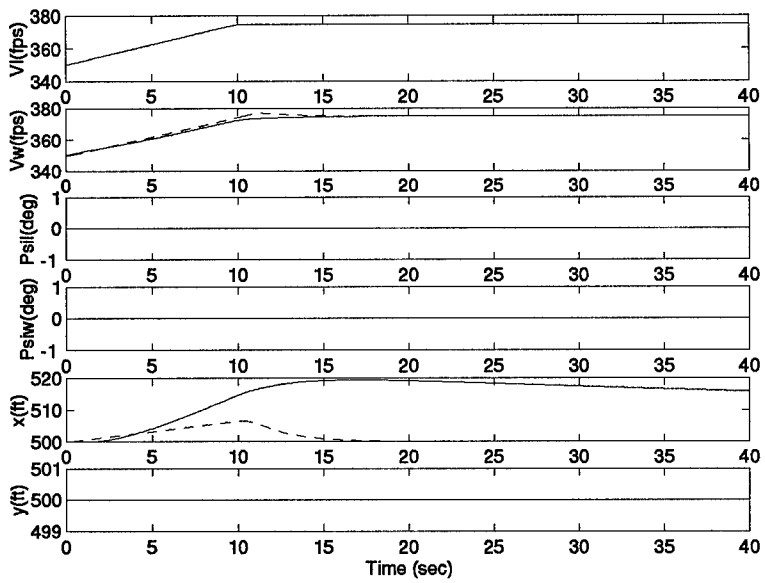

Figure 4.10 C-130A: Diamond Formation, Nonlinear Response, $25\frac{ft}{sec}$ Velocity Change
Reyna: solid; New: dashed

4.5 Development (Second-Order Models)

The controller is now redesigned incorporating second-order models developed by Buzogany [3]. The same loop closure design technique is used as in Section 4.3.2. The design is then analyzed using identical test conditions. Comparisons are made between the performance of the linearized models and the nonlinear simulation. Comparisons are not made with Reyna's controller since his design was based upon first-order models.

The linearized kinematics and second-order aircraft models are now combined into state space form (Equation 4.10).

$$\frac{d}{dt}\begin{bmatrix} x \\ v_W \\ y \\ \psi_W \\ \dot{\psi}_W \\ v_L \\ \psi_L \\ \dot{\psi}_L \end{bmatrix} = A\begin{bmatrix} x \\ v_W \\ y \\ \psi_W \\ \dot{\psi}_W \\ v_L \\ \psi_L \\ \dot{\psi}_L \end{bmatrix} + B\begin{bmatrix} v_{wc} \\ \psi_{wc} \end{bmatrix} + \Gamma\begin{bmatrix} v_{lc} \\ \psi_{lc} \end{bmatrix} \tag{4.10}$$

where the A,B, and Γ matrices are, respectively

$$A = \begin{bmatrix} 0 & -1 & 0 & 0 & \overline{Y} & 1 & 0 & 0 \\ 0 & -\frac{1}{\tau_{v2}} & 0 & 0 & 0 & 0 & 0 & 0 \\ 0 & 0 & 0 & -\overline{V} & -\overline{X} & 0 & \overline{V} & 0 \\ 0 & 0 & 0 & 0 & 1 & 0 & 0 & 0 \\ 0 & 0 & 0 & -\frac{1}{\tau_{\psi_a}\tau_{\psi_b}} & -\left(\frac{1}{\tau_{\psi_a}}+\frac{1}{\tau_{\psi_b}}\right) & 0 & 0 & 0 \\ 0 & 0 & 0 & 0 & 0 & -\frac{1}{\tau_{v2}} & 0 & 0 \\ 0 & 0 & 0 & 0 & 0 & 0 & 0 & 1 \\ 0 & 0 & 0 & 0 & 0 & 0 & -\frac{1}{\tau_{\psi_a}\tau_{\psi_b}} & -\left(\frac{1}{\tau_{\psi_a}}+\frac{1}{\tau_{\psi_b}}\right) \end{bmatrix}$$

$$B = \begin{bmatrix} 0 & 0 \\ \frac{1}{\tau_{v2}} & 0 \\ 0 & 0 \\ 0 & 0 \\ 0 & \frac{1}{\tau_{\psi a}\tau_{\psi b}} \\ 0 & 0 \\ 0 & 0 \\ 0 & 0 \end{bmatrix}$$

$$\Gamma = \begin{bmatrix} 0 & 0 \\ 0 & 0 \\ 0 & 0 \\ 0 & 0 \\ 0 & 0 \\ \frac{1}{\tau_{v2}} & 0 \\ 0 & 0 \\ 0 & \frac{1}{\tau_{\psi a}\tau_{\psi b}} \end{bmatrix}$$

4.6 Determination of Controller Gains

The controller gains are determined in an identical fashion as with the first-order models. Figures 4.11 and 4.12 illustrate the root locus for the Y and X loop closures, respectively. The gains are determined to be $K_{yp} = 1.87 \times 10^{-2}$ and $K_{xp} = 2.5 \times 10^{-2}$. With the control law in place, the system is now evaluated.

4.7 Evaluation of Controller with Second-Order Models

The performance of the formation hold autopilot controller is tested using the same maneuvers as in Section 4.4. Figures 4.13 and 4.14 show the responses using the linearized equations. The wing aircraft remains in formation without excessive excursions in the X and Y channel. In fact, the response has no signs of overshoot, which is quite desirable.

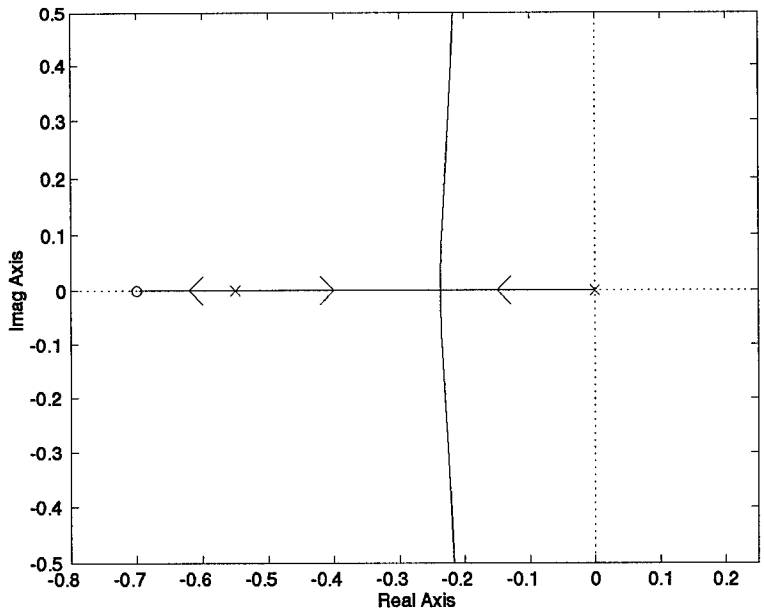

Figure 4.11 Proportional Inner Loop (Y) Feedback Root-Locus *Second-Order models*

The system is now simulated using fully nonlinear kinematics and rate-limit nonlinearities. The performance is compared to the linear prediction for identical maneuvers. Figures 4.15 and 4.16 illustrate the simulation results. The effects of the rate-limit nonlinearities are clearly indicated by the slower heading and velocity response. Although the performance of the controller is slightly reduced, it certainly meets the previously discussed criterion for success.

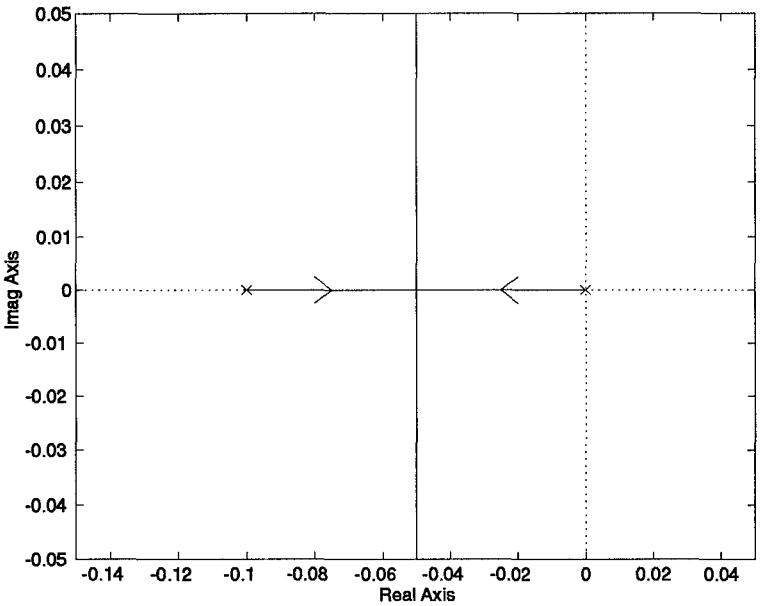

Figure 4.12 Proportional Outer Loop (X) Feedback Root-Locus *Second-Order Models*

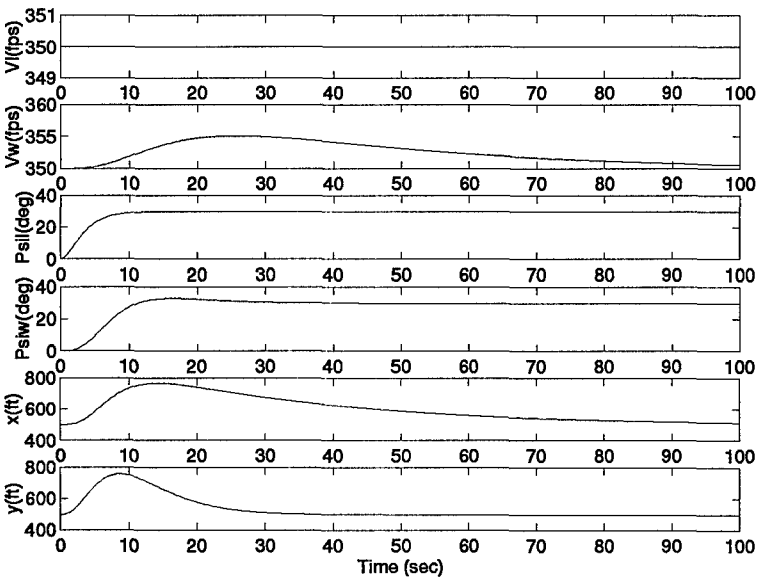

Figure 4.13 C-130A: Diamond Formation, Linear Response, 30 Degree Heading Change *Second-Order Models*

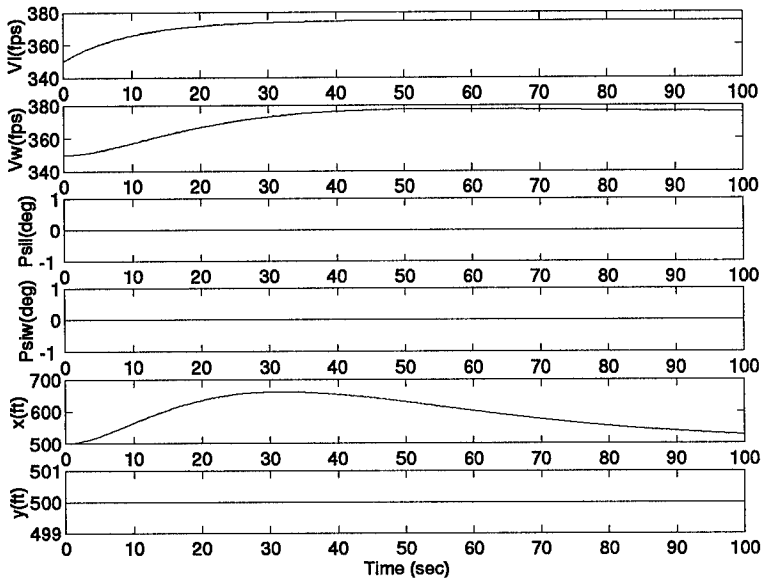

Figure 4.14 C-130A: Diamond Formation, Linear Response, $25\frac{ft}{sec}$ Velocity Change *Second-Order Models*

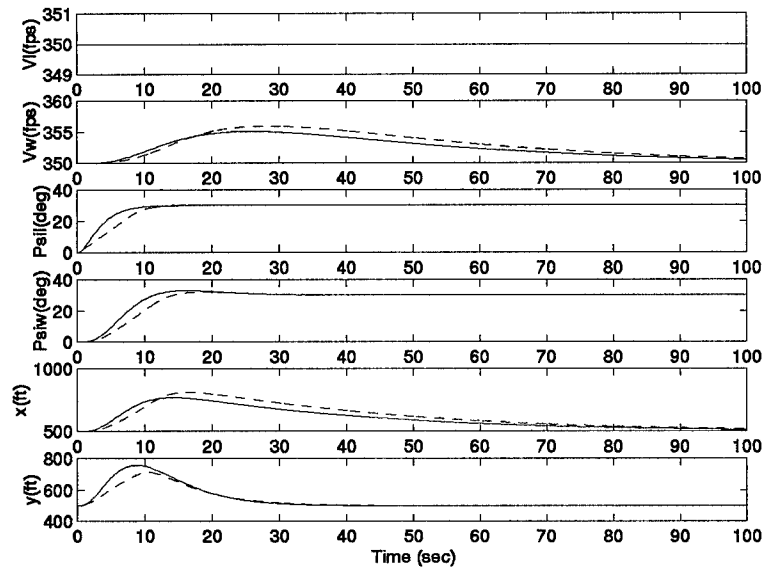

Figure 4.15 Heading Change Comparison. Linear: Solid, Nonlinear: Dashed

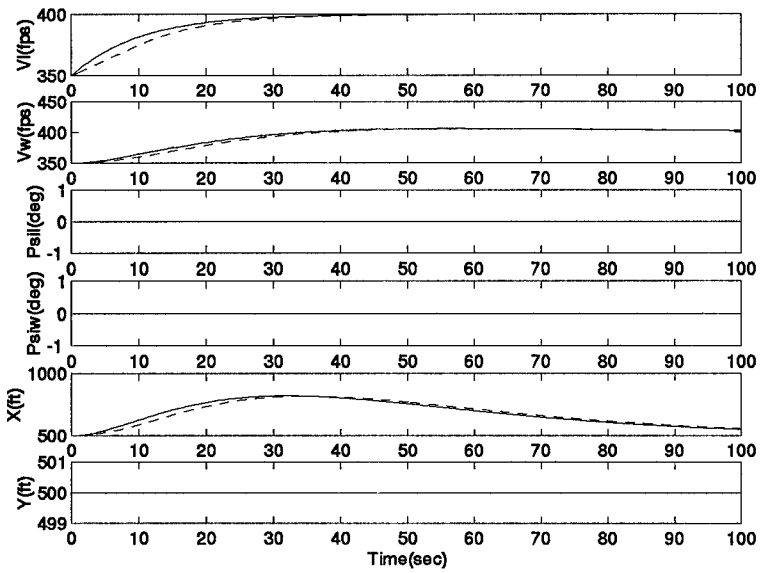

Figure 4.16 Velocity Change Comparison. Linear: Solid, Nonlinear: Dashed

4.8 Formation Geometry Change Maneuvers

In addition to the previous upper tier formation maneuvers, the formation flight controller is tested with respect to lower tier commands. From Chapter III, the lower tier consists of changes in formation geometry. The simulation is performed using second-order aircraft/autopilot models using the same controller as described in Sections 4.5 and 4.6. The Lissajous figure is introduced in this section to allow easy interpretation of the results. This figure plots the X and Y separations throughout the maneuver in the wing aircraft X-Y frame.

The following maneuvers are examined:

- Diamond to trail maneuver
- Left diamond to right diamond formation *during* a 30 degree left turn (Figure 4.17)

The diamond to trail maneuver simulation results are shown in Figures 4.18 and 4.19. The left turn transition maneuver simulation results are shown in Figures 4.20 and 4.21.

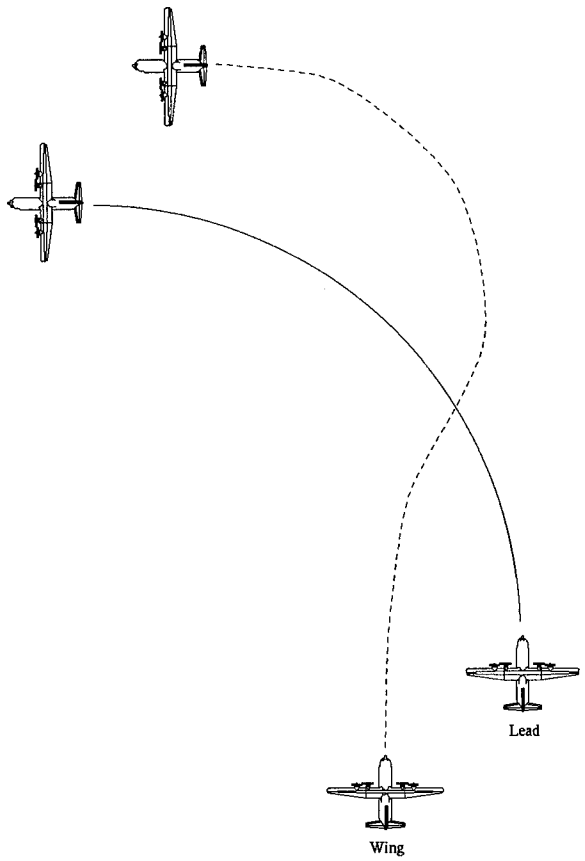

Figure 4.17 Left Turn with Formation Translation

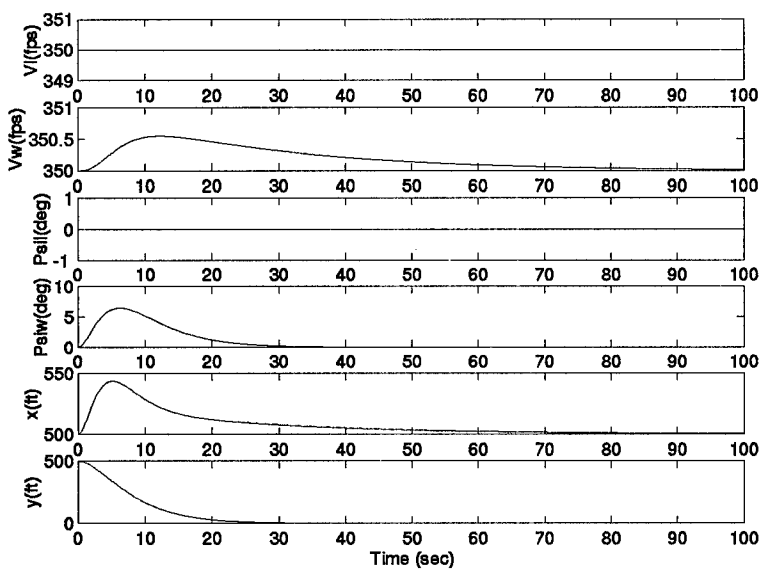

Figure 4.18 Left Diamond to Trail Formation Change

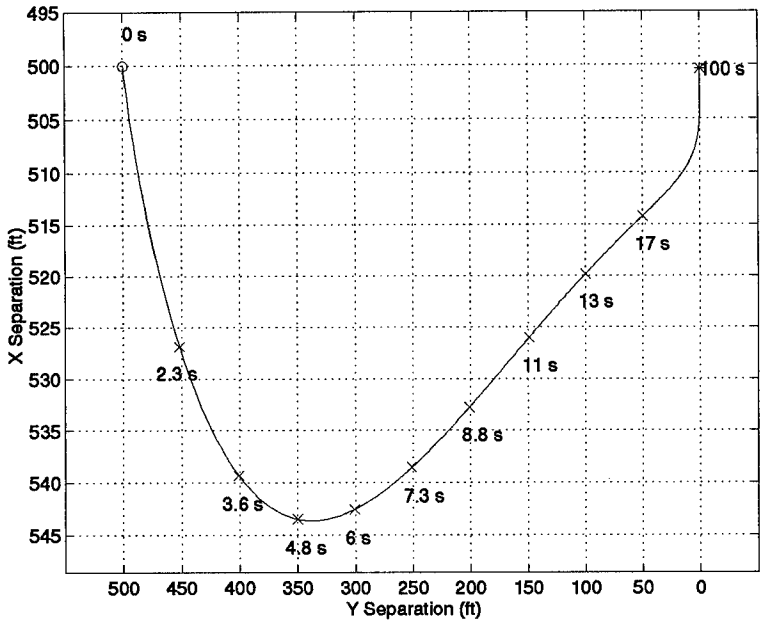

Figure 4.19 Left Diamond to Trail Formation Change Lissajous Figure

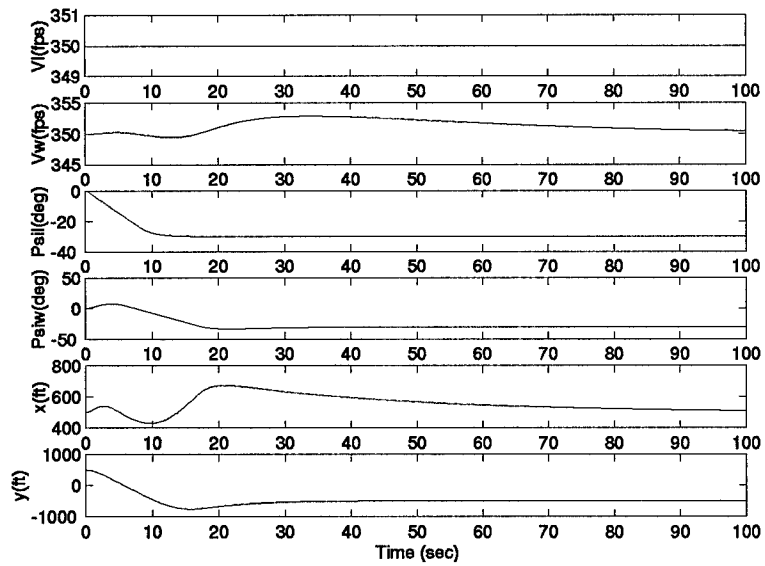

Figure 4.20 Left Diamond to Right Diamond with a 30 degree Left Turn

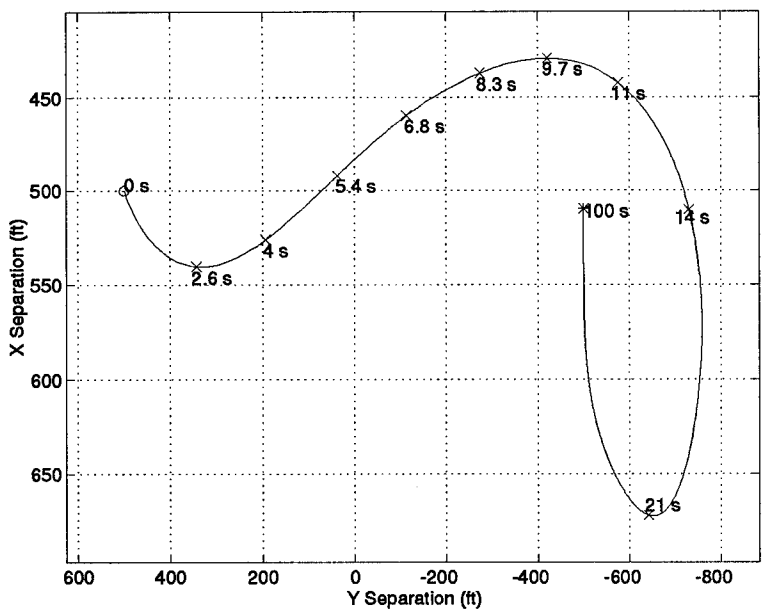

Figure 4.21 Left Diamond to Right Diamond with a 30 degree Left Turn Lissajous Figure

Parameter	Value
K_{xp}	2.50×10^{-2}
K_{yp}	1.87×10^{-2}

Table 4.1 Formation Flight Controller Gains

4.9 Controller Summary

The formation flight control laws are repeated below for clarity. Note that true states, *not* perturbations are used and represent the controller designed using second-order models. The controller gains are listed in Table 4.1.

$$V_{wc} = V_L + K_{xp}(X - X_{cmd}) \tag{4.11}$$

$$\Psi_{wc} = \Psi_L + K_{wp}(Y - Y_{cmd}) \tag{4.12}$$

4.10 Conclusion

The control law proposed in this chapter clearly demonstrates a performance improvement over the control law used in previous theses. Simulation results show that the new control law exhibits not only a shorter settling time but also has a higher damping ratio (Figs. 4.9 and 4.10). As discussed previously, an overdamped response reduces the wing aircraft excursions.

Another natural comparison arises when the second-order aircraft/autopilot models are utilized. The second-order aircraft/autopilot models differ from the first-order models in two distinct ways. First, the second-order models begin with an initial slope of zero. This is similar to the "onset delay" found in any real system. The second noteworthy difference is the conservativeness of the models. The second-order models exhibit slower responses, making them more conservative. While in the linear simulation this characteristic causes performance to suffer, when the rate-limit nonlinearities are included the response is much closer to that predicted by the linear case. This illustrates an important concept when designing controllers for nonlinear systems - small increases in the fidelity of the model can

enable the designer to design the linear system with less likelihood of unpleasant contact with hard nonlinearities.

Further conclusions are drawn from the "lower tier" commands. These formation changes push the controller harder because they are given as step commands whereas "upper tier" response is the result of disturbances *of a second-order nature.* Regardless, the response to the formation geometry commands meets desired specifications. The inside to outside diamond and left turn combination illustrates an example of maneuvers performed by real pilots to reduce energy excursions. The energy excursion minimization problem is discussed further in the next chapter.

V. Energy Tracking

5.1 Introduction

In previous research by Rohs [16] and Dargan [5], a two dimensional formation flight control system was designed. When evaluated, it was determined that during heading change maneuvers, the wing aircraft was forced to cycle throttle settings in order to maintain formation. These throttle variations caused an increase in fuel usage and inefficiency. This inherent limitation of two-dimensional maneuvers was addressed by Buzogany [3]. An "Energy Conserving" controller was developed which eliminated the ability of the wing aircraft to change specific energy levels. The resulting response was indeed efficient, but did not allow the wing aircraft to track the energy changes of the leader. To solve this problem, Reyna [14] developed an "Energy Minimizing" controller. The controller reduced energy excursions while enabling the wing aircraft to maintain formation. In this chapter, a controller is designed which minimizes unnecessary energy fluctuations in the wing aircraft while retaining identical formation response as in the planar design (Chapter IV).

This chapter is organized as follows. Section 5.2 begins by developing the energy conservation problem. Next, the energy conserving controller is designed in Section 5.2.1. Finally, the controller is evaluated using nonlinear simulations and the results are discussed.

5.2 Energy Conservation Problem

A discussion of energy conservation focuses on the changes in the energy state of the wing aircraft during formation maneuvers. Thus, the total specific energy of the wing aircraft is

$$E_W = \frac{1}{2}V_W^2 + gH_W \tag{5.1}$$

where g = gravitational acceleration and H_W = wing aircraft altitude. Differentiating equation (5.1) yields

$$\dot{E}_W = V_W\dot{V}_W + g\dot{H}_W \tag{5.2}$$

In the constant altitude (planar) maneuvers of the previous sections, the energy rate is defined by

$$\dot{E}_W = V_W \frac{T - D}{m} \tag{5.3}$$

where T = aircraft thrust, D = aircraft drag, and m = aircraft mass. It is clear that when cycling aircraft thrust, throttle variations cause changes in the energy state, thus decreasing efficiency. Hence, one must seek to reduce throttle cycling by reducing specific energy swings.

5.2.1 Controller Derivation. From equation (5.1), it is clear that the energy level of the wing aircraft is exclusively determined by velocity (true speed) and altitude. The velocity command input is already being utilized to maintain the formation. Thus, altitude must be controlled to minimize specific energy swings. Fortunately, the altitude aircraft/autopilot states are completely decoupled from the formation hold autopilot model, conveniently allowing direct control of the aircraft specific energy without altering the formation hold autopilot response.

At this point, it is tempting to apply control inputs to regulate the wing aircraft energy level to zero. This is an energy conserving technique and is a viable option if formation heading changes are exclusively considered. This concept is unsuitable if the leader chooses to change the energy level of the formation. In order to reduce energy swings and still maintain formation, the wing altitude must be manipulated such that the lead aircraft energy level is tracked. Thus, it is stipulated that

$$E_W = E_L \tag{5.4}$$

i.e.,

$$\frac{1}{2}V_W^2 + gH_W = \frac{1}{2}V_L^2 + gH_L \tag{5.5}$$

Solving eq. (5.5) for H_W yields

$$H_W = H_L + \frac{1}{2g}\left(V_L^2 - V_W^2\right) \tag{5.6}$$

Differentiating equation (5.6) twice,

$$\ddot{H}_W = \ddot{H}_L + \frac{1}{g}\left(\dot{V}_L^2 + V_L\ddot{V}_L - \dot{V}_W^2 - V_W\ddot{V}_W\right) \tag{5.7}$$

The aircraft/altitude-hold autopilot model as defined by Buzogany [3] is as follows,

$$\ddot{H} = -\frac{1}{\tau_{ha}+\tau_{hb}}\dot{H} - \frac{1}{\tau_{ha}\tau_{hb}}H + \frac{1}{\tau_{ha}\tau_{hb}}H_{cmd} \tag{5.8}$$

where,

$$\begin{aligned} \tau_{ha} &= 0.6154s^{-1} \\ \tau_{hb} &= 7.6923s^{-1} \end{aligned}$$

Substituting (5.8) into (5.7) and solving for the wing altitude command (H_{wc}) yields the optimal control law

$$H_{wc} = H_W + \frac{\tau_{ha}\tau_{hb}}{\tau_{ha}+\tau_{hb}}\dot{H}_W + \frac{\tau_{ha}\tau_{hb}}{g}\left(\dot{V}_L^2 + V_L\ddot{V}_L - \dot{V}_W^2 - V_W\ddot{V}_W\right) \tag{5.9}$$

Unfortunately, this optimal control law requires access to unobservable states. A suboptimal solution is proposed which ensures that an energy tracking path is *commanded* by the controller. Reevaluating equation (5.5) using wing commands yields,

$$\frac{1}{2}V_L^2 + gH_L = \frac{1}{2}V_{wc}^2 + gH_{wc} \tag{5.10}$$

$$H_{wc} = H_L + \frac{1}{2g}\left(V_L^2 - V_{wc}^2\right) \tag{5.11}$$

It is interesting to note the similarity between the velocity command and the new altitude command (5.11). Each consist of a base command which tracks the energy of the leader (V_L, H_L) and an energy conserving command to minimize energy swings. This is an intuitively satisfying state of affairs.

It is important to note that the new altitude control scheme is not completely rigorous as it fails to include the system dynamics. This is due to two main reasons:

- The energy state is nonlinear in nature.
- The aircraft/autopilot models are not considered "truth" models and are subject to variations in reality.

This allows a relatively simple controller design which is effective under a range of variations in the nonlinear plant.

5.2.2 Performance Metric. In order to properly analyze the results, a performance metric is needed. The integral of absolute error (IAE) type performance index [7:pp 548], P_{IAE}, is introduced

$$P_{IAE} = \int |\dot{E}_W(t)|\, dt \tag{5.12}$$

$P_{IAE} = 0$ corresponds to perfect energy conservation. Larger P_{IAE} values indicate greater energy excursions.

5.3 Energy Tracking Controller Analysis

The controller testing is divided into two types of maneuvers: static energy maneuvers and dynamic energy maneuvers. Static energy maneuvers consist of heading and formation geometry changes. Dynamic energy maneuvers include changes in lead altitude or speed.

The controller response for a 30 degree heading change is simulated (Figure 5.1). The solid line corresponds to the planar controller while the dashed line represents the response with the energy tracking controller. The wing specific energy perturbations are decreased by an order of magnitude when the energy tracking controller is implemented. The per-

formance index function comparing the cumulative energy variations helps to clearly show the advantages of the energy tracking controller (Figure 5.2).

A 10 fps lead velocity increase simulation demonstrates the controller's ability to track energy changes (Figure 5.3). Note that the energy tracking controller utilizes a decrease in altitude initially to reduce the rate of energy perturbation. This results in improved performance as shown in Figure 5.4.

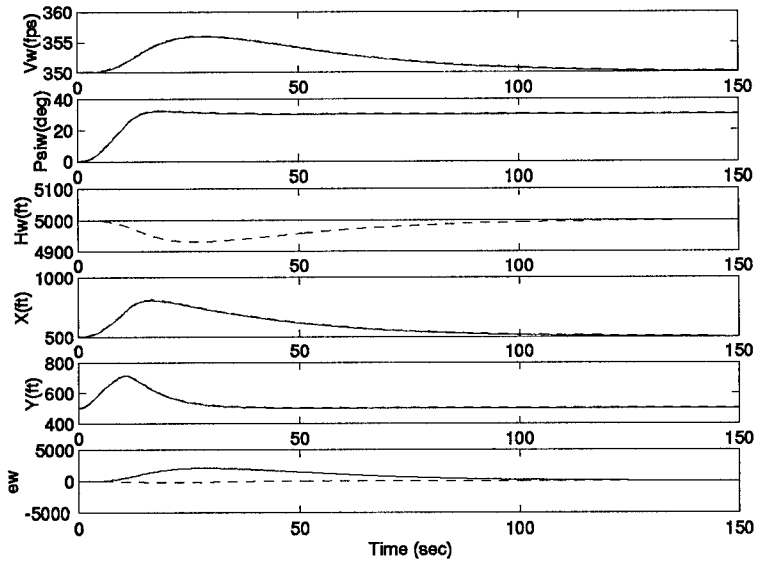

Figure 5.1 Comparison of Planar (Solid) and Energy Tracking Controller (dashed) *(30 Degree Heading Change)*

Finally, to illustrate the robustness of the controller, a combination maneuver is investigated. The lead aircraft simultaneously initiates a 30 degree heading change, a 100 foot altitude decrease and a 15 fps velocity increase (Figure 5.5). The resulting increases in efficiency clearly illustrate the value of the energy tracking formation flight controller (Figure 5.6).

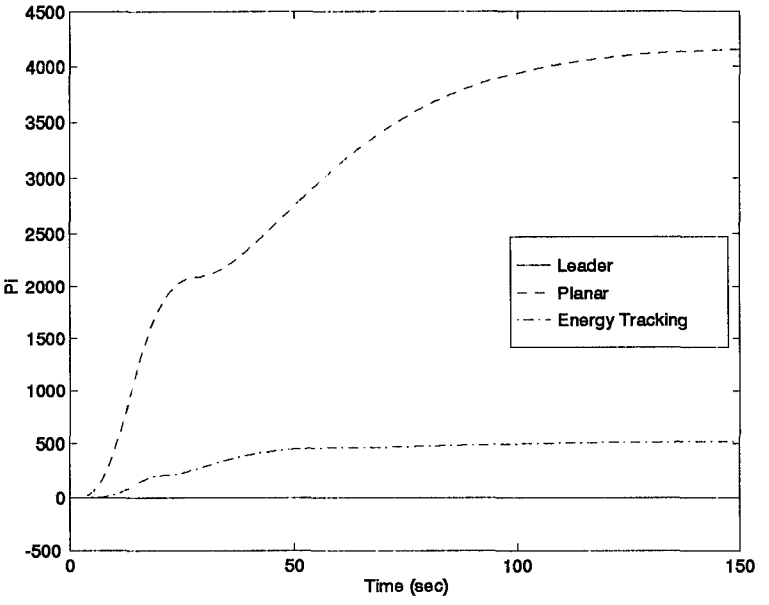

Figure 5.2 Performance Indices *(30 Degree Heading Change)*

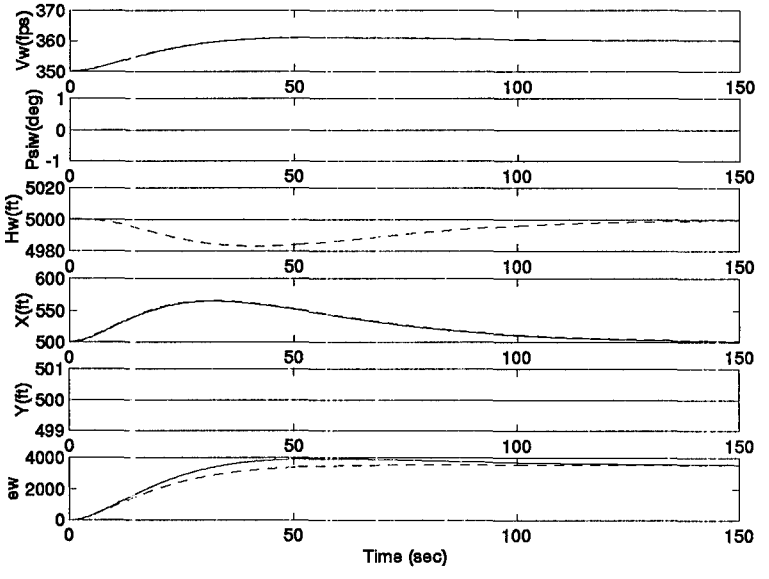

Figure 5.3 Comparison of Planar (Solid) and Energy Tracking Controller (dashed) *(10 fps Velocity Increase)*

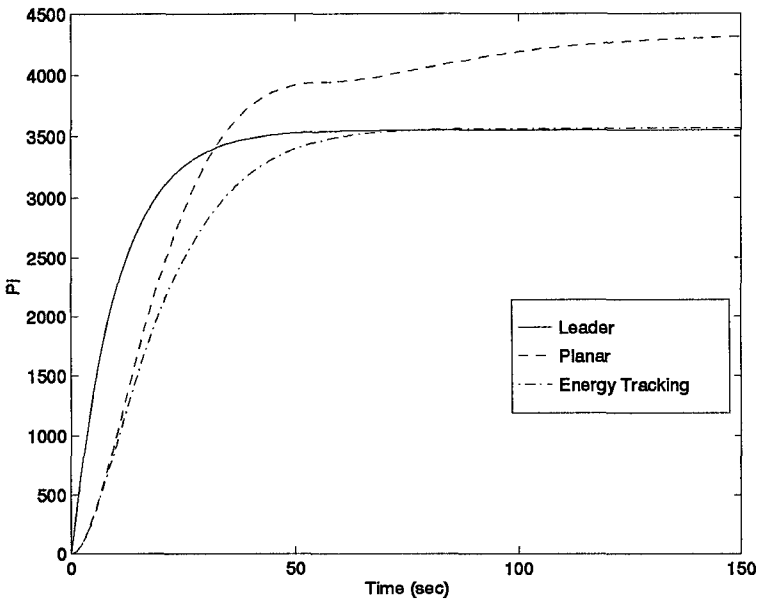

Figure 5.4 Performance Indices *(10 fps Velocity Increase)*

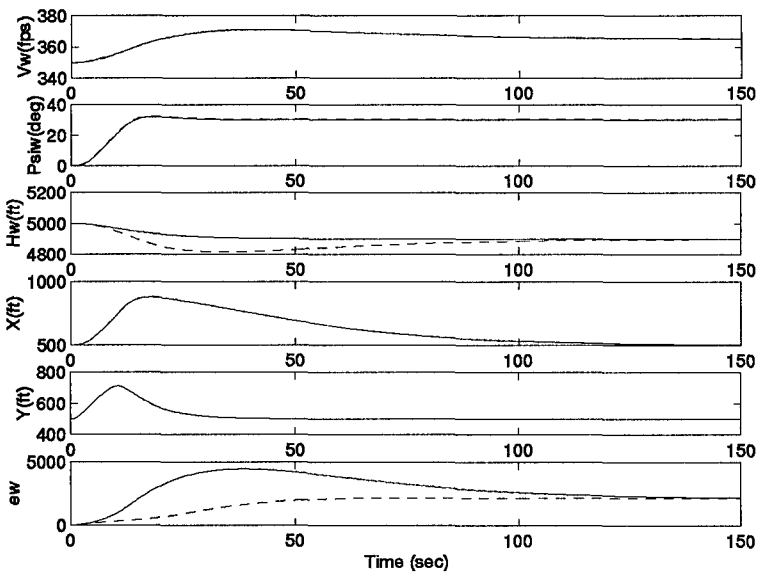

Figure 5.5 Comparison of Planar (Solid) and Energy Tracking Controller (dashed) *(Combination Maneuver) — 30° Heading Change, 100 ft Altitude Change, and 15 fps Velocity Increase)*

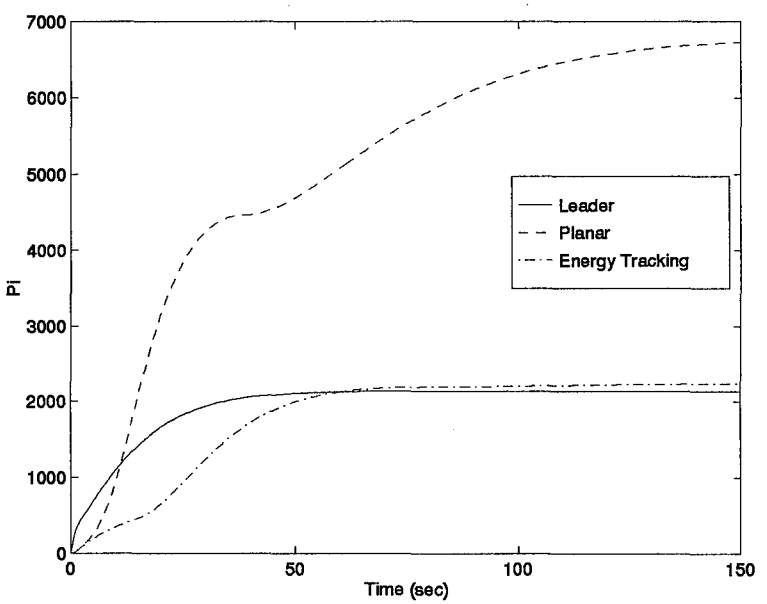

Figure 5.6 Performance Indices *(Combination Maneuver — 30° Heading Change, 100 ft Altitude Change, and 15 fps Velocity Increase)*

5.4 Formation Geometry Change Maneuvers

In addition to the previous upper tier formation maneuvers, the energy tracking formation flight controller is tested with respect to the lower tier commands used in Section 4.8.

The following maneuvers are examined:

- Diamond to trail maneuver
- Left diamond to right diamond formation *during* a 30 degree left turn (Figure 2.1)

The diamond to trail maneuver simulation results are shown in Figures 5.7 and 5.8. The left turn transition maneuver simulation results are shown in Figures 5.9 and 5.10.

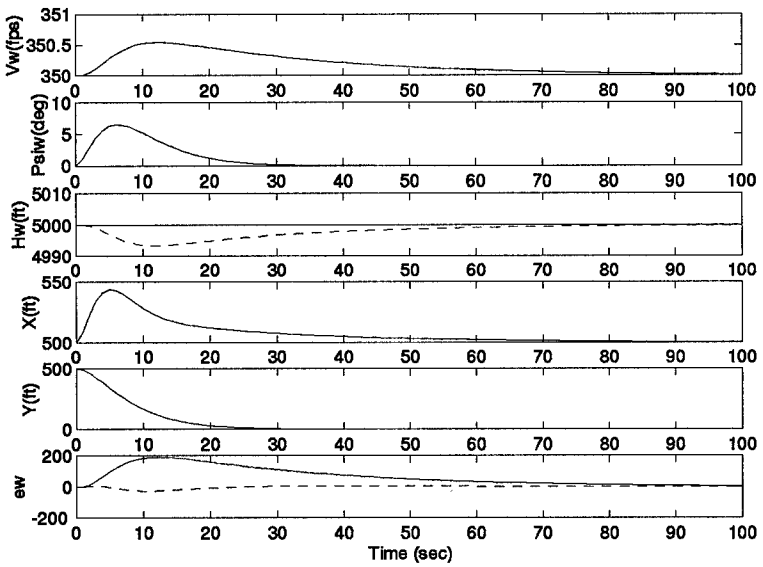

Figure 5.7 Left Diamond to Trail Formation Change — *Planar (Solid), Energy Tracking Controller (Dashed)*

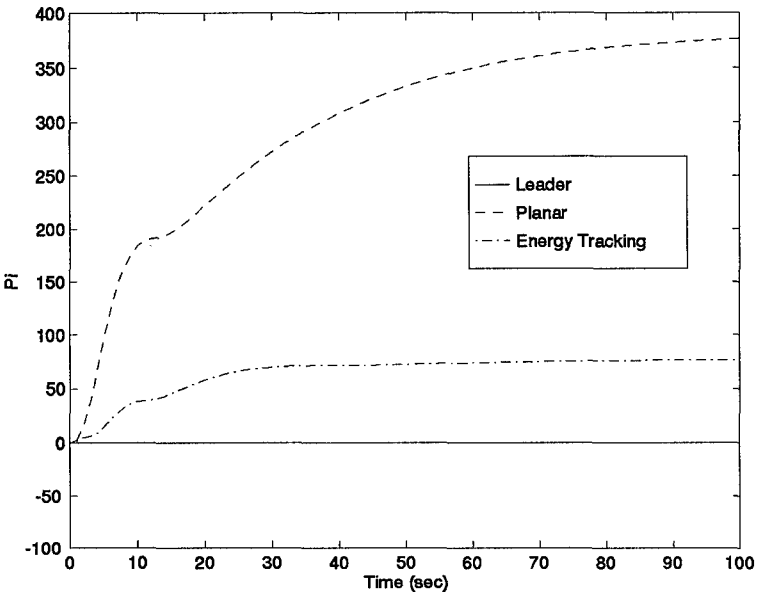

Figure 5.8 Left Diamond to Trail Formation Change Performance Index

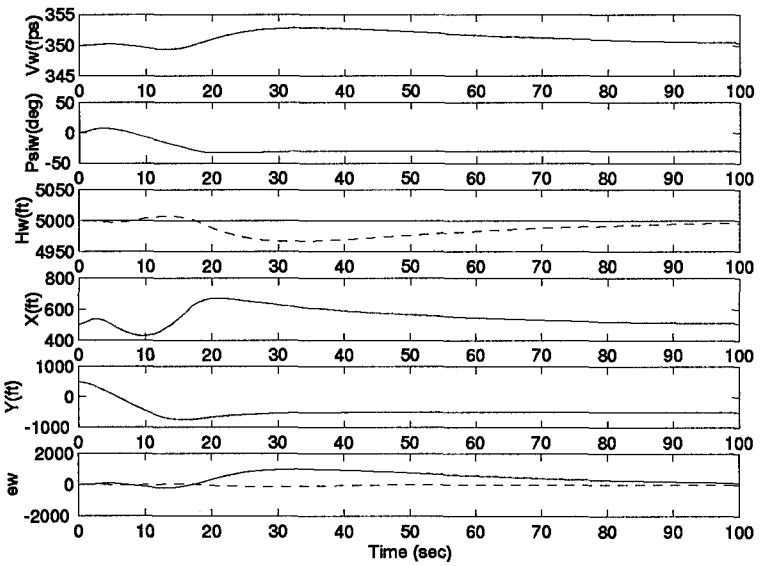

Figure 5.9 Left Diamond to Right Diamond with a 30 degree Left Turn — *Planar (Solid), Energy Tracking Controller (Dashed)*

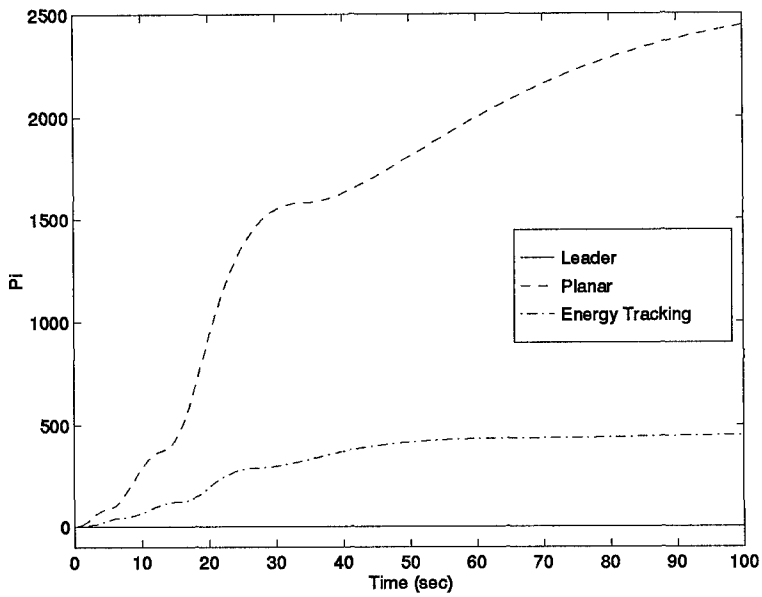

Figure 5.10 Left Diamond to Right Diamond with a 30° Left Turn Performance Index

Parameter	Value
K_{xp}	2.50×10^{-2}
K_{yp}	1.87×10^{-2}

Table 5.1 Energy Tracking Formation Flight Controller Gains

5.5 Controller Summary

The energy tracking formation flight control laws are repeated below for clarity. Note that true states, *not* perturbations are used. The controller gains are listed in Table 5.1.

$$V_{wc} = V_L + K_{xp}(X - X_{cmd}) \tag{5.13}$$

$$\Psi_{wc} = \Psi_L + K_{wp}(Y - Y_{cmd}) \tag{5.14}$$

$$H_{wc} = H_L + \frac{1}{2g}(V_L^2 - V_{wc}^2) \tag{5.15}$$

5.6 Conclusion

The formation hold autopilot now uses three-dimensional maneuvers to reduce wing aircraft energy excursions during formation maneuvers, thereby reducing throttle cycling. This yields improved fuel consumption and should reduce pilot fatigue. Utilization of natural decoupling of energy changing and energy conserving flight parameters results in an intuitive control law which allows wing aircraft energy tracking, while minimizing energy excursions about this energy trajectory. Nonlinear simulations verified the performance improvement and robustness of the proposed controller.

VI. Autopilots for Flying Circular Paths

6.1 Problem Description

In this chapter, the formation flight control concept is extended to automatically fly aircraft about a fixed point on the earth, at a specified range and velocity. Now, the leader is a computer-generated target (or "rabbit") following the ideal orbit path. The controller is thus responsible for maintaining the aircraft's desired position relative to the fictitious leader. The performance of the formation flight controller in this new mode is analyzed using nonlinear simulations. The autopilot for flying circular paths is designed to track commanded changes in airspeed and orbit radius, with a minimum of overshoot.

The chapter is organized as follows. The basic formation flight control system is developed in Section 6.2.1. The formation flight controller is designed in Section 6.2 using first-order aircraft/autopilot models. Both proportional, and proportional plus integral controllers are designed and tested using linear and nonlinear simulations. This procedure is repeated in Section 6.3 using second-order aircraft/autopilot models. The performance of the autopilot for flying circular paths when orbit parameter changes are commanded is demonstrated in Section 6.4. Concluding remarks are made in Section 6.6.

6.1.1 Linearization. The kinematic equations (3.18) and (3.19) contain nonlinear dynamics. In order to utilize linear design techniques these equations are linearized about a "trim" condition, or a nominal flight trajectory. In previous formation flight control work the dynamics were linearized about straight-line trajectories. In this thesis, however, it is stipulated that the wing aircraft is flying a nominal circular path in formation with the "leader", as illustrated in Figure 6.1. Hence, the nominal trajectory and perturbed variables used for this linearization are

$$
\begin{aligned}
X &= \overline{X} + x \\
Y &= \overline{Y} + y \\
V_L &= \overline{V} + v_L
\end{aligned}
$$

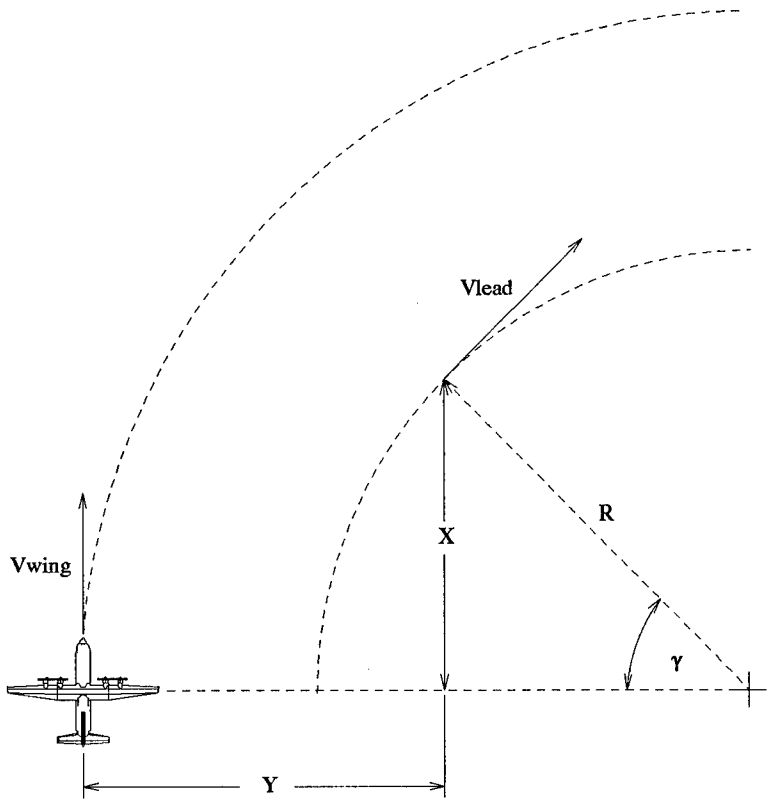

Figure 6.1 Circular Path Autopilot Visualization

$$
\begin{aligned}
V_W &= \overline{V}\left(\frac{R\cos\gamma + \overline{Y}}{R}\right) + v_W \\
\Psi_W &= \omega t + \psi_W \\
\Psi_L &= \omega t + \gamma + \psi_L
\end{aligned}
$$

where $\overline{X}$ and $\overline{Y}$ are the nominal separation distances in the x and y axes of the wing aircraft, respectively. R is the nominal radius of the circular path, ω is the angular rate, and γ is the toe-in angle of the lead aircraft. The angular rate (ω) and lead aircraft toe-in angle (γ) or

$$\omega = \frac{\overline{V}}{R} \tag{6.1}$$

$$\gamma = \sin^{-1}\left(\frac{\overline{X}}{R}\right) \tag{6.2}$$

Furthermore, the nominal commands are

$$\overline{V}_{wc} = \overline{V}\left(\frac{R\cos\gamma + \overline{Y}}{R}\right) \tag{6.3}$$

and

$$\overline{\Psi}_{wc} = \omega t + \omega\tau_{\psi w} \tag{6.4}$$

The latter is obtained by substituting the nominal wing aircraft heading $\Psi = \omega t$ into eq. (3.1) (or (3.4)) and solving for Ψ_{wc}.

Substituting the above nominal trajectory in equations (3.18) and (3.19), using the method of small perturbations, and eliminating the higher order terms, yields the linearized kinematics which are used in the linear analysis:

$$\dot{x} = v_L\cos\gamma + \overline{Y}\dot{\psi}_W + \omega y - v_W \tag{6.5}$$

$$\dot{y} = \overline{V}\cos\gamma\,(\psi_L - \psi_W) + v_L\sin\gamma - \omega x - \overline{X}\dot{\psi}_W \tag{6.6}$$

Note that in the limiting case of straight line trajectories where $R \rightarrow \infty \Rightarrow \omega = \gamma = 0$, eqns. (6.5) and (6.6) reduce to the equations used in Chapter IV.

6.2 First-order Models

In the initial analysis, first-order aircraft/autopilot models are used. The kinematic equations and aircraft models (eqs. (3.2), (3.1), (3.18), and (3.19)) are combined into the following state space form:

$$\frac{d}{dt}\begin{bmatrix} x \\ v_w \\ y \\ \psi_w \end{bmatrix} = A\begin{bmatrix} x \\ v_w \\ y \\ \psi_w \end{bmatrix} + B\begin{bmatrix} v_{wc} \\ \psi_{wc} \end{bmatrix} + \Gamma\begin{bmatrix} v_L \\ \psi_L \end{bmatrix} \tag{6.7}$$

where the state vector is $[x, v_W, y, \psi_W]^T$, the control vector is $[v_{wc}, \psi_{wc}]^T$, and the disturbance vector is $[v_L, \psi_L]^T$. The disturbances represent possible perturbations in the rabbit's nominal speed and heading. The output vector is $[x, y]^T$. The system matrices A, B, C, and Γ are, respectively:

$$A = \begin{bmatrix} 0 & -1 & \omega & -\frac{\overline{Y}}{\tau_\psi} \\ 0 & -\frac{1}{\tau_v} & 0 & 0 \\ -\omega & 0 & 0 & \frac{\overline{X}}{\tau_\psi} - \overline{V}cos\gamma \\ 0 & 0 & 0 & -\frac{1}{\tau_\psi} \end{bmatrix}$$

$$B = \begin{bmatrix} 0 & \frac{\overline{Y}}{\tau_\psi} \\ \frac{1}{\tau_v} & 0 \\ 0 & \frac{\overline{X}}{\tau_\psi} \\ 0 & \frac{1}{\tau_\psi} \end{bmatrix}$$

$$C = \begin{bmatrix} 1 & 0 & 0 & 0 \\ 0 & 0 & 1 & 0 \end{bmatrix}$$

$$\Gamma = \begin{bmatrix} cos\gamma & 0 \\ 0 & 0 \\ sin\gamma & \overline{V}cos\gamma \\ 0 & 0 \end{bmatrix}$$

It is possible that although the nominal path is not an equilibrium point, but rather, it is a time dependent trajectory, the linearized dynamical system is LTI.

6.2.1 Proportional Control Law. The control law which is initially evaluated is a proportional error feedback scheme for the linear control system (6.7),

$$V_{wc} = K_{xp}x \tag{6.8}$$

$$\psi_{wc} = K_{yp}y \tag{6.9}$$

Combining the system dynamics (6.7) and (6.8) and (6.9) results in the following closed loop dynamics:

$$A_{cl} = \begin{bmatrix} 0 & -1 & \omega + K_{yp}\frac{\overline{Y}}{\tau_\psi} & -\frac{\overline{Y}}{\tau_\psi} \\ K_{xp}\frac{1}{\tau_v} & -\frac{1}{\tau_v} & 0 & 0 \\ -\omega & 0 & -K_{yp}\frac{\overline{X}}{\tau_\psi} & \frac{\overline{X}}{\tau_\psi} - \overline{V}cos\gamma \\ 0 & 0 & K_{yp}\frac{1}{\tau_\psi} & -\frac{1}{\tau_\psi} \end{bmatrix} \tag{6.10}$$

The closed-loop system (6.10) is "driven" by the rabbit's velocity and heading perturbations v_L and ψ_L, respectively.

6.2.2 Stability Envelope Determination Using Routhian Analysis. A Routhian analysis of the system is used to determine the range of acceptable values for the controller gains K_{xp} and K_{yp}. This analysis begins with the determination of the characteristic equation. The characteristic equation is determined using the following formula:

$$Q(\lambda) = det\,[\lambda I - A] \tag{6.11}$$

Solving using the closed-loop A_{cl} matrix from (6.10) results in the following characteristic equation.

$$\begin{aligned} Q(\lambda) \;=\; & \lambda^4 + \frac{(\tau_v + \tau_v K_{yp}\overline{X} + \tau_\psi)}{\tau_\psi \tau_v}\lambda^3 \\ & + \frac{(\tau_v K_{yp}\overline{V}cos(\gamma) + 1 + K_{yp}\overline{X} + \tau_v\omega^2\tau_\psi + \omega\tau_v K_{yp}\overline{Y} + K_{xp}\tau_\psi)}{\tau_\psi \tau_v}\lambda^2 \\ & + \frac{(K_{yp}\overline{V}cos(\gamma) + \tau_v\omega^2 + \omega^2\tau_\psi + K_{xp}K_{yp}\overline{X} + \omega K_{yp}\overline{Y} + K_{xp})}{\tau_\psi \tau_v}\lambda \\ & + \frac{\omega^2 + K_{xp}K_{yp}\overline{V}cos(\gamma)}{\tau_\psi \tau_v} \end{aligned} \tag{6.12}$$

The specific parameters used in the analysis are

$$\begin{aligned} \frac{1}{\tau_v} &= 3 \\ \frac{1}{\tau_\psi} &= 1.5 \\ \overline{V} &= 350\left(\frac{ft}{sec}\right) \\ \omega &= \frac{\pi}{180}\left(\frac{rads}{sec}\right) \\ \overline{X} &= 0 \\ \overline{Y} &= 0 \\ \gamma &= 0 \end{aligned}$$

Substituting these values into equation (6.12) yields the quartic characteristic equation.

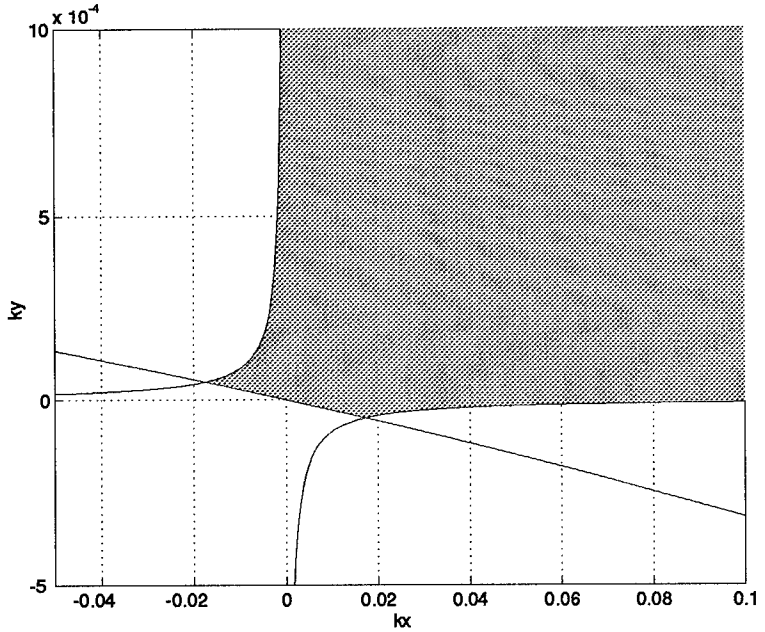

Figure 6.2 Range of Stability for Values of K_{xp} and K_{yp} *(Shaded Region)*

$$\begin{aligned} Q(\lambda) &= \lambda^4 + \frac{9}{2}\lambda^3 + (525K_{yp} + \frac{9}{2} + \frac{\pi^2}{32400} + 3K_{xp})\lambda^2 \\ &\quad + (1575K_{yp} + \frac{\pi^2}{7200} + K_{xp}\frac{9}{2})\lambda + \frac{\pi^2}{7200} + 1575K_{xp}K_{yp} \end{aligned} \tag{6.13}$$

The characteristic equation is now used to construct the following Routhian array.

$$\begin{array}{c|cc} \lambda^4 & 1 & 525K_{yp} + 3K_x + \frac{9}{2} + \frac{\pi^2}{32400} \quad 1575K_{xp}K_{yp} + \frac{\pi^2}{7200} \\ \lambda^3 & \frac{9}{2} & 1575K_{yp} + \frac{9}{2}K_{xp} + \frac{\pi^2}{7200} \\ \lambda^2 & 175K_{yp} + 2K_{xp} + \frac{9}{2} & 1575K_{xp}K_{yp} + \frac{\pi^2}{7200} \\ \lambda^1 & \frac{1984500000K_{yp}^2 + (51030000 + 175\pi^2)K_{yp} - 22680000K_{xp}K_{yp} + (2\pi^2 + 145800)K_{xp} + 64800K_{xp}^2}{3600(350K_{yp} + 4K_{xp} + 9)} & \\ \lambda^0 & 1575K_{xp}K_{yp} + \frac{\pi^2}{7200} & \end{array}$$

In order to guarantee system stability, the first column of the array must be positive definite. Utilizing this requirement allows the determination of the stable areas in the K_{yp}-K_{xp} plane. This is illustrated in Figure 6.2.

The results show that the system is stable for all positive values of K_{yp} and K_{xp}. This gives a large range for parameter variation. It is interesting to note that there are

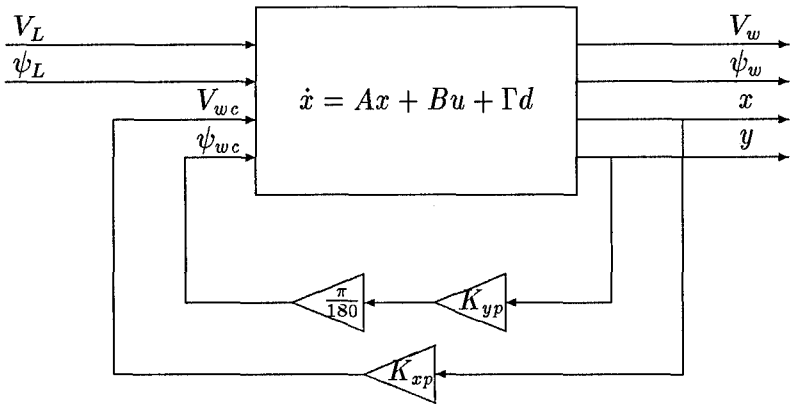

Figure 6.3 Linearized Formation Flight Control System with Proportional Feedback

restricted ranges where either K_{xp} or K_{yp} could be negative, while maintaining system stability. This has been verified through simulation.

6.2.3 Choosing K_{xp} and K_{yp}. The controller gains K_{xp} and K_{yp} are determined using successive loop closures. This is accomplished by analyzing the root locus for each loop. The goal is to determine gains which cause a slightly underdamped response ($\zeta \cong 1$). This ensures that the maneuvers are accomplished in "minimum" time without excessive heading and velocity excursions. The control scheme is shown in Figure 6.3.

The procedure begins by examining the root-locus for the $\frac{Y(s)}{\Psi_{cmd}(s)}$ transfer function obtained from the original system (6.7). The gain is chosen to produce a slightly underdamped response. The resulting K_{yp} value is 6.3×10^{-2}. The ψ_{cmd} loop is now closed, changing the original A matrix.

This new A matrix is now used to determine the $\frac{X(s)}{V_{cmd}(s)}$ outer loop transfer function. A gain $K_{xp} = 0.7496$ is chosen which gives a slightly underdamped response. Applying this SISO technique to the 2x2 MIMO plant is not completely rigorous, but it does yield insights into the inner workings of the autopilot as well as giving a general idea of acceptable controller gains. For a more rigorous treatment of MIMO control system stability, the reader is referred to reference [12].

6.2.4 Proportional Controller Analysis. The performance of the proportional controller is now examined under two test conditions. First, the control system is given a 10 ft perturbation in the X and Y channels. Figure 6.4 shows the controller response with $\overline{X}, \overline{Y} = 0$. As predicted in Section 6.2.3, the system exhibits a slightly underdamped response.

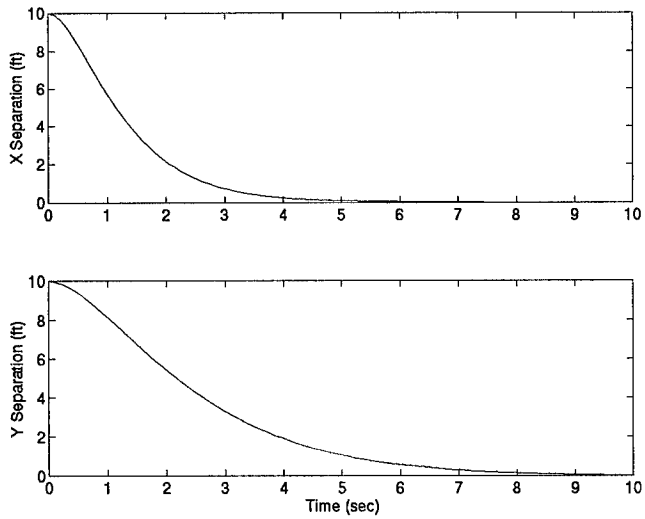

Figure 6.4 First-order, Proportional Linear Autopilot Response ($\overline{X} = \overline{Y} = 0$)

In order to examine the robustness of the controller, the system is also tested with $\overline{X}, \overline{Y} = 500$ ft. The results are shown in Figure 6.5. As in the previous case, the system once again displays acceptable response.

To affect a change in airspeed, the leader, i.e., the "rabbit", is given a velocity step command and the disturbance rejection capability of the controller is called into action. To affect a change in orbit radius, the "rabbit" is commanded to have an instantaneous change in radius.

The disturbance rejection of the controller is now evaluated. The leader, viz., the "rabbit", is given a 10 ft/sec velocity step and a 10 degree step heading change. Figure 6.6 shows the velocity disturbance rejection and Figure 6.7 shows the heading disturbance rejection. From the results shown in Figures 6.6 and 6.7, it is clear that a steady-state error is present and the disturbances are not rejected by the proportional controller. Hence,

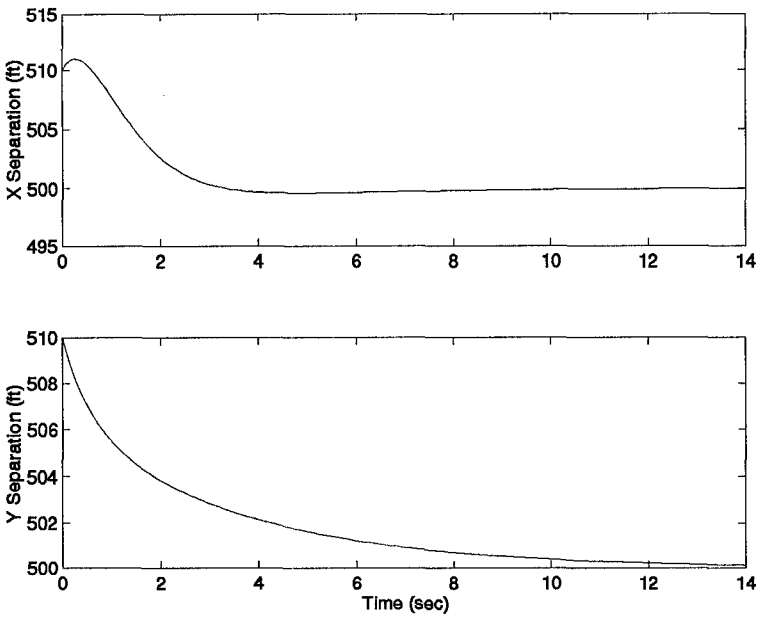

Figure 6.5 First-order, Proportional Linear Autopilot Response ($\overline{X} = \overline{Y} = 500$)

changes in "rabbit" speed and heading cannot be tracked, and integral action is needed for tracking and disturbance rejection.

Another possible source of disturbance to the system comes from modeling errors. These effects become apparent when using linearization-based methods to design linear controllers for the control of nonlinear processes. In the specific problem under investigation, these errors are introduced during the initiation of the orbiting maneuver from an initial straight-line formation flight. This additional problem is fully discussed in Chapter VII and in [18].

Figures 6.8 and 6.9 compare the proportional controller responses using linear and nonlinear dynamics. It is interesting to note that the linear system model predicts a zero steady-state error. When the nonlinear dynamics are used, this prediction is rendered untrue. In order to be robust, the system needs the inherent disturbance rejection characteristics provided by integral action. Note that this disturbance rejection capability is not initially posed as part of the circular path autopilot problem because the "rabbit" is not expected to maneuver. While not explicitly stated, a built-in degree of disturbance rejection capability is nevertheless required in nonlinear control, in view of unavoidable

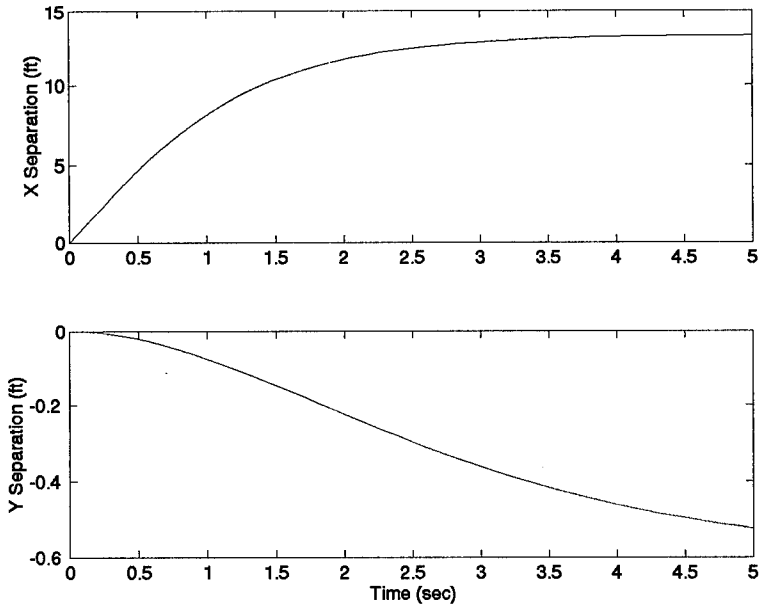

Figure 6.6 First-order, Proportional Linear Autopilot. 10 $\frac{ft}{sec}$ Velocity Increase Response $(\overline{X} = \overline{Y} = 0)$

"modelling mismatches" brought about by the use of linear design methods for nonlinear plants.

6.2.5 Adding Integral Action. In order to meet anticipated disturbance rejection requirements, and in order to operate in the nonlinear environment of the formation flight control problem integral action is used. The controller design proceeds in a manner similarly to Section 6.2.3. Root-locus analysis is used to close successive feedback loops, beginning with the "inner-loop" Y channel and ending with the "outer-loop" X channel. Equation (6.14) shows the new control law with integral action in the Y channel.

$$\psi_{cmd} = K_{yp} y + K_{yi} \int_0^t y \, dt \tag{6.14}$$

From the root-locus, acceptable gain values are determined to be $K_{yp} = 6.3 \times 10^{-2}$ and $K_{yi} = 6.3 \times 10^{-3}$. The system is now augmented and evaluated. The integral action in the Y channel has added a system pole at the origin. Equation (6.15) shows the new control law used in the X channel.

$$V_{cmd} = K_{xp}x + K_{xi}\int_0^t x\,dt \tag{6.15}$$

Gain values are determined to be $K_{xp} = 0.75$ and $K_{xi} = 0.075$.

6.2.6 Proportional Plus Integral Controller Analysis. The performance of a controller with proportional plus integral action is tested and compared to the proportional controller. First, the controller is given a 10 ft perturbation in the X and Y channels for trim separations of $\overline{X} = \overline{Y} = 0$ ft and $\overline{X} = \overline{Y} = 500$ ft, respectively. The two results are compared in Figures 6.10 and 6.11. It is important to note that the addition of integral action slows down the response in both channels. This is the inherent drawback of adding integral action. While it does add robustness to the system, it somewhat compromises performance. In this case, the specifications require the addition of integral action.

As in Section 6.2.4, the disturbance rejection of the two controllers is evaluated. The leader is given a 10 ft/sec velocity step and a 10 degree step heading change. Figure 6.12 shows the results for the velocity step. Figure 6.13 shows the heading step disturbance response.

Examination of Figures 6.12 and 6.13 clearly demonstrates the performance improvements realized by the integral controller. The addition of integral action has reduced steady-state error to zero in both cases. The disturbance rejection characteristics of integral action is essential when compensating for modeling errors caused by nonlinearities, which is demonstrated in the next section.

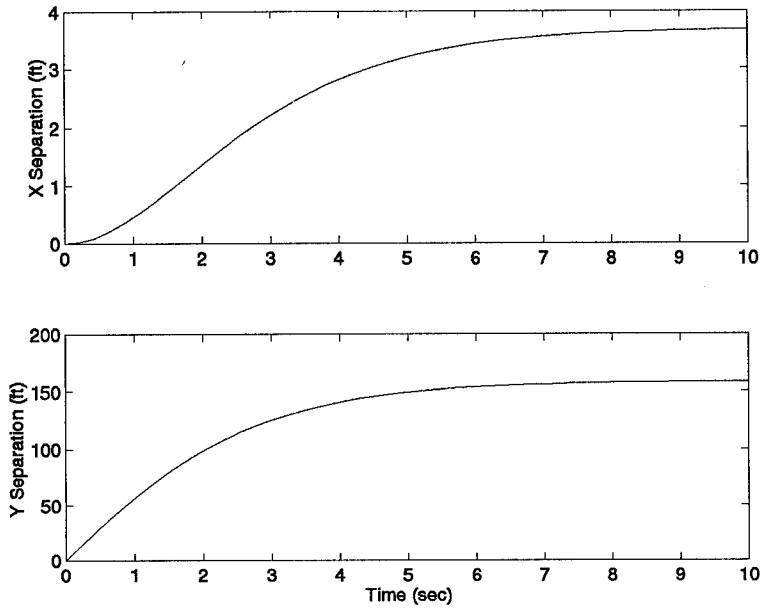

Figure 6.7 First-order, Proportional Linear Autopilot. 10 degree Heading Change Response ($\overline{X} = \overline{Y} = 0$)

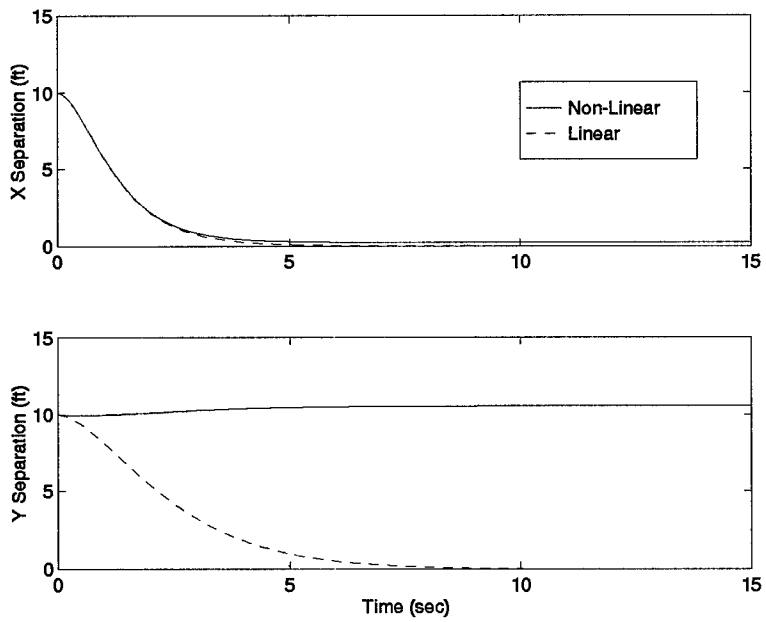

Figure 6.8 First-order, Proportional Linear and Nonlinear Autopilot Response ($\overline{X} = \overline{Y} = 0$)

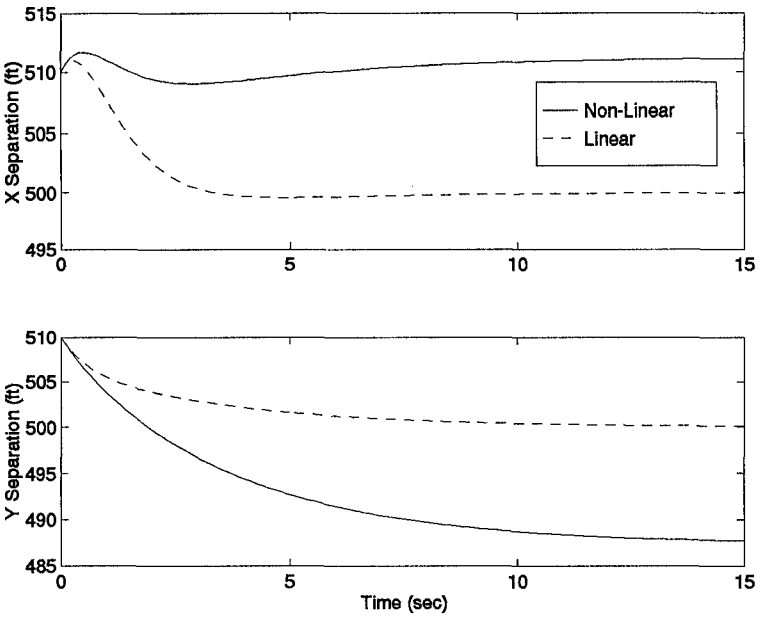

Figure 6.9 First-order, Proportional Linear and Nonlinear Autopilot Response ($\overline{X} = \overline{Y} = 500$)

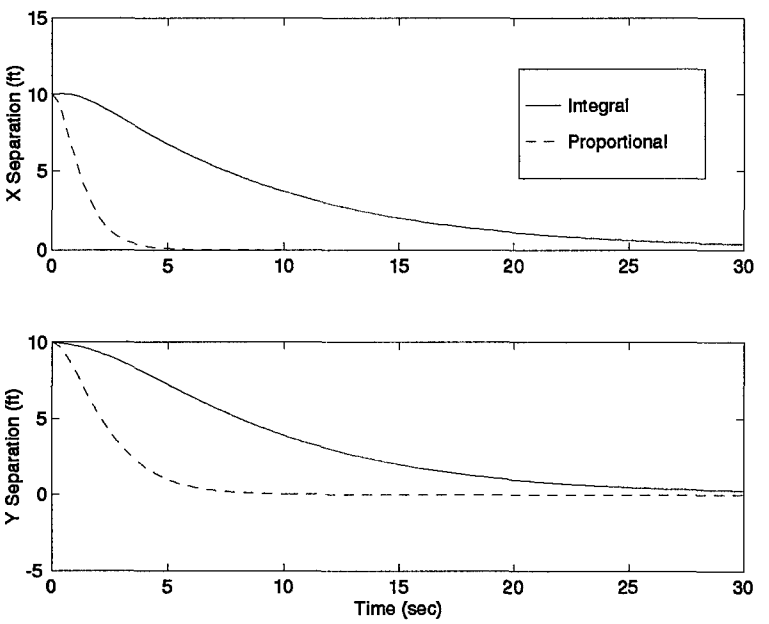

Figure 6.10 First-order, Proportional Plus Integral, Linear Autopilot Response ($\overline{X} = \overline{Y} = 0$)

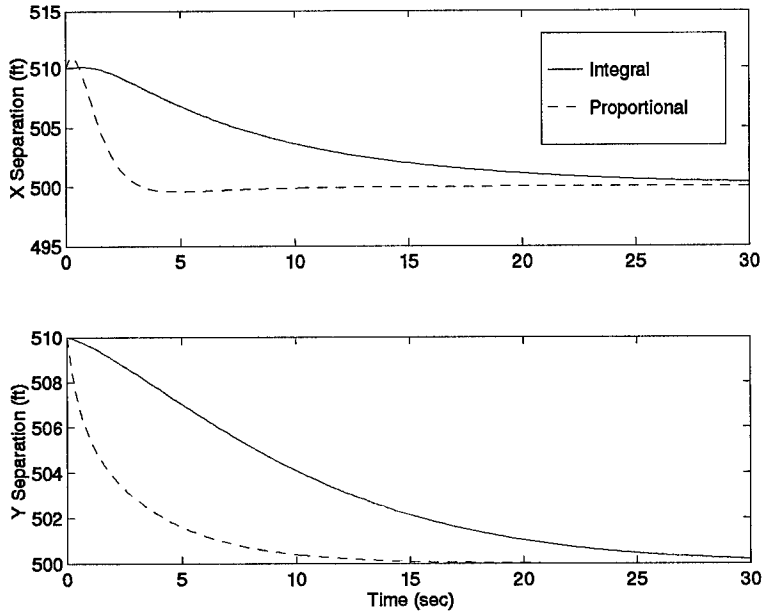

Figure 6.11 First-order, Proportional Plus Integral, Linear Autopilot Response ($\overline{X} = \overline{Y} = 500$)

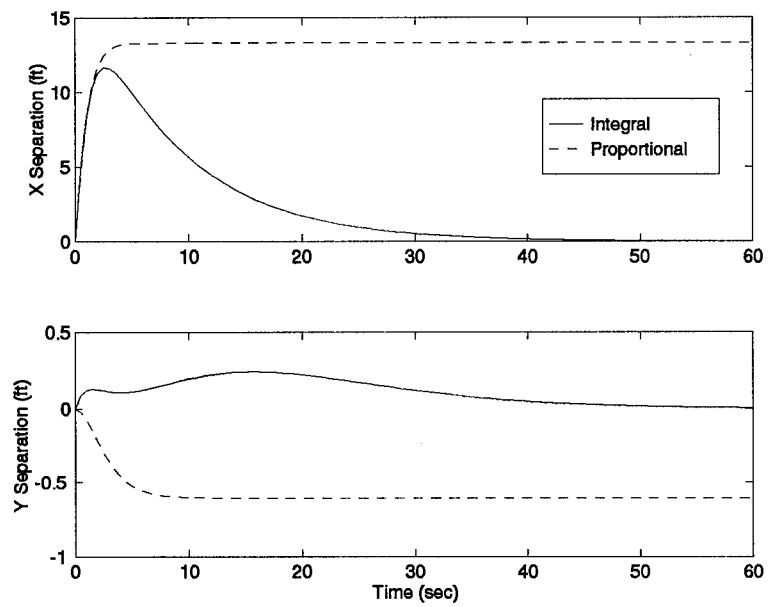

Figure 6.12 First-order, Proportional Plus Integral, Linear Autopilot. 10 $\frac{ft}{sec}$ Velocity Increase Response ($\overline{X} = \overline{Y} = 0$)

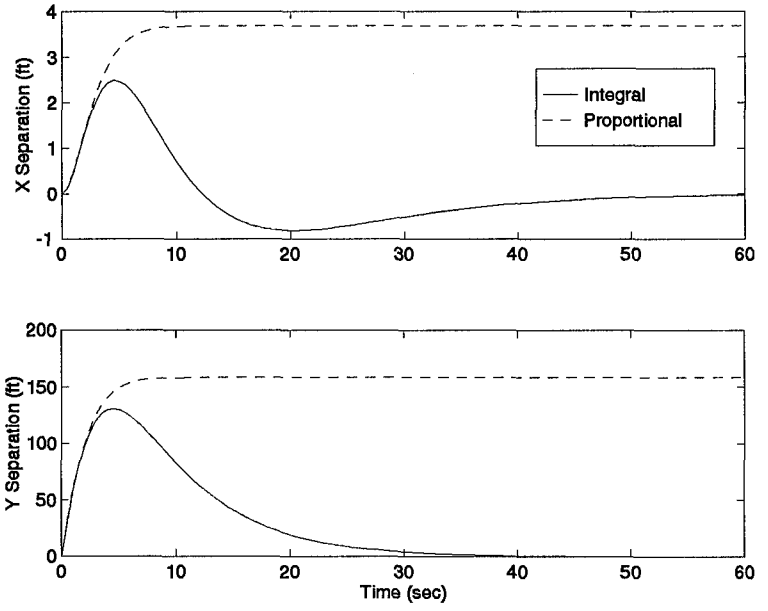

Figure 6.13 First-order, Proportional Plus Integral, Linear Autopilot. 10 degree Heading Change Response ($\overline{X} = \overline{Y} = 0$)

6.2.7 Simulation Using Nonlinear Dynamics. The integral control laws (6.14) and (6.15) are now tested using nonlinear dynamics (3.18) and (3.19). The results obtained give insights into the validity of the linearized design procedure. As in the previous analyses, the wing aircraft is initially tested with a 10 ft perturbation in the X and Y channels for commanded separations of $X_{cmd} = Y_{cmd} = 0$ ft and $X_{cmd} = Y_{cmd} = 500$ ft. The system is tested using the gains determined by the design procedures in Sections 6.2.3 and 6.2.5. Figures 6.14 and 6.15 compare the linear results to the nonlinear simulation.

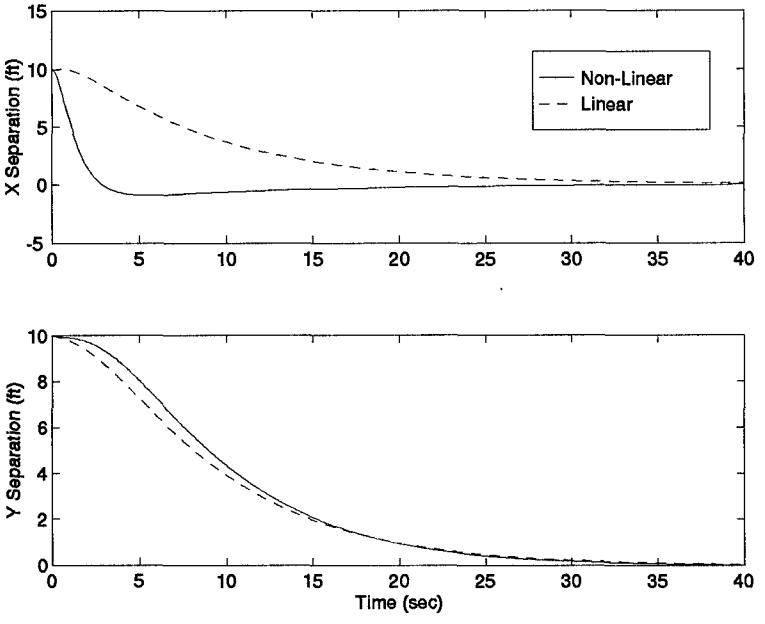

Figure 6.14 First-order, Proportional Plus Integral, Nonlinear Autopilot Response ($\overline{X} = \overline{Y} = 0$)

The nonlinear dynamic effects are easily seen, but the integral action of the controllers is able to compensate for these disturbances. It is important to note the differences due to initial separation distances. Due to the underdamped nature of its response, the Y channel seems to be especially sensitive to larger separations.

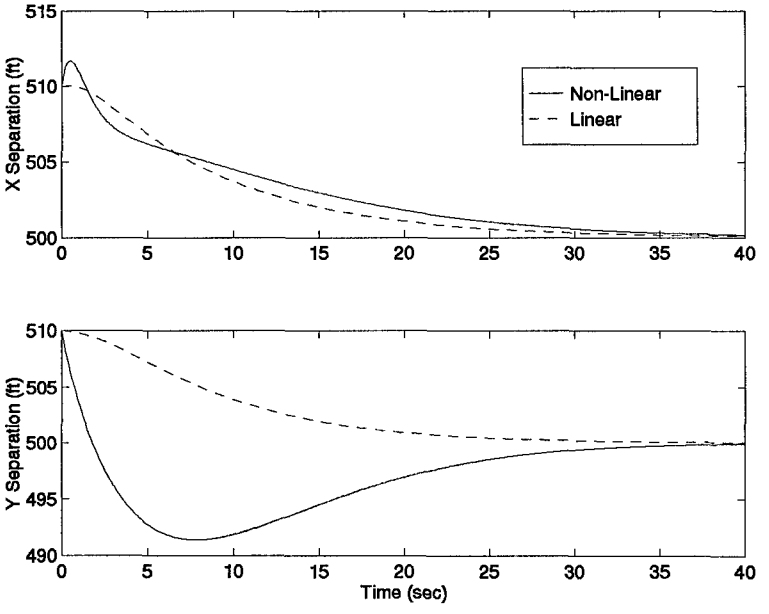

Figure 6.15 First-order, Proportional Plus Integral, Nonlinear Autopilot Response ($\overline{X} = \overline{Y} = 500$)

6.2.8 Simulation Using Nonlinear Dynamics and Rate Limits. The nonlinear effects of rate limits in the aircraft/autopilot models are now examined. The effect of rate limits on the autopilot performance in compared in Figures 6.16 and 6.17.

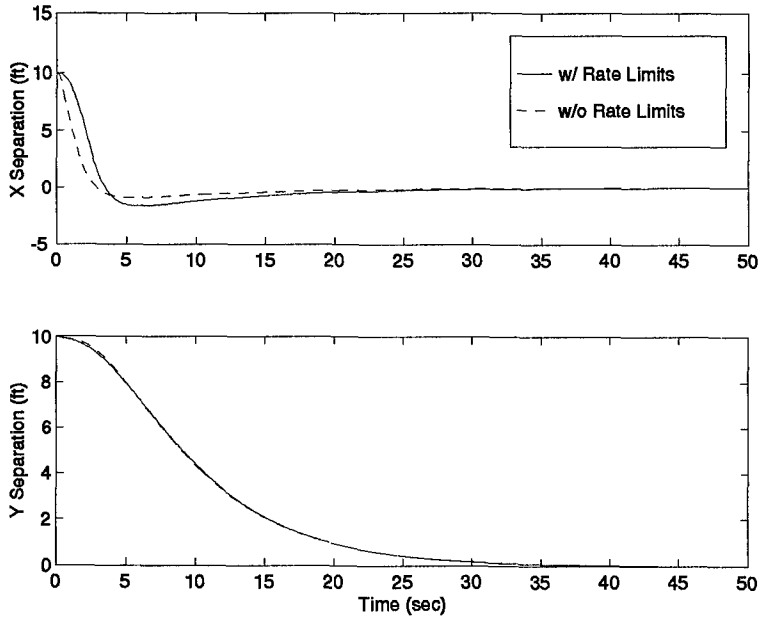

Figure 6.16 First-order, Proportional Plus Integral, Nonlinear Autopilot Response w/ Rate Limits ($X_0 = Y_0 = 10ft$)

The rate limits do not affect the response greatly in the initial case of $\overline{X} = \overline{Y} = 0$ ft. The small separation conditions create rather benign dynamics, thus the controller is relatively unaffected by rate limits. Alternatively, the $\overline{X} = \overline{Y} = 500$ ft case clearly shows the effects of rate limits in the X channel. The heading change caused by the Y channel creates an increasing X separation, which the aircraft is unable to overcome initially. The rate limit effects are illustrated in Figure 6.18.

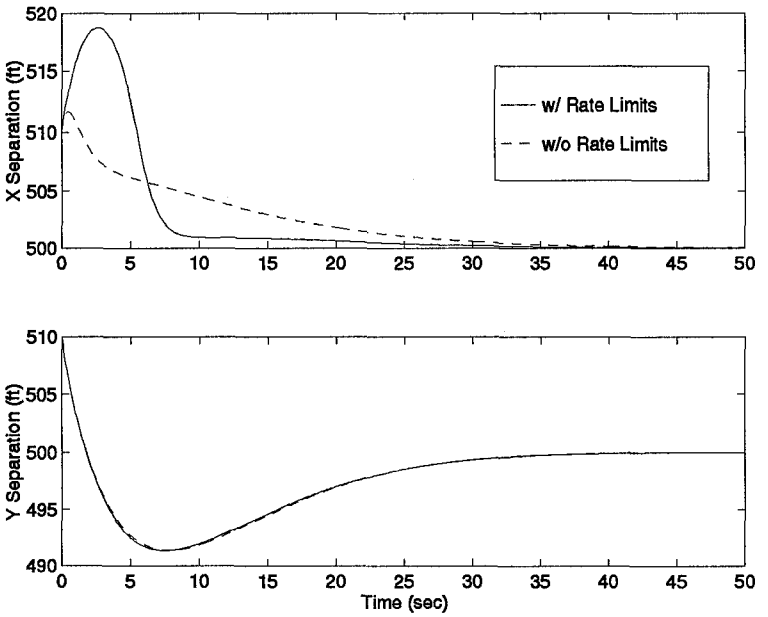

Figure 6.17 First-order, Proportional Plus Integral, Nonlinear Autopilot Response w/ Rate Limits ($X_0 = Y_0 = 510ft$)

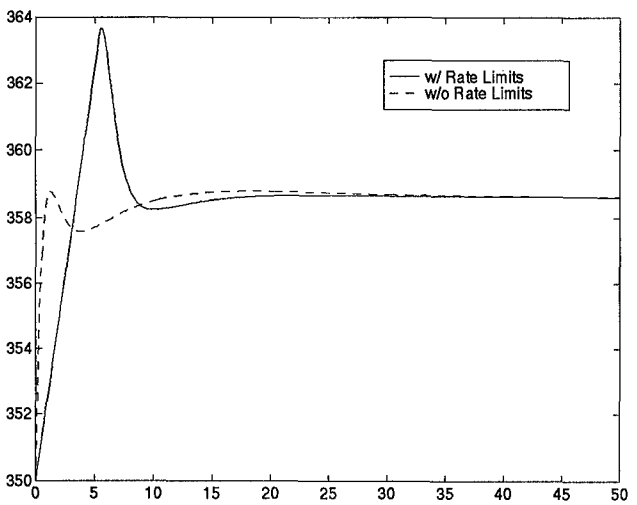

Figure 6.18 First-order, Proportional Plus Integral, Nonlinear Velocity Response w/ and w/o Rate Limits ($X_0 = Y_0 = 510ft$)

6.3 Second-order Models

Next, second-order aircraft/autopilot models are employed in the simulation. The equations of motion and aircraft models are combined into the augmented state space form

$$\frac{d}{dt}\begin{bmatrix} x \\ V_w \\ y \\ \psi_w \\ \dot{\psi}_w \end{bmatrix} = A\begin{bmatrix} x \\ V_w \\ y \\ \psi_w \\ \dot{\psi}_w \end{bmatrix} + B\begin{bmatrix} V_{wc} \\ \psi_{wc} \end{bmatrix} + \Gamma\begin{bmatrix} V_L \\ \psi_L \end{bmatrix} \tag{6.16}$$

where the system matrices are

$$A = \begin{bmatrix} 0 & -1 & \omega & 0 & \overline{Y} \\ 0 & -\frac{1}{\tau_v} & 0 & 0 & 0 \\ -\omega & 0 & 0 & -\overline{V}cos\gamma & -\overline{X} \\ 0 & 0 & 0 & 0 & 1 \\ 0 & 0 & 0 & -\frac{1}{\tau_{\psi_a}\tau_{\psi_b}} & -\frac{1}{\tau_{\psi_a}} - \frac{1}{\tau_{\psi_b}} \end{bmatrix}$$

$$B = \begin{bmatrix} 0 & 0 \\ \frac{1}{\tau_v} & 0 \\ 0 & 0 \\ 0 & 0 \\ 0 & \frac{1}{\tau_{\psi_a}\tau_{\psi_b}} \end{bmatrix}$$

$$C = \begin{bmatrix} 1 & 0 & 0 & 0 & 0 \\ 0 & 0 & 1 & 0 & 0 \end{bmatrix}$$

$$\Gamma = \begin{bmatrix} cos\gamma & 0 \\ 0 & 0 \\ sin\gamma & \overline{V}cos\gamma \\ 0 & 0 \\ 0 & 0 \end{bmatrix}$$

6.3.1 Proportional Controller Design Using Successive Loop Closures. As in Section 6.2.3, a proportional control law is initially used. The procedure begins by examining the root-locus for the $\frac{Y(s)}{\Psi_{cmd}(s)}$ transfer function obtained from the original system (6.16). The presence of complex poles indicates that the system exhibits an underdamped response. Thus, a gain is chosen which minimizes the overshoot. The resulting value for K_{yp} is 1.33×10^{-2}. The ψ_{cmd} loop is now closed and the corresponding changes to the A matrix are made. This A matrix is used to determine the $\frac{X(s)}{V_{cmd}(s)}$ outer loop transfer function.

Again, a gain is chosen which minimizes system overshoot. The resulting value for K_{xp} is 2.19×10^{-2}. This is a marked difference from the gains used in Section 6.2.3. The second-order system is much more sensitive to high gains and is less stable than the first-order system.

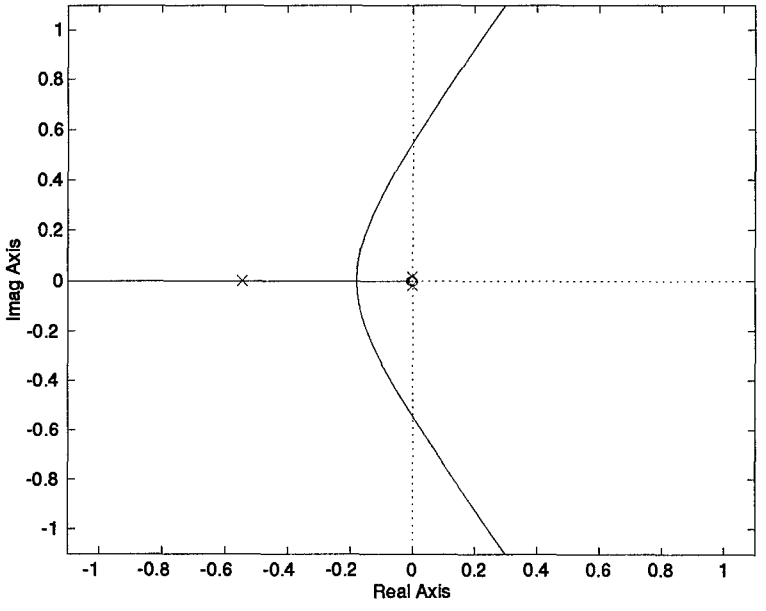

Figure 6.19 Proportional Inner Loop (Y) Feedback Root-Locus *(Second-Order Models)*

6.3.2 Proportional Controller Analysis. The performance of the second-order proportional controller is examined under the same test conditions of Section 6.2.4. First, the controller is given a 10 ft perturbation in the X and Y channels. Figure 6.21 shows the autopilot response with $\overline{X}, \overline{Y} = 0$ ft. The second-order models create a much slower

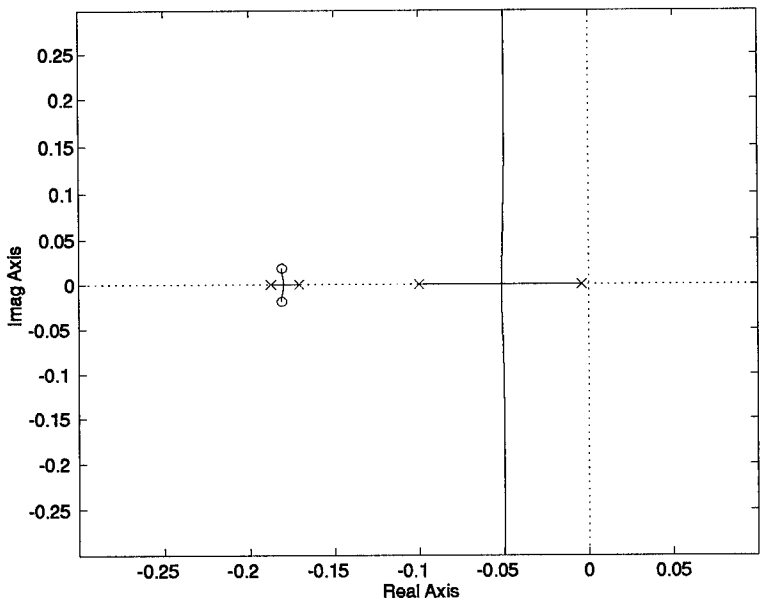

Figure 6.20 Proportional Outer Loop (X) Feedback Root-Locus *(Second-Order Models)*

response than first-order models. Also, as predicted in the previous section, the system exhibits some overshoot in the Y channel; however the response is acceptable.

Again, in order to examine the robustness of the controller, the system is also tested with "formation" parameters of $\overline{X}, \overline{Y} = 500$ ft. The results are shown in Figure 6.22. As in the previous case, the system once again displays acceptable response.

The disturbance rejection of the controller is now evaluated. The leader is given a 10 ft/sec velocity step and a 10 degree step heading change. Figure 6.23 shows the disturbance rejection for the velocity step. Figure 6.24 shows the results for the heading step.

From the results shown in Figures 6.23 and 6.24 it is clear that a steady-state error is present. The proportional controller response using linear and nonlinear dynamics is compared in Figure 6.25. Once again, the disturbances due to modeling error create steady-state tracking errors when the nonlinear dynamics are used. Thus, integral action is required when second-order aircraft models are introduced.

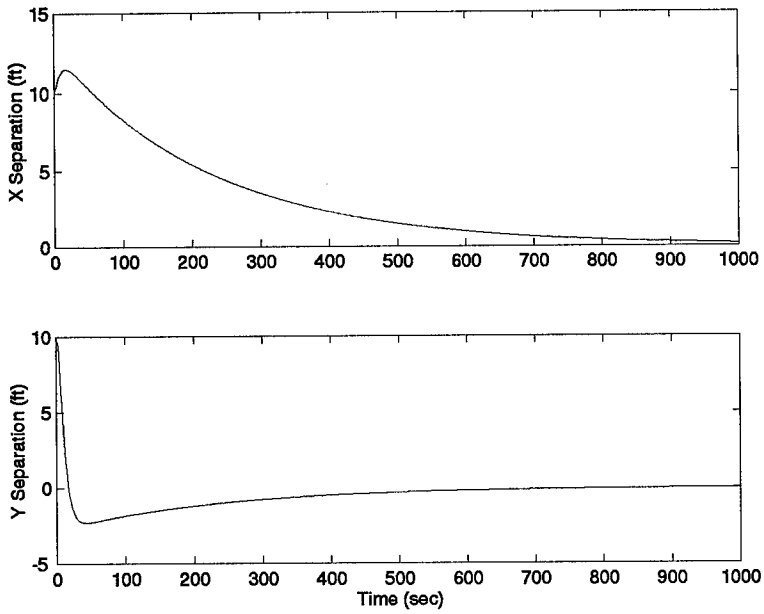

Figure 6.21 Second-Order, Proportional, Linear Autopilot Response ($\overline{X} = \overline{Y} = 0$)

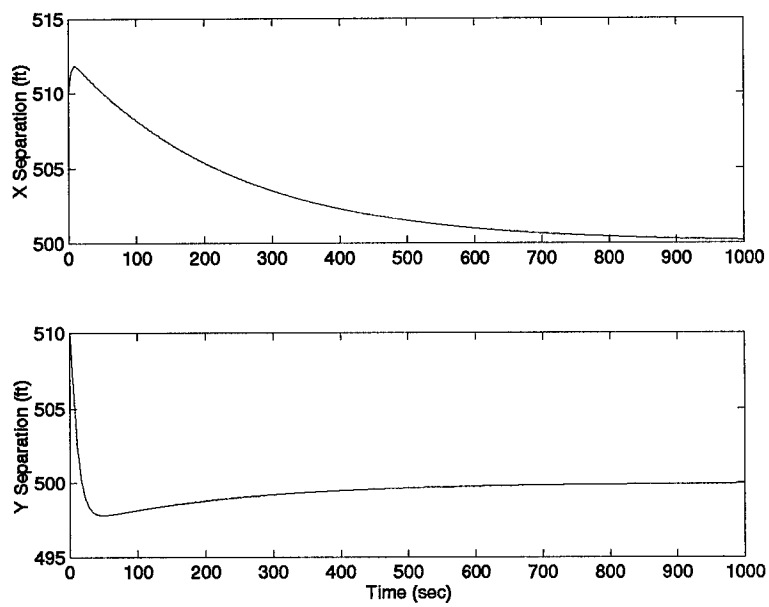

Figure 6.22 Second-Order, Proportional, Linear Autopilot Response ($\overline{X} = \overline{Y} = 500$)

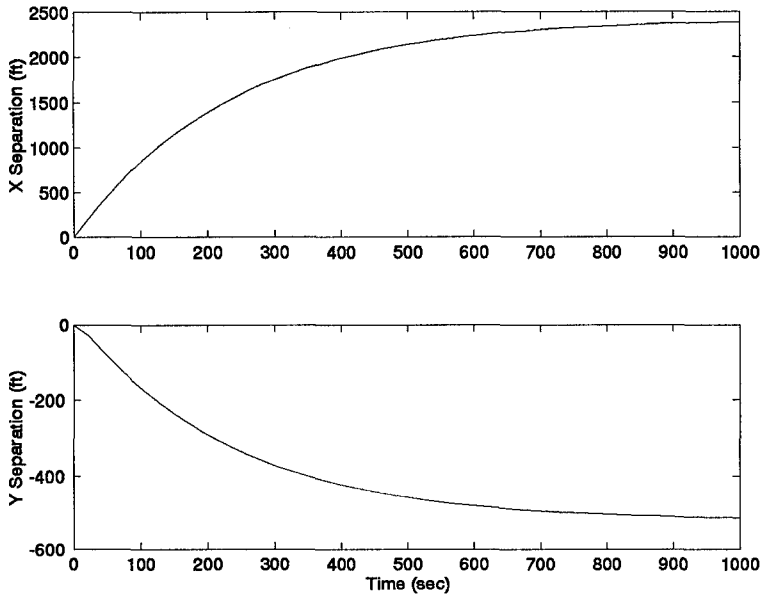

Figure 6.23 Second-Order, Proportional, Linear Autopilot 10 $\frac{ft}{sec}$ Velocity Increase Response $(\overline{X} = \overline{Y} = 0)$

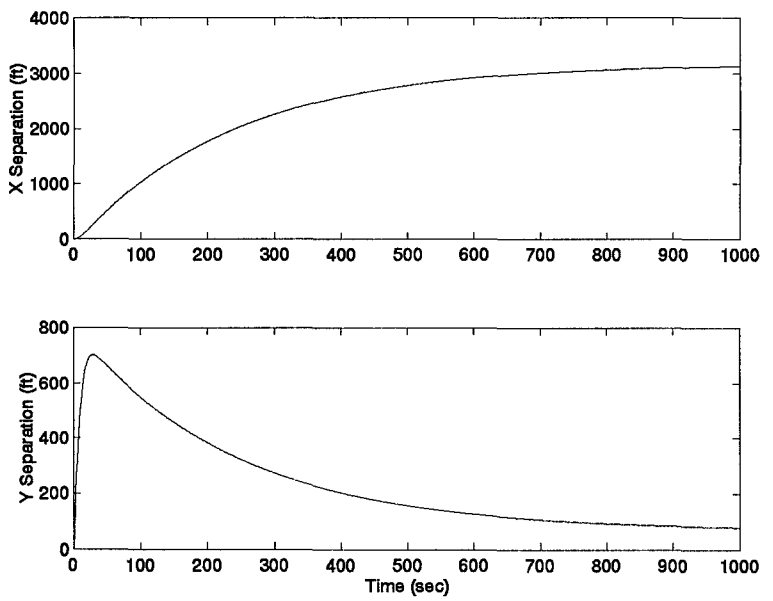

Figure 6.24 Second-Order, Proportional, Linear Autopilot 10 degree Heading Change Response $(\overline{X} = \overline{Y} = 0)$

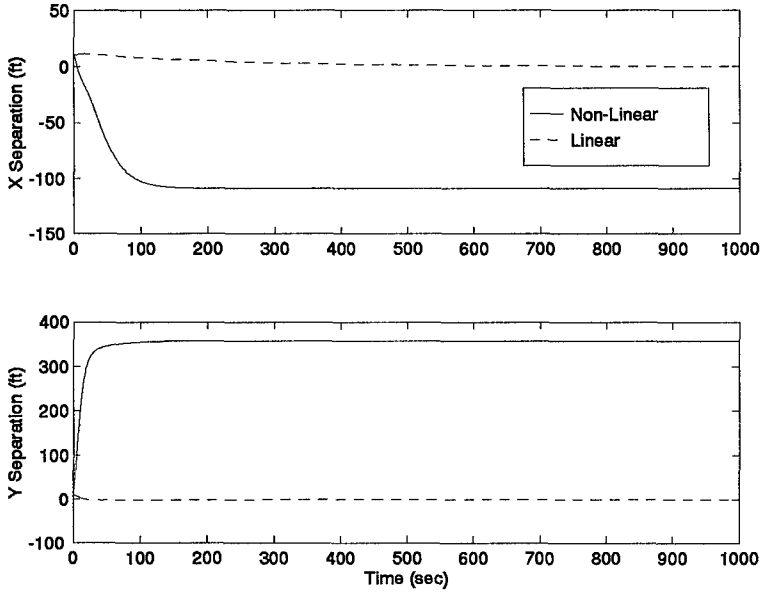

Figure 6.25 First-Order, Proportional, Linear and Nonlinear Autopilot Response ($\overline{X} = \overline{Y} = 0$)

6.3.3 Adding Integral Action. Integral action is added using a procedure identical to that described in Section 6.2.5. The control laws used are identical to equations 6.14 and 6.15. From the $\frac{Y(s)}{\psi_{cmd}}$ root-locus (Figure 6.26), acceptable gain values are determined to be $K_{yp} = 1.5 \times 10^{-2} and K_{yi} = 5.0 \times 10^{-4}$. The system is now augmented and evaluated. Again, the integral action in the Y channel has added a system pole at the origin. From the $\frac{X(s)}{V_{cmd}}$ root-locus (Figure 6.27), gain values are determined to be $K_{xp} = 4.5 \times 10^{-2} and K_{xi} = 4.5 \times 10^{-4}$.

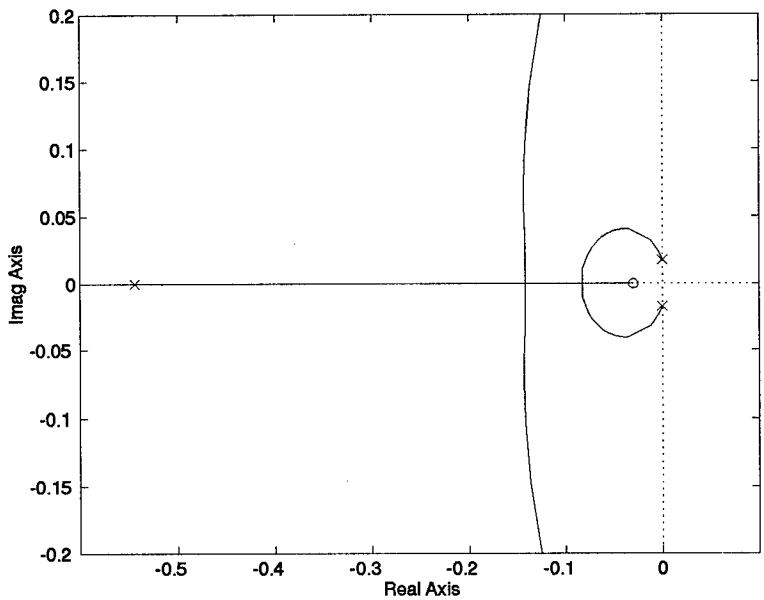

Figure 6.26 Proportional Plus Integral Inner Loop (Y) Feedback Root-Locus *(Second-Order Models)*

6.3.4 Proportional Integral Controller Analysis and Comparison. The performance of a controller with proportional and integral action is tested and compared to the proportional controller. First, the controller is given a 10 ft perturbation in the X and Y channels for trim separations of $\overline{X} = \overline{Y} = 0$ ft and $\overline{X} = \overline{Y} = 500$ ft, respectively. The results are compared in Figures 6.28 and 6.29.

As in Section 6.2.4, the disturbance rejection of the two controllers is evaluated. The leader is given a 10 ft/sec velocity step and a 10 degree step heading change. Figure 6.30 shows the results for the velocity step. Figure 6.31 shows the heading step disturbance response.

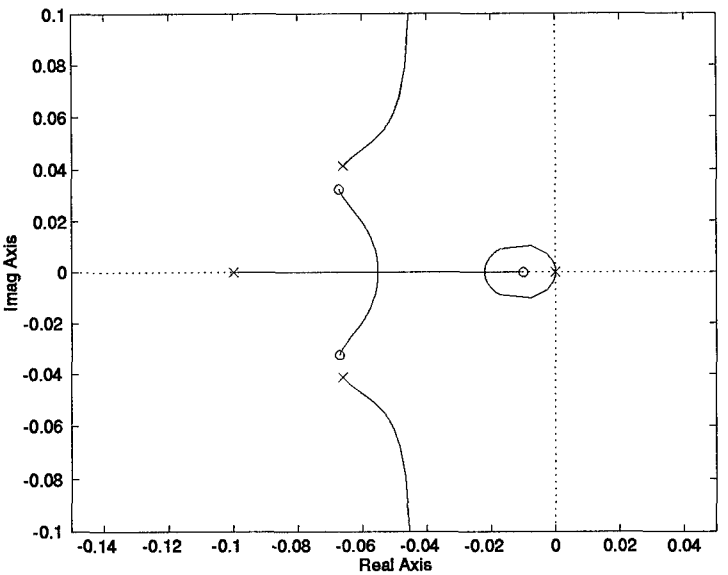

Figure 6.27 Proportional Plus Integral Outer Loop (X) Feedback Root-Locus *(Second-Order Models)*

Examination of Figures 6.30 and 6.31 clearly demonstrates the performance improvements realized by the proportional plus integral controller. The addition of integral action has reduced steady-state error to zero in both cases. Hence, the disturbance rejection characteristics of integral action is essential when compensating for modeling errors caused by nonlinearities, which is demonstrated in the next section.

6.3.5 Simulation Using Nonlinear Kinematics. The integral control laws are now tested using nonlinear kinematics (3.18) and (3.19). The results obtained give insights into the validity of the linearized design procedure. As in the previous analyses, the wing aircraft is initially tested with a 10 ft perturbation in the X and Y channels for commanded separations of $X_{cmd}, Y_{cmd} = 0$ ft and $X_{cmd}, Y_{cmd} = 500$ ft. The system is tested using the gains determined by the design procedures in Section 6.3.3. Figures 6.32 and 6.33 compare the linear simulations to the nonlinear simulation.

The effects of the nonlinear dynamics are evident, but the integral action of the controllers is able to compensate for these disturbances. It is important to note the differences due to initial separation distances. Due to the underdamped nature of its response, the Y channel seems to be especially sensitive to larger separations.

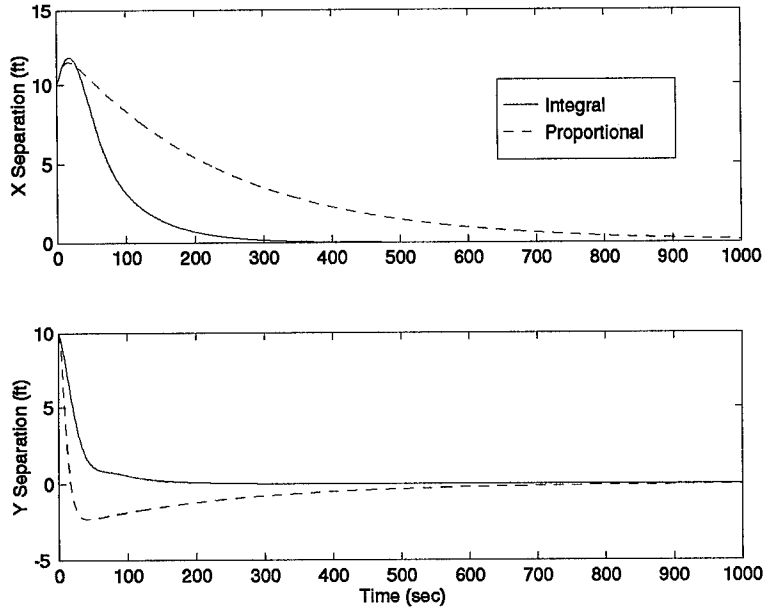

Figure 6.28 Second-order, Proportional Plus Integral, Linear Autopilot Response ($\overline{X} = \overline{Y} = 0$)

6.3.6 Simulation Using Both Nonlinear Kinematics and Rate Limits. The nonlinear effects of rate limits in the autopilot are now examined. The effects of the rate limits on control system performance are compared in Figures 6.34 and 6.35.

The rate limits do not significantly effect the response in the case where $X_0 = Y_0 = 10$ ft. The small separation conditions create rather benign dynamics, thus the controller is relatively unaffected by rate limits. Alternatively, the $X_0 = Y_0 = 2500$ ft case shows the effects of rate limits much more clearly. The heading change caused by the Y channel creates an increasing X separation, which the aircraft is unable to overcome initially. The rate limits are illustrated in Figure 6.36. It is also important to note that the V_{max} limiter has been reached in addition to the standard rate limits. The effects of the nonlinear saturations can clearly be correlated between Figures 6.36 and 6.35.

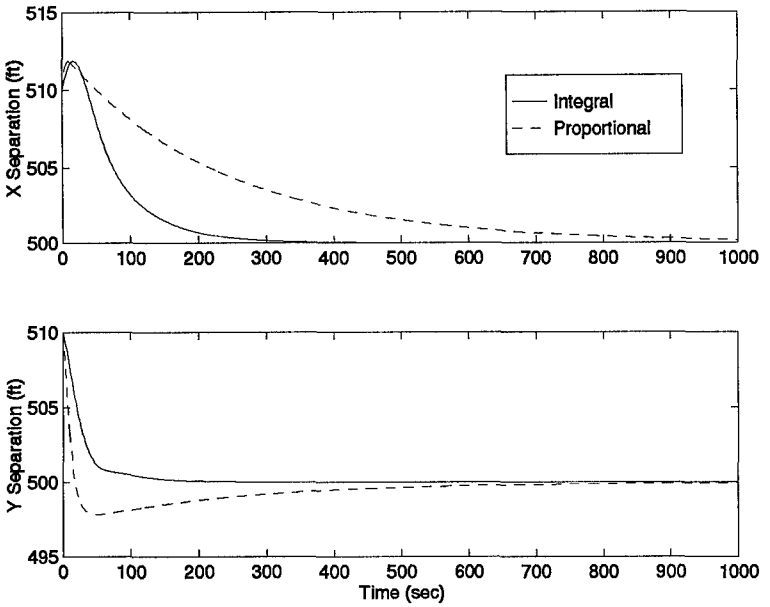

Figure 6.29 Second-order, Proportional Plus Integral, Linear Autopilot Response ($\overline{X} = \overline{Y} = 500$)

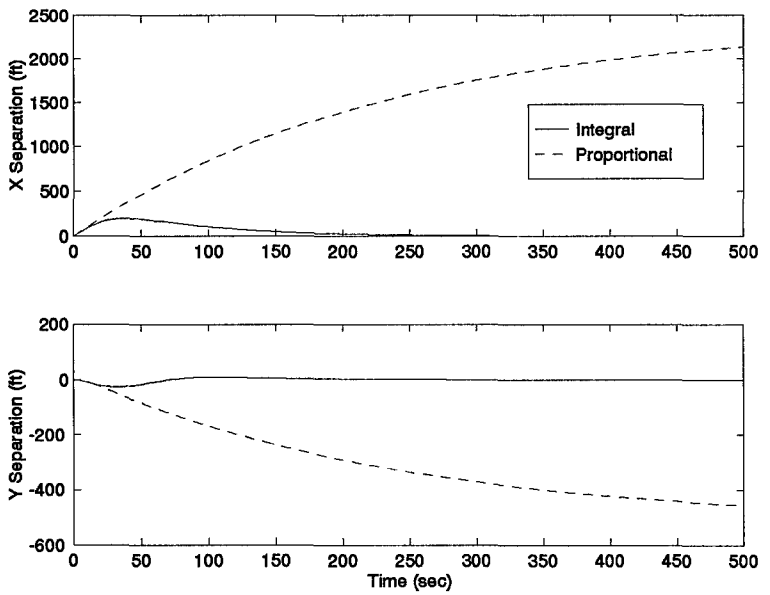

Figure 6.30 Second-order, Proportional Plus Integral, Linear Autopilot. 10 $\frac{ft}{sec}$ Velocity Increase Response ($\overline{X} = \overline{Y} = 0$)

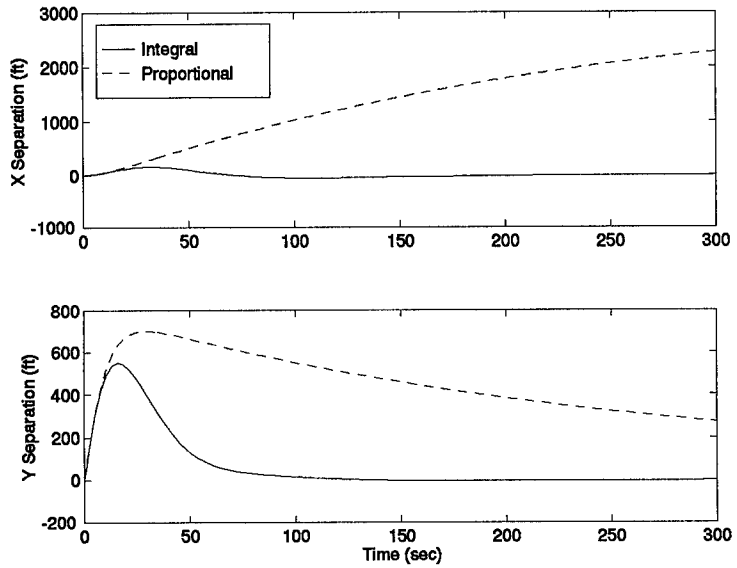

Figure 6.31 Second-order, Proportional Plus Integral, Linear Autopilot. 10 degree Heading Change Response ($\overline{X} = \overline{Y} = 0$)

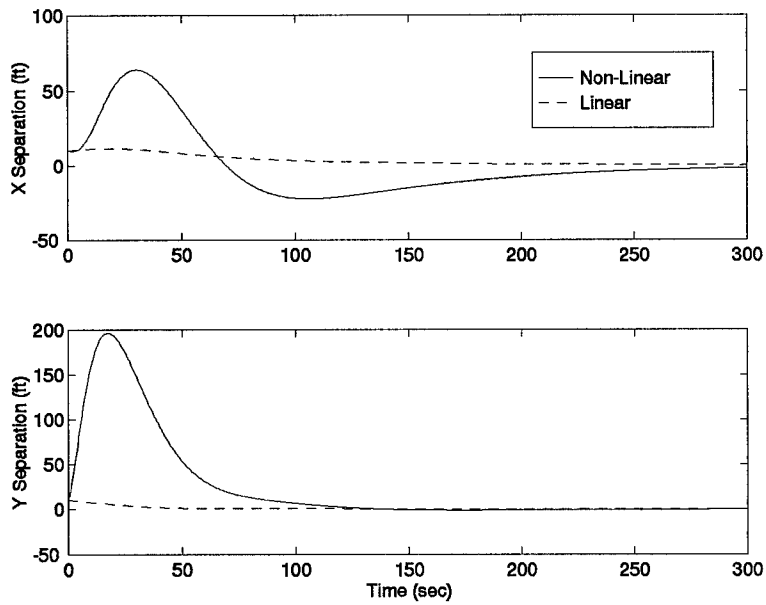

Figure 6.32 Second-order, Proportional Plus Integral, Nonlinear Autopilot Response ($\overline{X} = \overline{Y} = 0$)

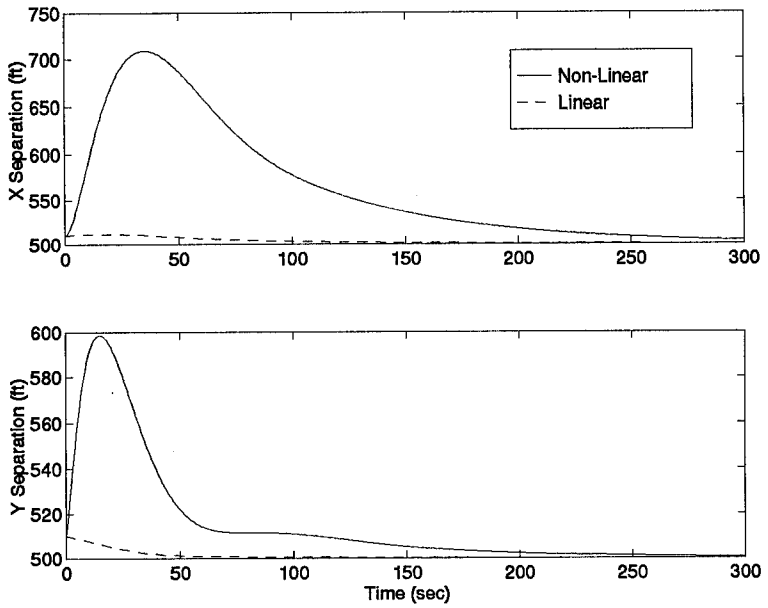

Figure 6.33 Second-order, Proportional Plus Integral, Nonlinear Autopilot Response ($\overline{X} = \overline{Y} = 500$)

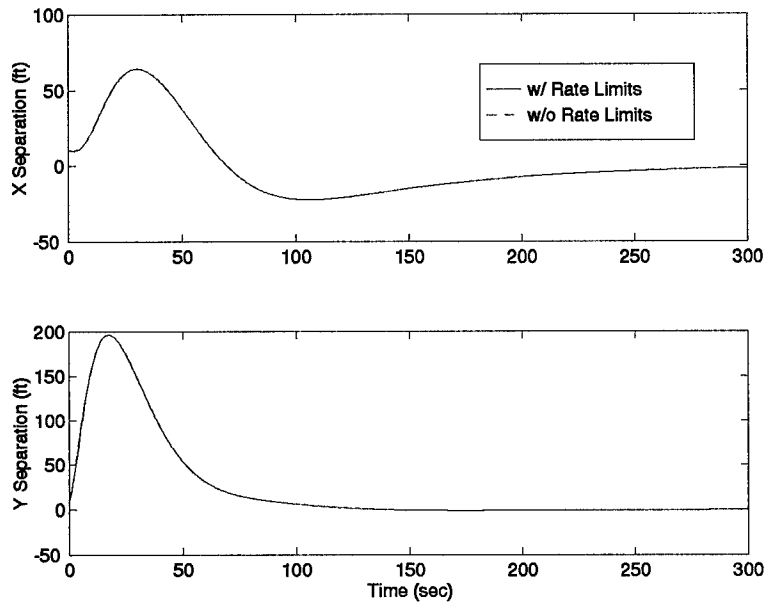

Figure 6.34 Second-order, Proportional Plus Integral, Nonlinear Autopilot Response w/ Rate Limits ($X_0 = Y_0 = 10ft$)

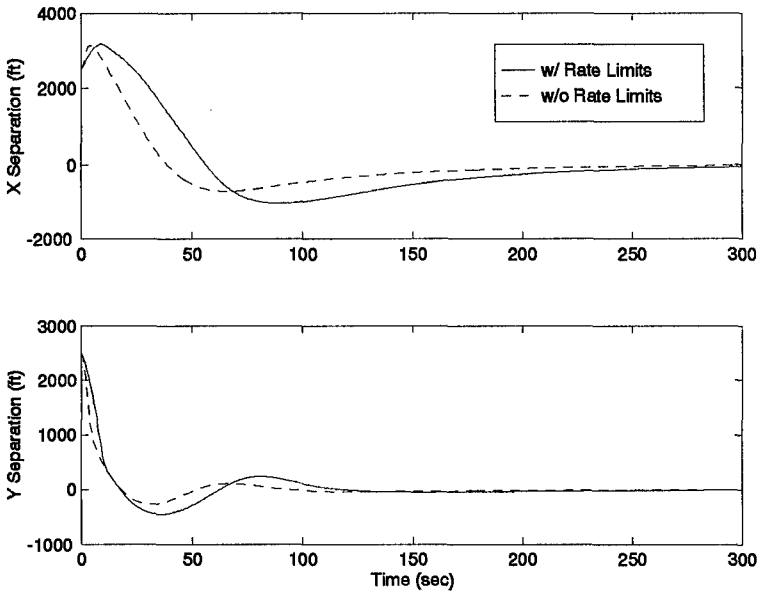

Figure 6.35 Second-order, Proportional Plus Integral, Nonlinear Autopilot Response w/ Rate Limits ($X_0 = Y_0 = 2500ft$)

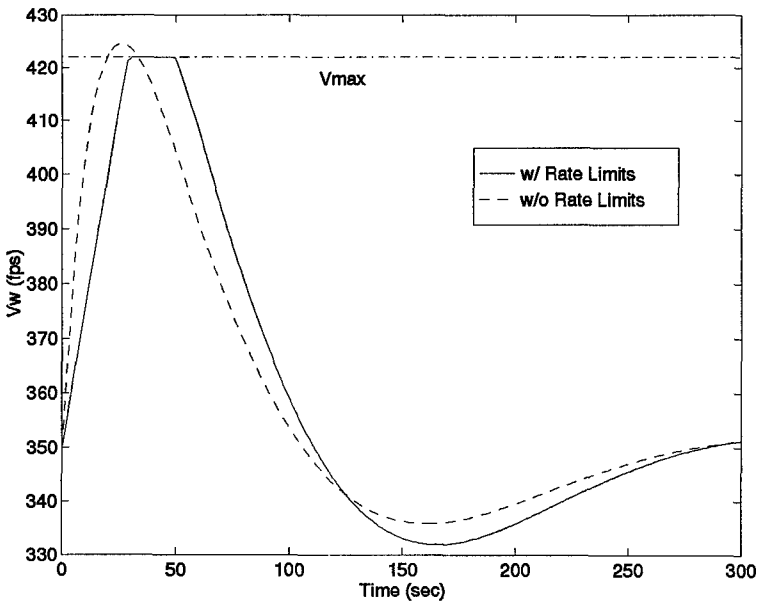

Figure 6.36 Second-order, Proportional Plus Integral, Nonlinear Velocity Response w/ and w/o Rate Limits ($X_0 = Y_0 = 2500ft$)

6.4 Trajectory Variations

The performance of the circular path autopilot is tested with regard to its response to commanded changes in the desired path trajectory, namely changes in the velocity and orbit radius. The tests involve three maneuvers: a decrease in radius, an increase in velocity, and a simultaneous change in airspeed and orbit radius. All maneuvers are accomplished by instantaneously changing the trajectory of the rabbit.

In each test, the formation initial conditions are straight and level flight. The circular path autopilot is engaged at t = 0 s. At t = 300 s, the change in "lead", viz. rabbit, trajectory is made. The wing aircraft response to a reduction in radius from 20054 feet to 10000 feet is shown in Figure 6.37. Note the disturbance rejection of the controller as seen in the X and Y channels. Next, the rabbit's velocity is increased from 350 fps to 375 fps (Figure 6.38). Finally, the rabbit is given a radius change command from 20054 ft to 10000 ft *and* velocity is increased from 350 fps to 375 fps (Figure 6.39). The circular path autopilot exhibits acceptable tracking performance in each case.

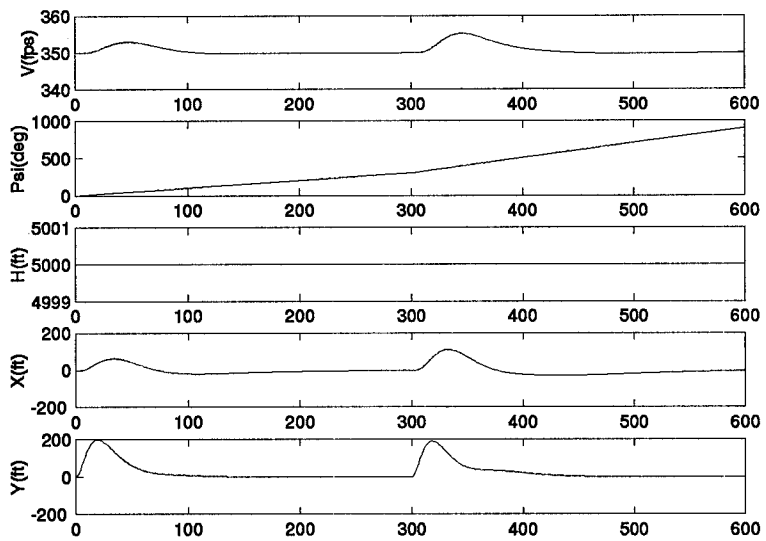

Figure 6.37 Trajectory Radius Change from 20054 ft to 10000 ft (at T = 300s)

The X-Y response of the wing aircraft in its own rotating reference frame for the combination maneuver is shown in Figures 6.40 and 6.41. The complete response is divided into two halves — the circular path initialization response and the response to the rabbit trajectory change.

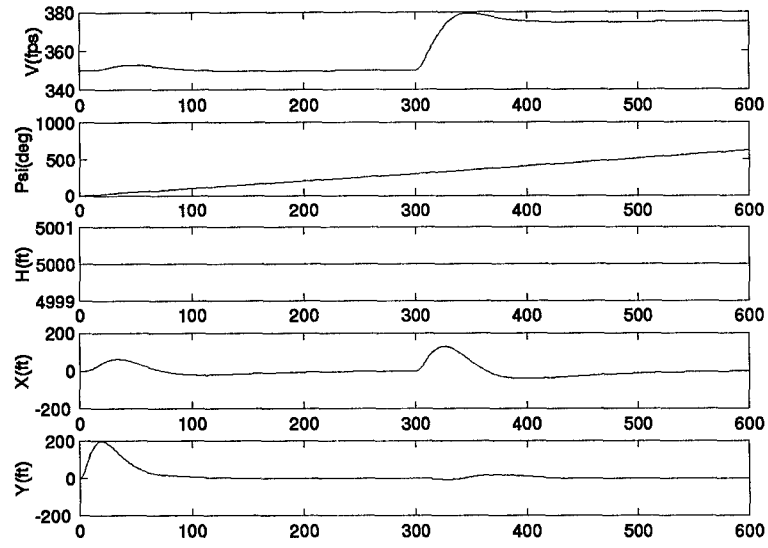

Figure 6.38 Trajectory Velocity Change from 350 fps to 375 fps, ($atT = 300s$)

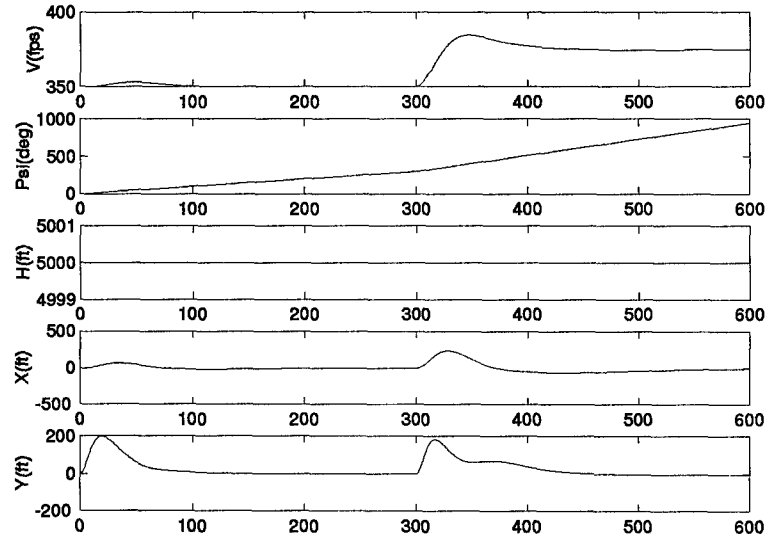

Figure 6.39 Combination Trajectory Radius and Velocity Change, ($atT = 300s$)

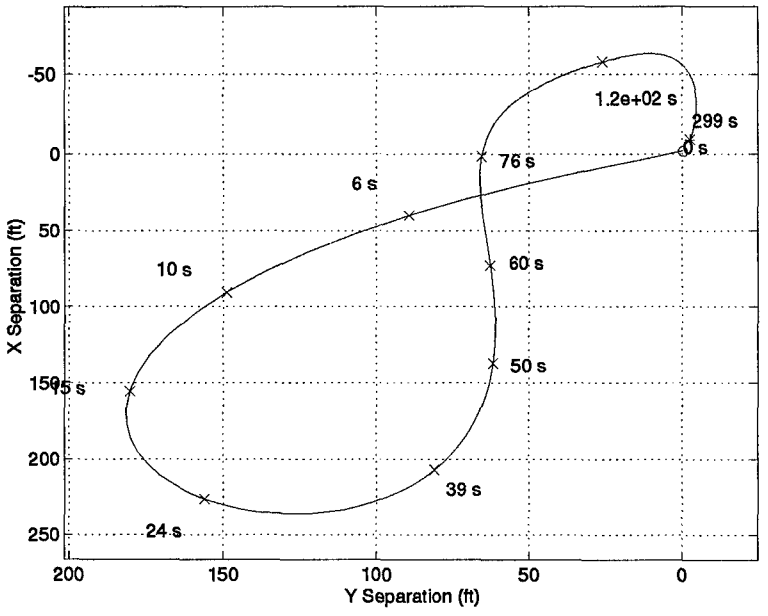

Figure 6.40 Circular Path Initialization, $(0 \leq T \leq 300s)$

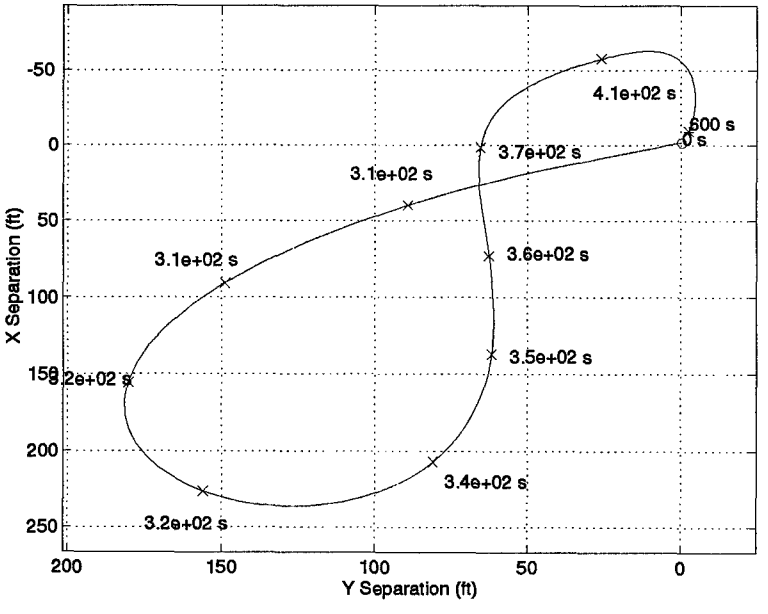

Figure 6.41 Combination Trajectory Radius and Velocity Change Lissajous Figure, $(300 \leq T \leq 600s)$

Parameter	Value
K_{xp}	4.50×10^{-2}
K_{xi}	4.50×10^{-4}
K_{yp}	1.50×10^{-2}
K_{yi}	5.00×10^{-4}

Table 6.1 Circular Path Formation Flight Controller Gains

6.5 Controller Summary

The circular path formation flight control laws are repeated below for clarity. Note that true states, *not* perturbations are used. The controller gains are listed in Table 6.1.

$$V_{wc} = V_L + K_{xp}(X - X_{cmd}) + K_{xi}\int_0^t (X - X_{cmd})\,dt \tag{6.17}$$

$$\Psi_{wc} = \Psi_L + K_{wp}(Y - Y_{cmd}) + K_{yi}\int_0^t (Y - Y_{cmd})\,dt \tag{6.18}$$

$$H_{wc} = H_L + \frac{1}{2g}(V_L^2 - V_{wc}^2) \tag{6.19}$$

6.6 Conclusion

Using a clear, step by step process, an autopilot for flying aircraft in a circular path is designed and validated through nonlinear simulation. The development of the autopilot for flying the aircraft in a circular path is an interesting extension of, and yields valuable insights into, the formation flight control problem.

The conclusion which can be drawn relates to the importance of integral action in nonlinear control systems. While integral action can somewhat degrade the performance of the system, its inherent disturbance-rejection capability compensates for unavoidable disturbances introduced by the quintessential linearization step of the control design process. Unfortunately, these disturbances are ubiquitous in real world nonlinear control systems. Hence, the control system engineer must take these factors into account during the design process.

Another important item of note is related to the use of second-order aircraft/autopilot models which more closely approximate reality. A beneficial effect is observed when the rate-limits are included in the simulation. This enables the designer to more confidently use conventional linear design techniques with less likelihood of encountering the hard rate limits. Hence, it is in fact beneficial to use realistic models, for this facilitates the control design process.

VII. Proportional and Integral Control of Nonlinear Systems

The subtle factors involved when designing linear controllers for nonlinear systems are investigated in greater detail regarding the design of the formation flight controller in Chapters IV and VI. This chapter reveals insights into possible pitfalls and motivations for the use of proportional-integral control in this thesis.

7.1 Introduction

Most control system design paradigms are centered on linear plant models. It is therefore preordained that when nonlinear plants need to be controlled, the linearization of the attendant nonlinear dynamics is the first step in the design process. The linearization is performed about a known and desired equilibrium point ("trim condition"), or, the nonlinear dynamics are linearized about a prespecified nominal trajectory. The method of small perturbations about a trim condition, or about a nominal trajectory, is invoked, and dynamics linear in the perturbations are obtained. Linear control design methods are then applied to the ensuing linearized plant. Finally, the synthesized linear control law is applied to the nonlinear plant.

Linear state feedback control, also referred to as "proportional" control, and control employing integral action, are popular control methods. Proportional and Integral (PI) control is an effective control synthesis method, whose beneficial attributes in nonlinear systems control are investigated in this work. Although, based on the linear analysis alone, the need for integral control might not be evident, it is shown that when linear controllers are applied to nonlinear plants, integral action not only yields improved performance, but is in fact necessary.

The chapter is organized as follows. In Section 7.2 a detailed investigation of the steps taken in the linearization procedure is undertaken. The well known PI controller design method is briefly outlined in Section 7.3, with special reference to those attributes of PI control which positively interact with certain facets of the linearization process. The role of integral action in nonlinear control is discussed in Section 7.4, where the concepts at work are illustrated in an example. In Section 7.5 the role of integral action in mitigating certain

subtle deleterious effects introduced by the linearization process is further emphasized. The need for integral action is further motivated in Section 7.6 where linear robust control is discussed. The discussed concepts are illustrated in the context of the nonlinear aircraft formation flight control problem. Concluding remarks are made in Section 7.7.

7.2 Linearization

The nonlinear control system is considered

$$\dot{X} = f(X,U)\ ,\quad X(0) = X_0\ ,\quad t \geq 0\ , \tag{7.1}$$

where the state X$\in R^n$ and the control $U \in R^m$. Two types of control problems are routinely considered: 1) Regulation about a prespecified equilibrium/trim point, or, 2) Regulation about a prespecified nominal trajectory.

In the first instance, the said trim point (or equilibrium point) is $\overline{X}$, $\overline{U}$, and it satisfies the equation

$$0 = f(\overline{X},\overline{U}) \tag{7.2}$$

The state perturbation is x and the control perturbation is u, viz.,

$$X = \overline{X} + x \tag{7.3}$$

$$U = \overline{U} + u \tag{7.4}$$

Hence, in view of eqs. (7.1) - (7.4), the perturbations equation is a Linear Time Invariant (LTI) control system

$$\dot{x} = Ax + Bu\ , x(0) = x_0 = X_0 - \overline{X}\ ,\quad t \geq 0\ , \tag{7.5}$$

containing the Jacobian matrices $A = \frac{\partial f}{\partial x}\,|_{\overline{X},\overline{U}}$ and $B = \frac{\partial f}{\partial u}\,|_{\overline{X},\overline{U}}$.

If regulation about a prespecified nominal trajectory $\overline{X}(t)$, $\overline{U}(t)$, $t \geq 0$ is desired, the state and control perturbations satisfy

$$X = \overline{X}(t) + x \tag{7.6}$$

$$U = \overline{U}(t) + u \tag{7.7}$$

In this case,

$$\dot{\overline{X}} = f(\overline{X}(t), \overline{U}(t)) \ , \ \overline{X}(0) = \overline{X}_0 \ , \ t \geq 0 \tag{7.8}$$

and the ensuing linearized control system (see, e.g., eqs. (7.1) and (7.6) - (7.8)) is time-dependent, viz.,

$$\dot{x} = A(t)x + B(t)u \ , \ x(0) = x_0 = X_0 - \overline{X}_0 \ , \ t \geq 0 \ . \tag{7.9}$$

In either case, second-order terms are neglected in the linearized dynamics in both eqs. (7.5) and (7.9). Indeed,

$$\dot{x} = A(t)x + B(t)u + H.O.T.\,(x, u) \ . \tag{7.10}$$

Next, optimal linear control laws $u^*(t, x)$ are synthesized for the linear plants (7.5) or (7.9); finally, the respective control signals (7.11) or (7.12)

$$U^*(t, X) = \overline{U} + u^*(t, X - \overline{X}) \tag{7.11}$$

$$U^*(t, X) = \overline{U}(t) + u^*(t, X - \overline{X}(t)) \tag{7.12}$$

are applied to the original nonlinear plant (7.1), and are used in the type 1 or type 2 control problems.

7.3 PI Control

PI control entails the augmentation of the state vector. In the linear design step, the control law

$$u^* = K_P x + K_I z \ , \tag{7.13}$$

where

$$\dot{z} = x \ , \ z(0) = 0 \tag{7.14}$$

is synthesized. Next, define

$$Z = \int_0^t X(t)dt \tag{7.15}$$

Thus, eqs. (7.11) and (7.13) - (7.15) yield the control law

$$U(X,Z,t) = K_P X + K_I Z - K_I \overline{X} t + \overline{U} - K_P \overline{X} \tag{7.16}$$

Similarly, eqs. (7.12) and (7.13)-(7.15) yield the control law

$$U(X,Z,t) = K_P X + K_I Z + \overline{U}(t) - K_P \overline{X}(t) - K_I \int_0^t \overline{X}(t)dt \tag{7.17}$$

The PI control laws (7.16) and (7.17) are applied to the nonlinear plant (7.1).

Now, Lyapunov's classical stability theorem applies to "unforced" nonlinear dynamical systems, i.e.,

$$\dot{X} = f(X,\overline{U}) \ , \ X(0) = X_0 \ , \ t \geq 0 \ , \tag{7.18}$$

or

$$\dot{X} = f(X,\overline{U}(t)) \ , \ X(0) = X_0 \ , \ t \geq 0 \ . \tag{7.19}$$

It states that if the Jacobian A is a stability matrix, or, if the homogeneous time-dependent linear dynamical system

$$\dot{x} = A(t)x \ , \ x(0) = x_0 \ , t \geq 0$$

is asymptotically stable, then there exists a neighborhood of $\overline{X}$, or there exists a neighborhood of $\overline{X}_0$, such that the nonlinear systems (7.18) or (7.19) are asymptotically stable.

PI control laws are easily synthesized for LTI dynamical systems. Thus, proportional control is employed to stabilize linear (or linearized) plants such as (7.5). Now, Lyapunov's stability result is easily extended to apply to *stabilizability*, viz., there exists a neighborhood of $\overline{X}$ in R^n such that the closed loop control system (7.1) and (7.20)

$$U = K_P X + \overline{U} - K_P \overline{X} \tag{7.20}$$

is stabilizable, provided that the linearized control system (7.5) and (7.21)

$$u^* = K_P x \tag{7.21}$$

is asymptotically stable. Note that stable linear systems are globally stable whereas Lyapunov's stabilizability theorem guarantees the stability of the closed-loop nonlinear system (7.1), (7.20) in a "sufficiently small" neighborhood of the trim point $\overline{X}$.

Concerning the linearized system (7.9): Our "bag of tricks" for the control of non autonomous plants is rather limited. Obviously, it is more difficult to synthesize a control law which stabilizes the time dependent linearized plant (7.9) than it is to synthesize a control law which stabilizes the LTI plant (7.5). However, if a stabilizing control law is available, Lyapunov's stabilizability result can also be applied to non LTI scenarios which arise from the application of linearization to regulation about a known and desirable nominal trajectory $\overline{X}(t)$, $\overline{U}(t)$. Thus, if the linearized control system (7.9) is stabilizable, then a neighborhood of $\overline{X}_0$ exists such that the response of the control system (7.1) satisfies $lim_{t \to \infty} \mid X(t) - \overline{X}(t) \mid = 0$.

So far, integral control has not been used. Only proportional control is needed for stabilization. Integral action is employed in linear control theory for disturbance rejection. Specifically, *persistent* disturbances are considered. Now, in design practice, integral action is oftentimes employed even in the absence of explicitly modeled disturbances, although the possible presence of the latter is implied. Since, according to Lyapunov's Theorem, integral control is not needed for stabilization in the linear design phase, the practice of employing integral action is sometimes hard to justify on theoretical grounds only. The situation is somewhat similar to the open-loop/feedback control quandary in optimal control, where existing optimization theory searches for, and provides, open-loop optimal controls, yet, based on a belief in the possible existence of disturbances acting on the system, the synthesis of feedback control laws is sought. Obviously, this is an intellectually unsatisfying state of affairs, for the disturbances whose postulated existence is alluded to, were not included in the model in the first place.

In the case of integral action, an explanation is provided by a close examination of the linearization - based control synthesis procedure. Disturbances are created during the linearization process, as is evident in eq. (7.9). Alas, the disturbances affecting the linear plant don't fall into the category of disturbances normally considered in linear control design, namely

- They are not persistent (which is good news)
- They are of feedback nature (which is bad news)

Although these disturbances are not of the type routinely considered, their rejection is of utmost importance. Their rejection by integral action will extend the range of applicability of the "linear" results — see, e.g., Sect. 7.4. In other words, the extent of the Lyapunov stabilizability theorem - guaranteed stable neighborhood of the trim state will be enlarged. Hence, integral control, by virtue of its disturbance rejection action, helps to make the linearization - based design procedure outlined in Section 7.2 work.

7.4 Example

The concepts discussed in Section 7.3 are illustrated in the context of a scalar nonlinear control problem

$$\dot{X} = X + X^2 + U \ , \ X(0) = X_0 \in R^1 \ , \ t \geq 0 \ . \tag{7.22}$$

Regulation about the trim point $\overline{X} = \overline{U} = 0$ is considered. Hence, the linearized control system is

$$\dot{x} = x + u \tag{7.23}$$

Note that the disturbance induced by linearization is x^2.

The proportional control law employed is

$$u^*(x) = -K_P x \ ,$$

viz.,

$$U^*(X) = -K_P X \ , \tag{7.24}$$

where $K_P > 1$. The domain of stability of the proportional control law is $-\infty < X_0 < K_P - 1$. Note that the domain of stability of the closed-loop system can be made arbitrarily large by increasing the gain K_P.

The addition of integral action will help to augment the realm of stability of the system (7.22) and (7.29) for a fixed K_P. For example, let $K_P = 2$. The proportional-integral control law,

$$U^* \ = \ -2(X + \int_0^t X \, dt) \tag{7.25}$$

is experimentally evaluated using a phase plane analysis (Figure 7.1). This proportional-integral control system increases the region of stability from $-\infty < X_0 < 1$ to $-\infty < X_0 \leq 1.75$.

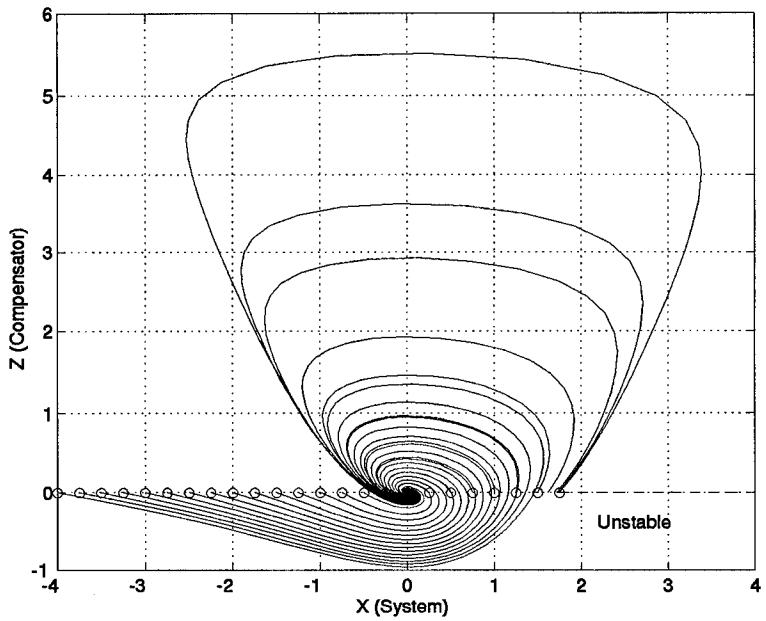

Figure 7.1 Phase Plane Response of Proportional/Integral Controller

The disturbances induced by linearization encountered in Sects. 7.3 and 7.4 are due to the neglect of higher order terms in the linearization process. Nevertheless, if the linearized closed - loop control system is stable and it affords the tracking of a reference signal, then Lyapunov's stabilizability result guarantees a degree of stability and reference signal tracking performance also in the nonlinear control system. Proportional control alone suffices to accomplish this. Integral control will increase the above mentioned degree of stability and tracking performance in the nonlinear control system.

7.5 Linearization - Induced Mismatches

It turns out that during the linearization process additional subtle mismatches are oftentimes introduced into the control problem. The latter have the effect of a persistent disturbance. Although the linear control synthesis methodology might not explicitly prescribe integral control, integral action is nevertheless required in nonlinear control in order to alleviate the ill effects of the above mentioned mismatches. Hence, integral action is a

crucial element that needs to be included in the classical linearization - based nonlinear control design paradigm discussed in Section 2. Indeed, integral action plays a decisive role in making linearization - based control laws work in a nonlinear environment.

In Chapter IV, a proportional flight control system is designed. The governing nonlinear kinematic equations are repeated:

$$\dot{X} = V_L cos(\Psi_L - \Psi_W) + \dot{\Psi}_W Y - V_W \tag{7.26}$$

$$\dot{Y} = V_L sin(\Psi_L - \Psi_W) - \dot{\Psi}_W X \tag{7.27}$$

In the formation flight controller design process, the nonlinear kinematic equations (7.26) and (7.27) are linearized. In the case where leader heading or velocity step input changes are contemplated, the linearization is performed about the fixed initial formation velocity ($\overline{V}$) and fixed initial formation course ($\overline{\Psi} = 0$) "trim conditions", i.e.,

$$\begin{aligned} X &= \overline{X} + x \\ Y &= \overline{Y} + y \\ V_L &= \overline{V} + v_L \\ V_W &= \overline{V} + v_W \\ \Psi_L &= \psi_L \\ \Psi_W &= \psi_W \end{aligned}$$

The small perturbation assumption is made and higher-order terms are neglected to form the following linear perturbation model

$$\dot{x} = v_L - v_W + \overline{Y}\dot{\psi}_W \tag{7.28}$$

$$\dot{y} = \overline{V}(\psi_L - \psi_W) - \overline{X}\dot{\psi}_W \tag{7.29}$$

Furthermore, the plant includes the lead and wing aircraft dynamics, viz.,

$$\dot{v}_W = -\frac{1}{\tau_{V_W}} v_W + \frac{1}{\tau_{V_W}} v_{Wc} \tag{7.30}$$

$$\ddot{\Psi}_W = -\frac{\tau_{\psi_A} + \tau_{\psi_B}}{\tau_{\psi_A}\tau_{\psi_B}} \dot{\Psi}_W - \frac{1}{\tau_{\psi_A}\tau_{\psi_B}} \Psi_W + \frac{1}{\tau_{\psi_A}\tau_{\psi_B}} \Psi_{Wc} \tag{7.31}$$

$$\dot{v}_L = -\frac{1}{\tau_{V_L}} v_L + \frac{1}{\tau_{V_L}} v_{Lc} \tag{7.32}$$

$$\ddot{\Psi}_L = -\frac{\tau_{\psi_A} + \tau_{\psi_B}}{\tau_{\psi_A}\tau_{\psi_B}} \dot{\Psi}_L - \frac{1}{\tau_{\psi_A}\tau_{\psi_B}} \Psi_L + \frac{1}{\tau_{\psi_A}\tau_{\psi_B}} \Psi_{Lc} \tag{7.33}$$

where the command inputs are v_{Wc} and ψ_{Wc} and the disturbance inputs are ψ_{Lc} and v_{Lc}. This is a type 1 control problem.

An autopilot for flying an aircraft in a circle about a prespecified target extends the application of the formation hold autopilot concept to allow an aircraft to orbit about a fixed point on the earth and is addressed in Chapter VI. The control system is described by eqs. (7.26), (7.27), (7.30), (7.32) and (7.33). The rabbit disturbance inputs, if any, are V_L and Ψ_L.

Whereas the formation hold autopilot was linearized about a steady state "trim" plant, the autopilot for flying aircraft in a circular path requires linearization about a time varying nominal trajectory. Hence, the nominal trajectory and the perturbed variables used for the linearization are (see, e.g., Figure 6.1):

$$\begin{aligned}
X &= \overline{X} + x \\
Y &= \overline{Y} + y \\
V_L &= \overline{V} \\
V_W &= \overline{V}\left(\frac{R\cos\gamma + \overline{Y}}{R}\right) + v_W \\
\Psi_L &= \omega t + \gamma \\
\Psi_W &= \omega t + \psi_W \\
\dot{\Psi}_W &= \omega + \dot{\psi}_W
\end{aligned}$$

The control inputs are also expressed as perturbations about a nominal control signal:

$$V_{wc} = \overline{V}_{wc}(t) + v_{wc} \tag{7.34}$$

$$\Psi_{wc} = \overline{\Psi}_{wc}(t) + \psi_{wc} \tag{7.35}$$

To complete our trim analysis about the circular nominal trajectory, the trim command inputs $\overline{V}_{wc}(t)$ and $\overline{\Psi}_{wc}(t)$ must be determined. To this end, substitute the nominal trajectory $\overline{\Psi}_w(t) = \omega t$ and $\dot{\overline{\Psi}}_w(t) = \omega$ into the differential equations (7.30) and (7.31), and obtain the following:

$$\overline{V}_{wc} = \overline{V}\left(\frac{Rcos\gamma + \overline{Y}}{R}\right) \tag{7.36}$$

$$\overline{\Psi}_{wc}(t) = \tau_{\psi_A}\tau_{\psi_B}\omega + \omega t \tag{7.37}$$

Finally, substituting the nominal trajectory into the nonlinear dynamics and eliminating high order terms results in the linearized perturbation dynamics. It is remarkable that although a type 2 control problem is considered, the linearized dynamical system is LTI and it is given by eq. (7.38).

$$\frac{d}{dt}\begin{bmatrix} x \\ v_W \\ y \\ \psi_W \\ \dot{\psi}_W \end{bmatrix} = \begin{bmatrix} 0 & -1 & \omega & 0 & \overline{Y} \\ 0 & -\frac{1}{\tau_v} & 0 & 0 & 0 \\ -\omega & 0 & 0 & -\overline{V}cos(\gamma) & -\overline{X} \\ 0 & 0 & 0 & 0 & 1 \\ 0 & 0 & 0 & -\frac{1}{\tau_{\psi_a}\tau_{\psi_b}} & -\frac{1}{\tau_{\psi_a}} - \frac{1}{\tau_{\psi_b}} \end{bmatrix}\begin{bmatrix} x \\ v_W \\ y \\ \psi_W \\ \dot{\psi}_W \end{bmatrix}$$

$$+\begin{bmatrix} 0 & 0 \\ \frac{1}{\tau_v} & 0 \\ 0 & 0 \\ 0 & 0 \\ 0 & \frac{1}{\tau_{\psi_a}\tau_{\psi_b}} \end{bmatrix} \begin{bmatrix} v_{wc} \\ \psi_{wc} \end{bmatrix} \tag{7.38}$$

The LTV aspect of the problem is confined to the nominal time varying states and to the nominal time varying controls.

Since in this problem no "leader" disturbance inputs are anticipated, proportional output feedback is employed

$$v_{wc} = K_{xp}x \tag{7.39}$$

$$\psi_{wc} = K_{yp}y \tag{7.40}$$

where the gains are $K_{xp} = 0.022$ and $K_{yp} = 2.3 \times 10^{-3}$ — see Section 4.6. As expected, the resulting response to initial x and y perturbations meets regulation requirements in the linear system (7.38), where the control signal, (7.39) and (7.40) are used (see, e.g., Figure 7.2).

Next eqs. (7.12), (7.39) and (7.40) are employed to form the control in the nonlinear system. This results in a constant tracking error in the nonlinear simulation — see, e.g., Figure 7.3. Subtle mismatches introduced by the linearization process have created persistent, unmodelled disturbances in the nonlinear simulation. Investigation of this phenomenon yields insights into the pitfalls of using linear controllers derived from analyzing linearized models.

Both the linear model (7.37) and the nonlinear simulation were initiated with the wing and lead aircraft flying in formation along a straight trajectory. This violates the tacit assumption made in the linearization process, which envisages that the lead aircraft is offset by an angle γ — see, e.g., Figure 6.1. Also, in the linearization process it is assumed that the speed of the wing aircraft is not equal to the speed of the leader. The

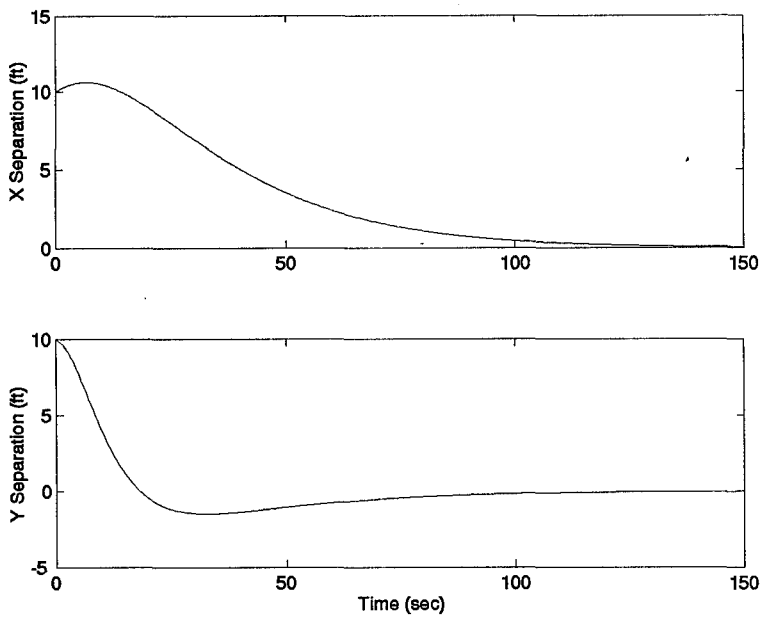

Figure 7.2 Linear Point Circle Autopilot Model

next sources of mismatches become apparent upon analysis of the naive control laws used in the nonlinear simulation:

$$\begin{aligned} V_{wc} &= \overline{V} + K_{xp}(X - \overline{X}) \\ \Psi_{wc} &= \omega t + K_{yp}(Y - \overline{Y}) \end{aligned} \tag{7.41}$$

Although the control laws look reasonable, the trim, or nominal, control signals in eqs. (7.36) and (7.37) should have been used. The latter yield the control law

$$\begin{aligned} V_{wc} &= \frac{R\cos(\gamma) + Y}{R}\overline{V} + K_{xp}(X - \overline{X}) \\ \Psi_{wc} &= \tau_{\psi_a}\tau_{\psi_b}\omega + \omega t + K_{yp}(Y - \overline{Y}) \end{aligned} \tag{7.42}$$

Indeed, using the control law (7.42), the tracking performance illustrated in Fig. 4 would be recovered for sufficiently small changes in formation geometry, and integral action would be unnecessary.

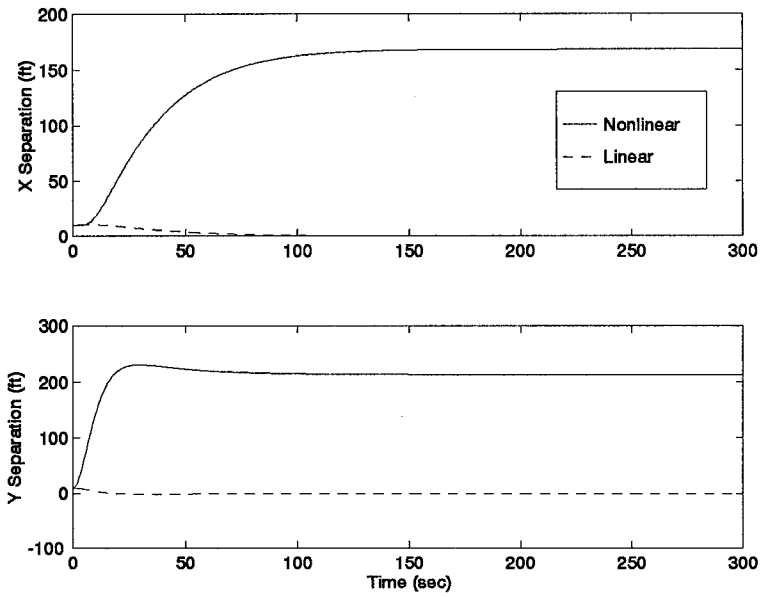

Figure 7.3 Linear and Nonlinear Comparison (Proportional)

Unfortunately, the desire to maintain robustness might preclude the use in the control law (7.42) of the:

- Time Constants $(\tau_{\psi_a}, \tau_{\psi_b})$
- Radius (R)
- Angular Rate (ω)
- Toe-in Angle (γ)

Adding integral action of the following form,

$$V_{wc} = \overline{V} + K_{xp}(X - \overline{X}) + \int_0^t K_{xi}(X - \overline{X})\, dt \tag{7.43}$$

$$\Psi_{wc} = \omega t + K_{yp}(Y - \overline{Y}) + \int_0^t K_{yi}(Y - \overline{Y})\, dt \tag{7.44}$$

and employing the above control laws, results in the nonlinear response shown in Figure 7.4 which shows that there is no steady-state error. Hence, the addition of integral action enables the controller to regulate the nonlinear system despite linearization induced mismatches.

Finally, additional robustness is incorporated into the control law when, in addition to positioning errors in the formation, one also uses the actual lead aircraft's state measurements V_L and Ψ_L, i.e.,

$$V_{wc} = V_L + K_{xp}(X - \overline{X}) + \int_0^t K_{xi}(X - \overline{X})\, dt \tag{7.45}$$

$$\Psi_{wc} = \Psi_L + K_{yp}(Y - \overline{Y}) + \int_0^t K_{yi}(Y - \overline{Y})\, dt \tag{7.46}$$

The latter somewhat robustifies the controller to improve performance in the presence of speed and heading disturbances of the "rabbit".

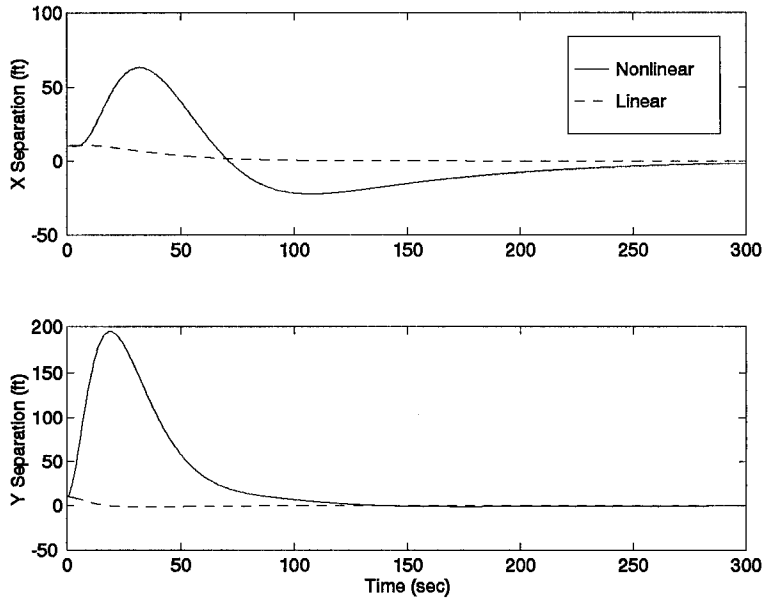

Figure 7.4 Linear and Nonlinear Comparison (With Integral Controller)

7.6 Integral Action in Robust Control

The available linear control design methods are brought to bear on nonlinear control problems. Thus, the robust control problem is oftentimes a product of an attack on nonlinearity. Strictly speaking, a known nonlinear plant is linearized about a set of N plausible operation points, $\left[(\overline{X}_i, \overline{Y}_i)\right]_{i=1}^{n}$, which cover its operational envelope. For example, in flight control, one then refers to a set of N representative "flight conditions" in the flight envelope. The ensuing N pairs of A_i and B_i matrices of the linear plants in eq. (7.5) are the Jacobians in X and U of the original nonlinear plant (7.1), evaluated at the respective N operating points. Thus, a robust control problem is posed of synthesizing a fixed controller that, within prespecified tolerances, yields uniformly acceptable tracking performance for the N linear plants.

In practice, it is required to control the original nonlinear plant (7.1). hence, the synthesized linear robust controller is used in eq. (7.11). Unfortunately, in eq. (7.11), the operating point information $\overline{X}_i$ and $\overline{U}_i$ is required. Thus, eq. (7.11) requires that the actually controlled i^{th} plant be identified. This, in turn, invalidates the proposed robust control approach, and it would appear that the proposed robust control attack on nonlinearity is doomed to failure. However, this need not be the case, and, in fact, it is sufficient in eq. (7.11) to use a middle of the envelope fixed trim point $\overline{X}$ and $\overline{Y}$. Therefore, a persistent control disturbance is at work. For example, if linear state feedback is used, then the control disturbance is

$$d = \overline{U} - \overline{U_i} + F(\overline{X} - \overline{X}_i) \tag{7.47}$$

The latter is a d_1 type input disturbance (see [7]), and it will be rejected by integral action. Hence, integral action is a must in linear robust control.

The above outlined approach is pursued in [9] and [10], where a full envelope flight control system for a high performance fighter is designed. In [9] and [10], information on the possible speed of movement of the aircraft from the neighborhood of one flight condition to the next is used to determine the bandwidth of the disturbance, and, moreover, the

disturbance rejection specification is set to make the disturbance imperceptible to the pilot.

7.7 Conclusions

For linear plants, a plethora of linear controller design paradigms are available. The unavoidable linearization step which is required in order to apply these linear control synthesis methods to nonlinear plants introduces disturbances into the control problem. These disturbances are of three kinds, namely

1. They are a direct consequence of the linearization procedure which calls for higher order terms in the dynamics to be neglected.
2. During the linearization process subtle mismatches are sometimes introduced into the control problem through the actually employed nominal control.
3. Disturbances arising during linear robust control of nonlinear plants.

These mismatches have the effect of a (persistent) disturbance.

Item 1. is discussed in Sects. 7.3 and 7.4. The nature of the disturbances mentioned in item 1. is such that integral control is not necessary, although integral action increases the domain of nonlinear stability. The disturbances referred to in item 2. above are discussed in Sect. 7.5. Item 3. is discussed in Section 7.6. They make integral action mandatory in nonlinear control systems employing the linear control synthesis paradigm.

Hence, even though integral control might not be mandated by the linear analysis, integral action is necessary for the control of nonlinear plants. Therefore, when controllers of nonlinear plants are synthesized using linearization - based control methods, integral action should be included in the control design paradigm.

VIII. Analysis and Conclusions

8.1 Objectives of Research Met

The objective of this research is to continue the work of Rohs, Dargan, Buzogany and Reyna by continuing the development of the formation flight control problem by including more accurate second-order aircraft/autopilot models. The energy conservation problem is also considered using the second-order aircraft/autopilot models. The goals continue with the development of an autopilot to automatically fly and aircraft in a circular path about a earth fixed point. Finally, a visual medium for examining the intra-formation positions during maneuvers is designed. These objectives have been met.

8.1.1 Incorporation of Second-Order Models - Analysis. The incorporation of second-order aircraft/autopilot models is accomplished in Chapter IV. After determining that the formation control law proposed by Reyna for first-order aircraft/autopilot models is unsatisfactory when second-order models are used, a new proportional MIMO output feedback control law is advanced. The gains are determined using a single loop closure technique and root-locus analysis. Care is taken to limit gains in anticipation of the rate limit nonlinearities present in the nonlinear model. Using extensive nonlinear simulations, it is shown that the new proportional control achieves superior performance for first and second-order aircraft/autopilot models.

8.1.2 Energy Tracking. The energy conservation problem is addressed in Chapter V. Comparisons are made between the "energy conserving" and "energy minimizing" techniques of Buzogany and Reyna, respectively. A new control law which seeks to track the specific energy of the leader is proposed. This "energy tracking" controller uses nonlinear feedback to command excursions in the altitude channel which seek to reduce unnecessary energy swings in the wing aircraft. The energy tracking controller shows improvement in energy minimizing capability and greater robustness over Reyna's approach. It is noted that the energy tracking controller's performance is limited by the tacit assumptions made when the aircraft autopilots were designed, namely the desire to provide decoupling between the heading, altitude, and airspeed states.

8.1.3 Circular Path Autopilot. In Chapter VI, the formation flight control system is extended to allow the wing aircraft to automatically fly a circular path about a earth fixed point and at a prespecified radius and velocity. The design method is conceptually identical to that of Chapter IV, with one important difference: the linearization is now made about a time varying trajectory versus a single "trim" condition as is par for most flight control problems. The initial controller is designed and, through simulation, it is determined that purely proportional control is unable to achieve a desirable response. The addition of proportional plus integral control is needed. The new control law is evaluated and the circular path autopilot is shown to meet specified requirements.

8.1.4 Analysis of Subtleties Encountered in the Linearization Design Process. Subtleties involved in the linearization of nonlinear systems are investigated in response to questions raised in the analysis of the circular path autopilot. The linearization process is outlined in detail and the benefits of integral action are noted. The analysis shows that the higher order terms as well as linearization induced mismatches and robustness desires create an inherent need for the addition of integral action when using linear compensators to control nonlinear systems. The benefits of integral action are illustrated with examples from the traditional formation hold autopilot and the circular path autopilot.

8.2 Conclusions and Specific Lessons Learned

The following conclusions are drawn from this thesis:

- The addition of MIMO partial state feedback improves performance and robustness of the formation flight controller.
- Second-order aircraft/autopilot models more accurately represent the true system, reducing the tendency to encounter rate-limit nonlinearities. This enables the designer to be more confident of the initial linear design.
- The MIMO control system can be designed using the successive loop-closure technique when the system states are loosely coupled.

- A nonlinear control law which commands altitude excursions to track the energy of the lead aircraft is shown to effectively reduce energy excursions and subsequent throttle variations in the wing aircraft using the aircraft/autopilot models developed by Buzogany [3].
- The formation hold autopilot design can be extended to fly circular paths. It is also shown that integral action is necessary in order to guarantee zero steady state error.
- Integral action improves the performance of controllers by rejecting disturbances and improving robustness.
- A three dimensional simulation can be displayed using the Aviator flight simulation package. The problem can be simulated with realistic real-time inputs.

8.3 Recommendations for Further Study

This thesis addresses one part of the formation flight control problem. The problem has proven to be quite rich and suggestions for future study are made:

- Develop models of sensors and include them into the simulation. Sensor noise should also be added to determine its effect on system performance. Limited testing in this research effort has shown that the system will exhibit acceptable performance in the presence of sensor noise.
- Investigate the incorporation of air-refuelling modes into the formation hold autopilot.
- The system should be implemented digitally and analyzed in the presence of limited sampling rates and sensing delays and the subsequent performance of the system researched.
- Investigate the incorporation of anti-collision circuitry into the formation flight controller.
- Develop a more accurate aircraft/autopilot model which includes the effects of cross-coupling. This will help to improve the realism of the simulation.

- Extend the formation hold autopilot design to other aircraft, including helicopters, high-performance aircraft and hovercraft.
- Utilize optimal control techniques to develop solutions for the formation assembly problem. Research into this area has been started during this thesis effort, but is incomplete due to time constraints. An initial development of the problem is addressed in Section 8.4

8.4 Formation Assembly Problem

The formation assembly problem is initiated in this research effort, but is left incomplete due to time constraints. An overview of the research completed is given to provide future researchers a basis with which to continue.

Determination of optimal solutions to problems depends greatly on the exact problem description. The formation assembly problem is specified in the following manner.

- Determine a control law which will assemble a formation of N independent aircraft into a prespecified formation geometry in minimum time.
- Other aircraft and terrain obstacles must be avoided.
- Initial conditions are N aircraft at arbitrary altitude, heading and airspeed — see, e.g. Figure 8.1.

Obviously, this is a quite complicated problem. To help reach a tractable solution, the following sub-optimal reformulation is offered. Assume the following — see, e.g. Figure 8.2:

1. The lead aircraft is initially located at the desired final conditions, i.e., desired heading, altitude and airspeed.
2. The leader begins a circular holding pattern at $t = t_0$, thus returning to the desired final conditions at intervals determined by the orbit period $T_{orb} = 2\pi\frac{R}{V}$, namely $t_i = \{0, T, 2T, ...\}$.
3. The wing aircraft is commanded to fly in a path which reaches the final conditions in the minimum time which is in the set $\{0, T, 2T, ...\}$.

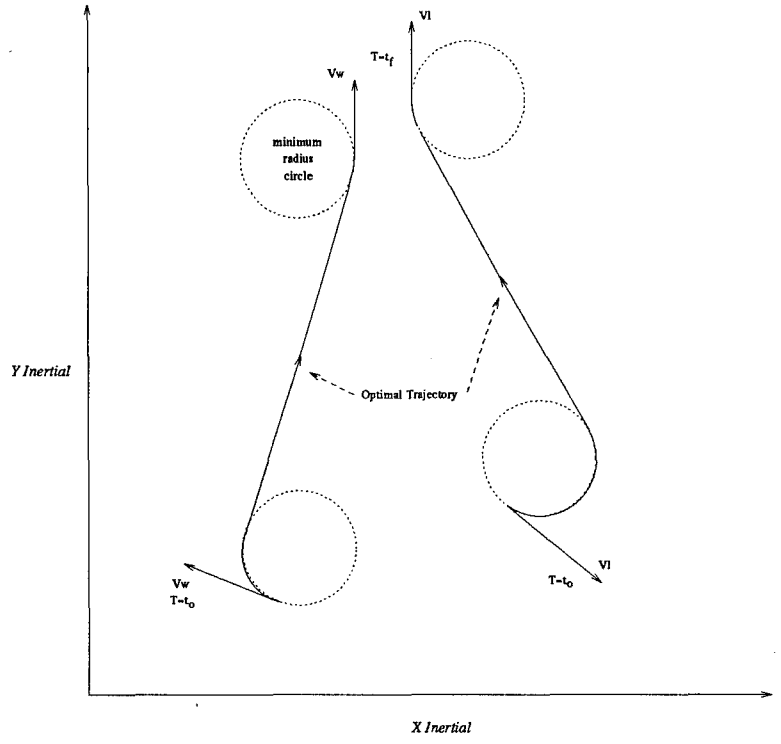

Figure 8.1 Optimal Formation Assembly (Two Aircraft)

4. Restrict the optimality to the commanded path of the wing aircraft. In other words, instead of including true wing position in the cost function, use the "rabbit" position as the baseline for optimization.

Using this strategy, the leader would be orbiting at the desired formation assembly location. The formation assembly controller would command a minimum time trajectory which intercepts the leader at the desired heading, altitude, and velocity. The difference between commanding a trajectory and controlling the wing aircraft to fly a desired trajectory are subtle. Commanding a trajectory acts as an outer loop to the formation flight control system and relies on the FFCS to guarantee tracking. The tracking capability of the FFCS and limits thereof are proven in Chapter VI in the design of the circular path autopilot. Actually controlling the aircraft to fly a trajectory is much more complicated and involves the design of complex control laws which model the performance of the FFCS.

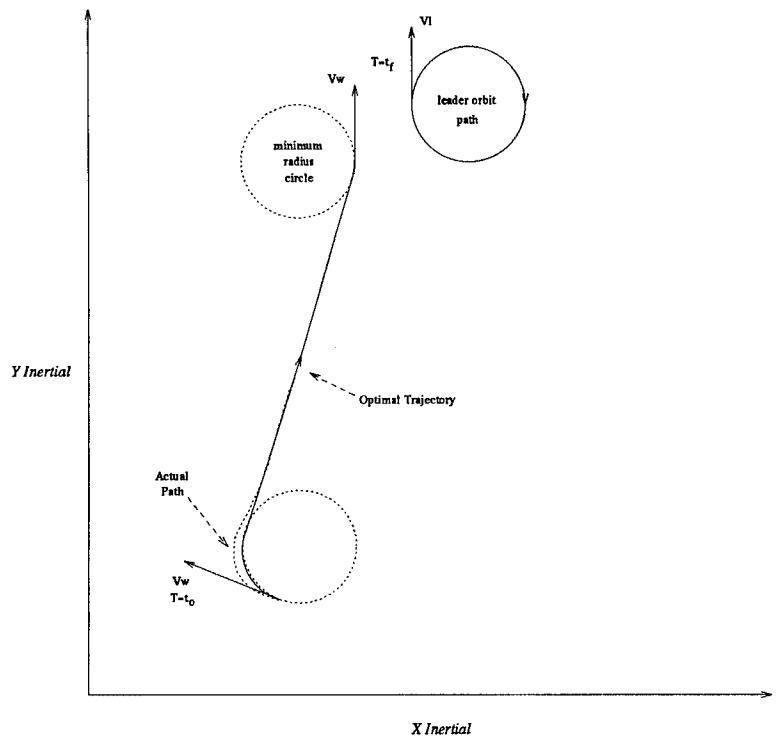

Figure 8.2 Formation Assembly (Suboptimal Reformulation)

8.5 Summary

In this thesis, a formation flight control system is designed. Two control laws are implemented. A proportional, partial state feedback formation flight control system is designed utilizing more accurate second-order models for an aircraft/autopilot developed by Buzogany [3]. Second-order models are also shown to be helpful for the control system designer when aircraft/autopilot rate limit nonlinearities are present. A new three-dimensional energy tracking controller is designed to reduce energy excursions of the wing aircraft by commanding appropriate altitude changes. With proportional plus integral control, the formation flight controller is extended to automatically fly an aircraft in a circular path. Finally, the formation flight control system can be simulated in machine code and the real time formation positions displayed using the Aviator flight simulation package.

Bibliography

1. Artificial Horizons, Inc., *Aviator Reference Manual*, Post Office Box 51847, Palo Alto, CA.
2. Blakelock, John H., *Automatic Control of Aircraft and Missiles* (Second Edition), John Wiley & Sons, Inc., 1991.
3. Buzogany, Louis E., *Automated Control of Aircraft in Formation Flight*, MS thesis, AFIT/GE/ENG/92D-07, School of Engineering, Air Force Institute of Technology (AU), Wright-Patterson AFB OH, December 1992.
4. Buzogany, Louis E., M. Pachter and J.J. D'Azzo, *Automated Control of Aircraft in Formation Flight*, Proceedings of the 1993 AIAA Guidance, Navigation, and Control Conference, pp 1349 - 1369, Monterey, CA, August 1993.
5. Dargan, John L., *Proportional Plus Integral Control of Aircraft for Automated Maneuvering Formation Flight*, MS thesis, AFIT/GE/ENG/91D-14, School of Engineering, Air Force Institute of Technology (AU), Wright-Patterson AFB OH, December 1991.
6. Dargan, John L., M. Pachter and J.J. D'Azzo, *Automatic Formation Flight Control*, Proceedings of the 1992 AIAA Guidance, Navigation, and Control Conference, pp 838 - 857, Hilton Head, SC, June 1992.
7. D'Azzo, John J. and Constantine H. Houpis, *Linear Control System Analysis and Design* (Third Edition), McGraw-Hill Book Company, 1988.
8. Kang, Ki H., A-10 Avionics Test Engineer, McClellan AFB CA, Personal interview, Air Force Institute of Technology, Wright-Patterson AFB OH, May 1994.
9. Reynolds, Odell R., *Design of a Subsonic Envelope Flight Control System for the VISTA F-16 Using Quantative Feedback Theory*, MS thesis, School of Engineering, Air Force Institute of Technology (AU), Wright-Patterson AFB OH, December 1994.
10. Reynolds, Odell R., M. Pachter and C.H. Houpis, *Full Envelope Flight Control System Design Using QFT*, American Control Conference, pp 350-354, Baltimore, MD, June 1994.
11. Pachter, M., J.L. Dargan, and J.J. D'Azzo, *Automatic Formation Flight Control*, To appear in the AIAA Journal of Guidance, Control, and Dynamics.
12. Pachter, M., T. Kobylarz and C.H. Houpis, *Literal Nyquist Stability Criterion for MIMO Control Systems*, To appear in the International Journal of Control.
13. Pachter, M., J.J. D'Azzo, and L.E. Buzogany, *Second - Order System Models of High - Order Plants*, International Journal of Systems Science, Vol. 25, No. 10, pp 1653-1662, 1994.
14. Reyna, Vincent P., *Automation of Formation Flight Control*, MS thesis, AFIT/GE/ENG/94M-01, School of Engineering, Air Force Institute of Technology (AU), Wright-Patterson AFB OH, March 1994.
15. Reyna, Vincent P., *Formation Flight Control Automation*, Proceedings of the 1994 AIAA Guidance, Navigation, and Control Conference, pp 1379-1404, Scottsdale, AZ, August 1994.

16. Rohs, Paul R., *A Fully Coupled, Automated Formation Control System for Dissimilar Aircraft in Maneuvering, Formation Flight*, MS thesis, AFIT/GE/ENG/91M-03, School of Engineering, Air Force Institute of Technology (AU), Wright-Patterson AFB OH, March 1991.

17. Veth, Michael J., M. Pachter and J.J. D'Azzo, *Autopilots for Flying Circular Paths*, Submitted to the 1995 AIAA Guidance, Navigation and Control Conference.

18. Veth, Michael J., M. Pachter and J.J. D'Azzo, *Proportional and Integral Control of Nonlinear Systems*, Forthcoming.

19. Veth, Michael J., M. Pachter and J.J. D'Azzo, *Energy Preserving Formation Flight Control*, To be presented at the 1995 AIAA Guidance, Navigation, and Control Conference.

20. Wright Research and Development Center, Aeronautical Systems Division, Air Force Materiel Command, *Intraformation Positioning System (IFPS) Request for Proposal,* Number F33615-89-R-3605. Wright-Patterson AFB OH, 14 December 1990.

Vita

Mike Veth was born on 16 September 1971 in Kirkwood, Missouri. He grew up there and attended Lafayette High School. Upon graduation he attended Purdue University and enrolled in the 220th Cadet Wing of the Air Force Reserve Officer Training Corps. He graduated with a Bachelor of Science in Electrical Engineering in May 1993. Upon graduating as an Air Force Distinguished Gradate, he received a regular commission and reported to Wright-Patterson AFB, Ohio, where he entered the School of Engineering of the Air Force Institute of Technology in pursuance of a Masters Degree in Electrical Engineering. His academic specialty is aircraft guidance and control.

Permanent address: 1362 Bear Canyon Rd.
Ballwin MO 63021

REPORT DOCUMENTATION PAGE

Form Approved
OMB No. 0704-0188

1. AGENCY USE ONLY (Leave blank)	2. REPORT DATE	3. REPORT TYPE AND DATES COVERED
	December 1994	Master's Thesis

4. TITLE AND SUBTITLE
ADVANCED FORMATION FLIGHT CONTROL

5. FUNDING NUMBERS

6. AUTHOR(S)
Michael J. Veth

7. PERFORMING ORGANIZATION NAME(S) AND ADDRESS(ES)
Air Force Institute of Technology, WPAFB OH 45433-6583

8. PERFORMING ORGANIZATION REPORT NUMBER
AFIT/GE/ENG/94D-30

9. SPONSORING/MONITORING AGENCY NAME(S) AND ADDRESS(ES)
Capt Steve Rasmussen
WL/FIGS
2210 Eighth Street Suite 11
Wright-Patterson AFB, OH 45433

10. SPONSORING/MONITORING AGENCY REPORT NUMBER

11. SUPPLEMENTARY NOTES

12a. DISTRIBUTION/AVAILABILITY STATEMENT
Approved for public release; distribution unlimited

12b. DISTRIBUTION CODE

13. ABSTRACT *(Maximum 200 words)*

Abstract

In this thesis, the formation flight control problem is continued from four previous theses. Automatic formation flight involves controlling multiple aircraft equipped with standard Mach-hold, altitude hold, and heading-hold autopilots to maintain a desired distance from a lead aircraft or "rabbit". Changes in the rabbit's states are treated as disturbances to the system and rejected. Previous research is advanced in the following areas. Higher-order aircraft/autopilot models are included into the design and a new feedback control law is employed, resulting in more accurate simulations. An energy tracking scheme is developed and is shown to reduce wing aircraft energy excursions. Finally, the formation hold autopilot is modified to allow the wing aircraft to orbit a stationary reference point on the earth at a desired range, airspeed, and altitude. The importance of the disturbance rejection capability of the controller is demonstrated through comparisons of linearized model predictions with nonlinear simulations. The design tradeoffs between performance and robustness are emphasized.

14. SUBJECT TERMS	15. NUMBER OF PAGES
Formation Flight Control, Energy Tracking Maneuvers, Energy Minimizing Maneuvers, Energy Excursion Minimizing Maneuvers, Circular Path Autopilot	243
	16. PRICE CODE

17. SECURITY CLASSIFICATION OF REPORT	18. SECURITY CLASSIFICATION OF THIS PAGE	19. SECURITY CLASSIFICATION OF ABSTRACT	20. LIMITATION OF ABSTRACT
UNCLASSIFIED	UNCLASSIFIED	UNCLASSIFIED	UL

GENERAL INSTRUCTIONS FOR COMPLETING SF 298

The Report Documentation Page (RDP) is used in announcing and cataloging reports. It is important that this information be consistent with the rest of the report, particularly the cover and title page. Instructions for filling in each block of the form follow. It is important to *stay within the lines* to meet *optical scanning requirements*.

Block 1. Agency Use Only *(Leave blank)*.

Block 2. Report Date. Full publication date including day, month, and year, if available (e.g. 1 Jan 88). Must cite at least the year.

Block 3. Type of Report and Dates Covered. State whether report is interim, final, etc. If applicable, enter inclusive report dates (e.g. 10 Jun 87 - 30 Jun 88).

Block 4. Title and Subtitle. A title is taken from the part of the report that provides the most meaningful and complete information. When a report is prepared in more than one volume, repeat the primary title, add volume number, and include subtitle for the specific volume. On classified documents enter the title classification in parentheses.

Block 5. Funding Numbers. To include contract and grant numbers; may include program element number(s), project number(s), task number(s), and work unit number(s). Use the following labels:

C	- Contract	PR	- Project
G	- Grant	TA	- Task
PE	- Program Element	WU	- Work Unit Accession No.

Block 6. Author(s). Name(s) of person(s) responsible for writing the report, performing the research, or credited with the content of the report. If editor or compiler, this should follow the name(s).

Block 7. Performing Organization Name(s) and Address(es). Self-explanatory.

Block 8. Performing Organization Report Number. Enter the unique alphanumeric report number(s) assigned by the organization performing the report.

Block 9. Sponsoring/Monitoring Agency Name(s) and Address(es). Self-explanatory.

Block 10. Sponsoring/Monitoring Agency Report Number. *(If known)*

Block 11. Supplementary Notes. Enter information not included elsewhere such as: Prepared in cooperation with...; Trans. of...; To be published in.... When a report is revised, include a statement whether the new report supersedes or supplements the older report.

Block 12a. Distribution/Availability Statement. Denotes public availability or limitations. Cite any availability to the public. Enter additional limitations or special markings in all capitals (e.g. NOFORN, REL, ITAR).

- DOD - See DoDD 5230.24, "Distribution Statements on Technical Documents."
- DOE - See authorities.
- NASA - See Handbook NHB 2200.2.
- NTIS - Leave blank.

Block 12b. Distribution Code.

- DOD - Leave blank.
- DOE - Enter DOE distribution categories from the Standard Distribution for Unclassified Scientific and Technical Reports.
- NASA - Leave blank.
- NTIS - Leave blank.

Block 13. Abstract. Include a brief *(Maximum 200 words)* factual summary of the most significant information contained in the report.

Block 14. Subject Terms. Keywords or phrases identifying major subjects in the report.

Block 15. Number of Pages. Enter the total number of pages.

Block 16. Price Code. Enter appropriate price code *(NTIS only)*.

Blocks 17. - 19. Security Classifications. Self-explanatory. Enter U.S. Security Classification in accordance with U.S. Security Regulations (i.e., UNCLASSIFIED). If form contains classified information, stamp classification on the top and bottom of the page.

Block 20. Limitation of Abstract. This block must be completed to assign a limitation to the abstract. Enter either UL (unlimited) or SAR (same as report). An entry in this block is necessary if the abstract is to be limited. If blank, the abstract is assumed to be unlimited.

*U.S.GPO:1990-0-273-271